Modeling the Interactions of Antimicrobial Peptides with Cell Membranes

by

Suemin Lee

A thesis
presented to the University of Waterloo
in fulfillment of the
thesis requirement for the degree of
Master of Science
in
Phyiscs

Waterloo, Ontario, Canada, 2022

Examining Committee Membership

The following served on the Examining Committee for this thesis. The decision of the Examining Committee is by majority vote.

External Examiner:	Robert Wickham Associate Professor, Department of Physics, University of Guelph
Supervisor(s):	Bae-Yeun Ha Professor, Dept. of Physics and Astronomy, University of Waterloo
Internal Member:	Jeff ZY Chen Professor, Dept. of Physics and Astronomy, University of Waterloo

Author's Declaration

I hereby declare that I am the sole author of this thesis. This is a true copy of the thesis, including any required final revisions, as accepted by my examiners.

I understand that my thesis may be made electronically available to the public.

Abstract

Antimicrobial peptides (AMPs) are key molecules of the innate immune system, found among a wide variety of living organisms, including animals, plants, and humans. It is typically composed of cationic and has a unique property known as cell selectivity: It has a stronger affinity toward bacterial membranes, which contain a large fraction of anionic lipids; in contrast, the outer layer of eukaryotic cell membranes consists electrically neutral. This distinctive characteristic causes peptide selectivity toward bacterial cells over the host cells, allowing AMPs to bind and rupture bacterial membranes preferentially. Optimized AMPs are thus considered novel candidates for the next generation of antibiotics. Despite its significance, the detailed picture of how their interactions with cell membranes influence peptide selectivity still remains unclear. The work in this thesis is aimed at gaining a deeper understanding of how AMPs interact with and permeabilize cell membranes from a theoretical perspective. First, we investigate the cell-density dependence of peptide activity and selectivity. In particular, we examine how the presence of host cells is implicated in peptide activity and selectivity. Second, we explore the effects of salt ions on the interactions of AMPs with cell membranes and their impacts on peptide activity and selectivity. Last, we examine the interactions between the outer bacterial membranes, especially the lipopolysaccharide (LPS) layer, against AMPs. To this end, we view LPS molecules as forming a polymer brush grafted to a charged surface and clarify the relative significance of various factors such as brush-peptide interactions, the electrostatic interactions between peptides and LPS headgroups, and brush lengths. Through this thesis, we introduced biophysical models for describing the interactions of AMPs with cell membranes and quantified the activity and selectivity under various biologically-relevant conditions. Additional efforts related to the work carried out in this thesis will be beneficial in searching for ideal AMPs as therapeutic agents.

Acknowledgements

First and foremost, I would like to express my deepest gratitude to my advisor, Dr. Bae-Yeun Ha, who has guided me throughout the past two years with his great patience, engagement, and valuable advice during my Master's at Waterloo. I was fortunate to have met him as a supervisor who allowed me to participate in the fascinating field of the research project and paved the way to continue my next journey. With his guidance and advice, I was able to fill my two years of studies with very meaningful and valuable learning time. I am confident that this thesis would not have been achievable without his mentorship and guidance. Additionally, I would like to thank my advisory committee members, Dr.Jeff Chen and Dr.Robert Wickham, for their time and sharing their critical comments and feedback.

Due to the pandemic, many things were unusual starting from the first semester at the University of Waterloo. Although I was not able to gain the whole experience on campus, I greatly appreciate all the efforts that have been made among many people and within the departments to put everyone together through virtual or even small events in person during the pandemic.

While staying at Waterloo, I was fortunate to meet great friends. I am grateful to my friends in Applied Mathematics, who shared their office space, opened the door every weekend, and invited me over to dinners and fun activities, which made my days more pleasant. Also, my wonderful roommate shared her evenings with me to chat and eat, which brightened my days. Additionally, I am so grateful to my amazing friend in Vancouver, who blows away all my stress and shares fun stories by talking on the phone overnights.

Last but not least, I would like to convey my heartfelt gratitude to my loving parents and my brother for their unwavering support and for always being at my back, which means so much to me and cannot be filled with words.

Dedication

I dedicate this to my loving parents.

Table of Contents

List of Figures

Chapter 1

Introduction

Living organisms operate under complex biological regulatory systems. Over a long period of time, organisms have evolved to survive while facing various challenges, including infections from pathogens like bacteria or viruses. The advent of antibiotics has enhanced the long-term survivability of humans. In 1928, Alexander Fleming discovered Penicillin which is the first known form of antibiotic. [51, 101] Since then, with advanced development, additional forms of antibiotics have been developed. However, over-usage or prolonged exposure to antibiotics has created an unpleasant consequence, i.e., bacterial resistance. Thus experts have warned against the abuse of antibiotics and suggested to put much effort to find a new alternative. [2, 5, 42, 51] Antimicrobial peptides (AMPs), found in living organisms, are key components of the innate immune system. Optimized AMPs have been identified as promising candidates. They often rupture bacterial membranes. It is less likely for bacteria to develop resistance against membrane-rupturing AMPs than against conventional antibiotics. [92, 102, 15]

Good AMPs are cell-selective. AMPs are mostly cationic (positively charged) and amphipathic (both hydrophilic and hydrophobic). [47] Bacterial cell membranes contain anionic (negatively charged) lipids, whereas the anionic lipids in host cell membranes are segregated into the inner layer. [42, 92] As a result, AMPs have a stronger affinity toward bacterial cells. When AMP binds to the cell surface, it causes destruction of cell membranes and brings fatal damage to cell morphology, leading to cell rupture and death. They can kill bacteria selectively over the host cells and are considered to be a promising novel candidate for next-generation peptide antibiotics. [76, 102, 47]

Aside from the benefit of human medication, AMPs have a wide range of applications and share a positive influence on various fields such as food, agriculture, animal husbandry,

and aquaculture industries. [42] For instance, in the food industry, where foods get easily spoiled by environmental factors like temperatures, acidity, and packaging, AMPs are used for food preservation purposes. AMPs are considered a favorable option over synthetic chemicals since it is biologically more stable and less harmful to the human body. [42] In addition, when plants are susceptible to disease, AMPs help inhibit the growth of pathogens in plants and positively affect agricultural production. [42, 62]

Despite the growing interest in potential applications of AMPs in a number of areas, the detailed mechanisms of action behind AMPs have not been fully elucidated. According to the database (APD3) [94], as of May 25, 2022, approximately 3324 AMPs have been discovered. Due to the enormous diversity and quantity, many different properties are exhibited by AMPs, making it challenging to integrate AMPs into a single reaction system. The well-known characteristics of AMPs often include structural morphology, charge distributions, interactions with various cell types, environmental conditions, etc. [42] Depending on their characteristics, they behave differently. In this work, we are interested in resolving several open questions about the interactions between AMPs and cells, e.g., how does the cell density impact the activities of AMPs in a heterogeneous mixture of bacteria and host cells, referred to as a competitive medium? A homogeneous solution of either bacteria or host cells can be designated as non-competitive. How do AMPs behave under different salt conditions? What is the role of outer bacterial membranes in protecting the bacteria against the action of AMPs?

These questions merit consideration. First, the density of cells can vary in a biological setting depending on the degree of infection and is a key parameter in controlling peptide activity and selectivity. [76] Secondly, AMPs have been widely used for food preservation in the food industry, and changing environmental conditions is a sensitive matter. [42] Examining variations in salt concentration allows us to understand how microbes interact with cationic molecules (e.g., AMPs) and predict their responses under various conditions. Lastly, unlike Gram-positive bacteria or eukaryotic cells, Gram-negative bacteria are surrounded by two membranes: outer membranes (OMs) and inner membranes. Thus, understanding how AMPs interact with and perturb the OM is important for us in designing peptide antibiotics for fighting Gram-negative bacteria. [64]

In this work, these questions are addressed by constructing theoretical models. Aside from the benefits discussed above, the resulting models help to accurately analyze experiments and make predictions regarding the interactions of AMPs with cell membranes. Before presenting the models, we first provide background information about the interactions between cells and AMPs.

1.1 Biological Background

1.1.1 Antimicrobial Peptides (AMPs)

AMPs are essential molecules of the innate immune system found in various living organisms. It act as a first-line defense against other pathogens, including bacteria, fungi, parasites, yeast, and viruses. [101, 97] These are short peptide molecules that are typically classified as short lengths of proteins. In general, polypeptides are formed from combinations of amino acids linked by covalent peptide bonds, and when 50 or more amino acids are grouped, they are commonly referred to as proteins. Therefore, AMPs are known as a small class of proteins consisting of 15-50 amino acid residues. Although rare, some AMPs consist of more than 100 amino acids. [7] These unique sequences of amino acid compositions on the AMP give diversity to the types, structure configurations, and functions.

Characteristics and Structural features

AMPs are known to have amphipathic (both hydrophilic and hydrophobic) nature and cationic properties with a net charge ranging between +2 and +9 due to the high occurrence of arginine and lysine residues. [96] Although anionic AMPs exist, positively charged AMPs are more common. Most AMPs include more than 50% hydrophobic amino acids, allowing them to have amphipathic characteristics and facilitate interaction with target cells. In addition, AMPs are observed in various conformations. Mostly, they exist in the following secondary structures: α-helix, β-sheets, loop, and $\alpha\beta$. [37] Here, the β–sheets are composed of at least two β-strands, which are sustained by the disulfide bonds that anchor the structures. [27]

Types of AMPs

AMPs are challenging to classify due to their immense variety and abundance. Thus, many studies have proposed various classification systems based on structural composition, origin, and activity. [42, 102, 101] In particular, when classified according to structure, AMPs are typically distinguished based on their secondary structures, such as α-helix, β-sheets, linear, or both containing $\alpha\beta$ configurations. Moreover, depending on the species of origin, it is categorized into mammals, amphibians, and insect microorganisms. There are more classification methods that exist depending on purposes, such as amino acid abundance or AMP activity. In addition, the most extensively studied AMP families of

the group include cathelicidins, defensins, cecropins, and magainin. [93, 88, 81, 38] Here, we briefly introduce well-known examples of AMPs.

In the mammalian AMPs, there are only two family groups: cathelicidins, and defensins. [24] Particularly, the only cathelicidin type discovered in humans is the LL-37 peptide, which is frequently observed in the skin of newborn infants. [26] The LL-37 peptide exhibits essentially no secondary structure in aqueous solution but acquires an α-helical structure when exposed to a non-polar environment. [101] Moreover, defensins are the most abundant among all AMP families, more widely distributed across most eukaryotes organisms, and can be further divided into sub-families of α, β, and θ-defensins. [24] α-defensin was initially discovered in rabbit alveolar macrophages, and six β-defensins were identified in humans isolated from bovine tracheal epithelial cells. The other forms of α and θ-defensins exist among humans.

Among the amphibian AMPs, magainin is one of the well-known AMPs primarily found on the skin of frogs. It has the properties of amphipathic, cationic, and α-helical structure. It was first isolated from the African clawed frog *Xenopus laevis* [98] and also discovered in the other species of frogs such as *Silurana*, *Pseudhymenochirus*, and *Hymenochirus*. [16] It plays an important role in inhibiting growth and killing *Pseudomonas* cells.

Melittin is one example of insect AMPs frequently employed in numerous investigations. It is the major component in honey bee venom, making up roughly 52% of its dry mass. [10] It contains amphipathic, cationic characteristics composed of 26 amino acids. When melittin is exposed to the water, it is primarily unstructured, but upon binding to a lipid or hydrophobic surface, it transforms into an α-helical structure. [101] It has several positive effects. In particular, due to its high selectivity in microbes or cancer cells, it is considered a strong potential for the development of therapeutic peptides.

1.1.2 Cell membrane and Lipid composition

Living cells are surrounded by a cell membrane. This cell membrane separates the exterior environment from the cell interior. It is an essential component that serves as a compartmentalization, signal transduction, and transport pathways. It has a basic bilayer structure mainly composed of phospholipids, proteins, and cholesterol. [3]

In particular, phospholipids, which are the main components of cell membranes, exist in various types and can be distinguished according to the charge properties. [102] The most common neutral phospholipids are phosphatidylcholine (PC) and phosphatidylethanolamine (PE). Phosphatidylcholine (PC) comprises up to $\sim$50% of total phospholipids and helps maintain membrane permeability. [89, 91] In contrast, the properties of

negatively charged phospholipids include phosphatidylserine (PS), cardiolipin (CL), phosphatidylinositol (PI), and phosphatidylglycerol (PG). [53] Cell membranes are formed by these various lipid mixtures.

Mammalian Cell Membrane

Mammalian cell membranes are composed of a lipid bilayer, but the two layers not being identical. The outer membranes are composed of abundant PC, electrically neutral, and cholesterol elements. [91] Comparatively, the majority of the cellular inner layer of the membrane is made up of PS, PE and PI, which impart anionic phospholipid properties. [90] This asymmetrical tendency between the two layers induces biological phenomena such as blood coagulation and cell apoptosis when PS lipids get exposed to the outer layer of the membrane. [12]

Bacterial Cell Membrane

Bacterial cell membranes have a different lipid composition than mammalian cells and are devoid of cholesterol. The outer leaflets of membranes have anionic properties due to the compositions of PS, CL, and PG lipids. [53] Based on the characteristics of the membrane's cell envelope, the bacterial cells can further be divided into two groups: Gram-negative bacteria and Gram-positive bacteria. [80] Gram-negative bacteria are characterized by a thin peptidoglycan layer and the lipopolysaccharide (LPS) in the outer membrane (OM) that plays a protective role. [80] In contrast, Gram-positive bacteria have a thick peptidoglycan layer and a lipoteichoic acid (LTA) layer on the outer surface. These outer layers play an essential role in preventing the entry of external substances. [73] The overall negative charge of the bacterial outer leaflet of the membrane is reflected by LPS and LTA.

1.2 Overview of Actions of Mechanism on AMPs

1.2.1 Cell Selectivity

Cell selectivity is one of the crucial motives for choosing AMPs as a promising alternative to antibiotics. [99, 9] As discussed in the previous Sec. 1.1.1, a brief review of the fundamental properties of AMP and cell membranes showed that cationic AMPs could bind effectively to the surface of anionic bacterial cell membranes due to their opposite charge effects.

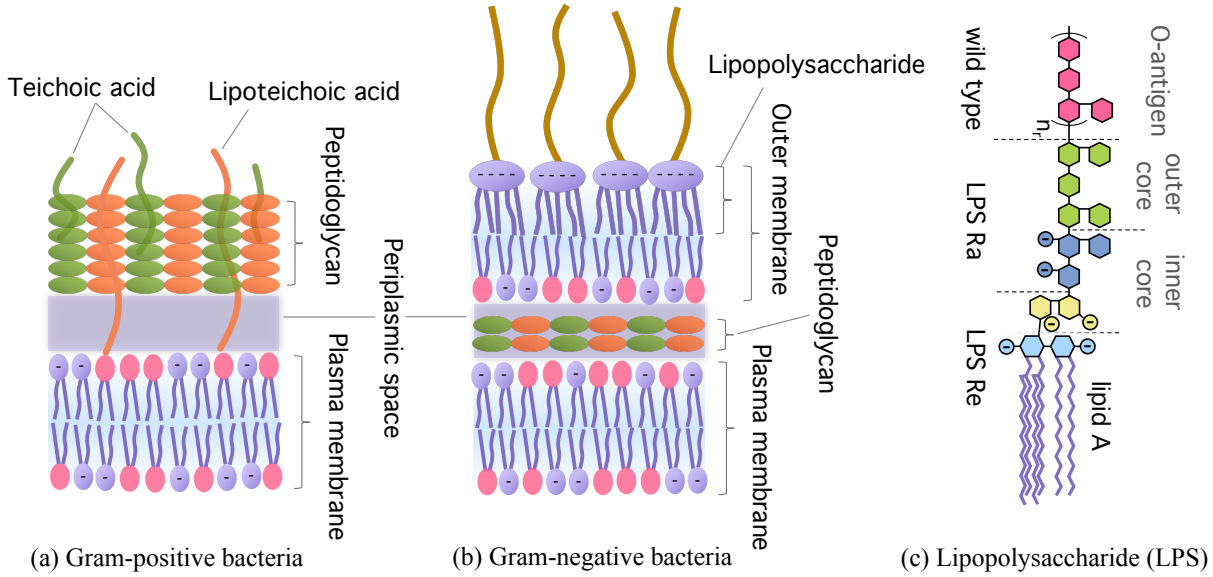

Figure 1.1: Basic structural diagram of the bacterial cell surface: (a) Gram-positive bacteria: It comprises thick layers of peptidoglycan, teichoic acid, and lipoteichoic acid on the outer layer. (b) Gram-negative bacteria: It comprises thin layers of peptidoglycan with the lipopolysaccharide attached to the outer membrane. (c) The three main structural domains of the lipopolysaccharide are Phospholipid A, Core oligosaccharides, and O antigens. Diagrams (a) and (b) were modified with permission from ref. [80]. Diagram (c) is adapted with permission from ref. [64]. (Copyright 2021 American Chemical Society.)

Mammalian cells, on the other hand, produce relatively weak binding attractions due to their uncharged surfaces. This higher binding affinity towards bacterial cells leads to rapid cell death and provides a favorable condition for host cells. Thus, we refer to this ability of AMPs to preferentially bind to microbes and destroy cells more effectively than host cells as "cell selectivity".

Despite the intriguing discovery of the special features of cell selectivity, the mechanism of action for positively charged AMPs has not been fully established. Therefore, the starting point of the research begins by understanding the interaction between cationic AMPs and anionic bacterial cell membranes. After AMPs bind to the surface of the membrane, it eventually leads to cell membrane destruction and cell death. Other than the charge-induced attraction, many other factors are involved in the binding process of the AMPs. In the following section, we reviewed the main driving forces behind the binding

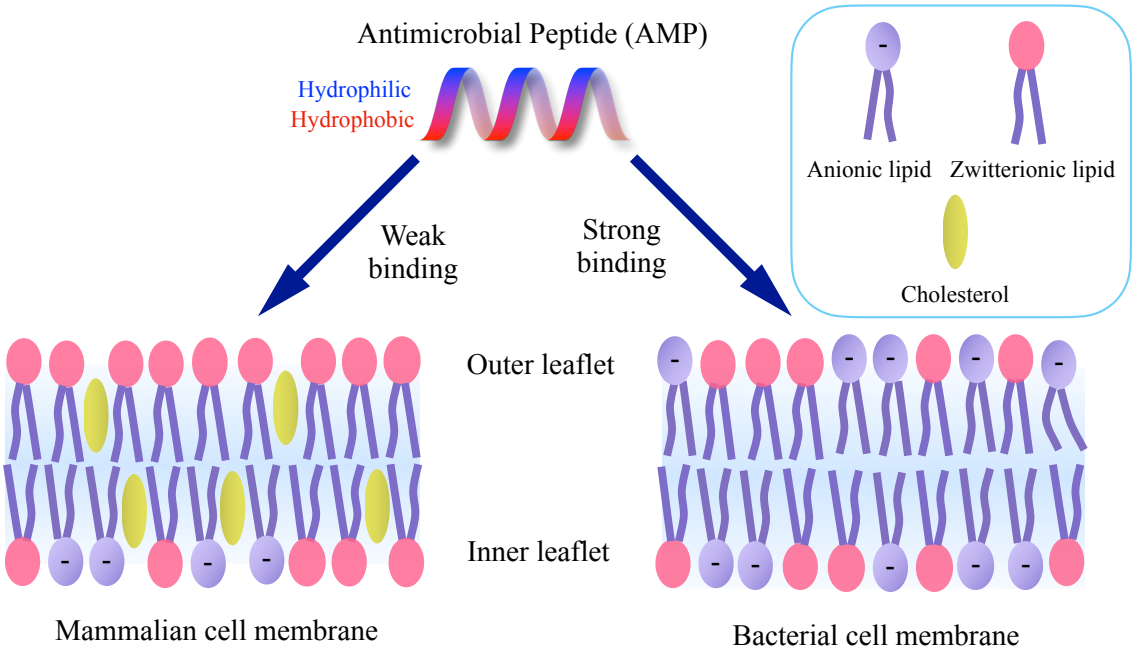

Figure 1.2: Schematic diagram of cell selectivity. Amphiphilic AMPs are colored differently to distinguish the hydrophobic and hydrophilic portions of the peptide. The hydrophobic portion of the AMP interacts with the hydrophobic region on the outer leaflet of the membrane, generating hydrophobic energy. Hydrophobic binding is observed in both mammalian cells and bacterial cells. The outer leaflet of the bacteria is composed of several anionic lipids. (e.g., phosphatidylserine (PS), cardiolipin (CL), and phosphatidylglycerol (PG) lipids). Mammalian membranes, are primarily composed of neutral lipids (e.g., phosphatidylcholine (PC)). The diagram adapted from Biochimica et Biophysica Acta (BBA) - Biomembranes, 1462, Katsumi Matsuzaki, 'Why and how are peptide–lipid interactions utilized for self-defense? Magainins and tachyplesins as archetypes', 1-10., Copyright (2022), with permission from Elsevier [55].

mechanism of the AMP. [8, 9, 99]

1.2.2 Binding mechanisms

Positively charged antimicrobial peptide (AMP) activity is initiated by interacting with negatively charged bacterial cell membranes. In particular, various mechanisms are im-

plicated in binding AMPs to cell membranes, and the most significant factors are the hydrophobic and electrostatic interactions.

Hydrophobic Interactions: Antimicrobial peptide (AMP) has amphipathic properties, and in particular; about 50% of amino acids in the primary sequence of AMPs are composed of hydrophobic residues. This allows the peptide to interact with the phospholipid bilayer. [7] The hydrophobic portion of the AMP interacts with the hydrophobic tail of the lipid cell membrane with the hydrophilic region of the AMP facing solution. [13, 78] It was found that stronger hydrophobic interactions were associated with rapid reactions and increased binding ability. However, an appropriate degree of hydrophobicity is essential for antimicrobial peptide function but needs to be taken with caution as excessive hydrophobicity is associated with toxicity and also results in loss of antimicrobial peptide specificity. [77]

Electrostatic Interactions: Electrostatic interactions are one of the most critical interactions involved in the binding process targeting microbial cells. AMP conserved the cationic feature over many organisms, enabling them to bind to other microorganisms through electrostatic interactions. Thus, AMPs attract charged phosphate groups and bind to bacterial membranes. [99] This explanation demonstrates that the initial binding process is triggered by electrostatic interactions. [27]

In particular, when an interaction occurs between a cationic AMP and Gram-negative bacteria, the interaction is initiated by replacing the divalent cations (e.g., Mg^{2+}, Ca^{2+}) from the LPS layer of the bacterial membrane. [82, 100] Moreover, Gram-positive bacteria have abundant teichoic acid polymers that provide ideal binding sites for cationic AMPs. In contrast, mammalian cells have an uncharged surface on the outer leaflets of the cell membrane, making them less attractive for a charged AMP to bind. Therefore, the fact that bacteria have more electrostatically favorable conditions indicates that AMPs have a higher selectivity for bacteria than mammalian cells.

1.2.3 Pore Forming mechanisms

When AMPs bind to cell membranes, the lipids get perturbed, and pores are created, ultimately leading to cell rupture and death. Different AMPS can form different pores. [9] The three most frequently observed models among the organisms are the Barrel-Stave model, the Carpet-like model, and the Toroidal Pore model. [78]

Barrel-Stave model: As the name suggests, when the peptide binds to the membrane, it creates a barrel-like ring to form a pore as depicted in Fig. 1.2.3 (b). In particular, the AMPs aggregate with each other, and the AMPs are inserted parallel to the bilayer to

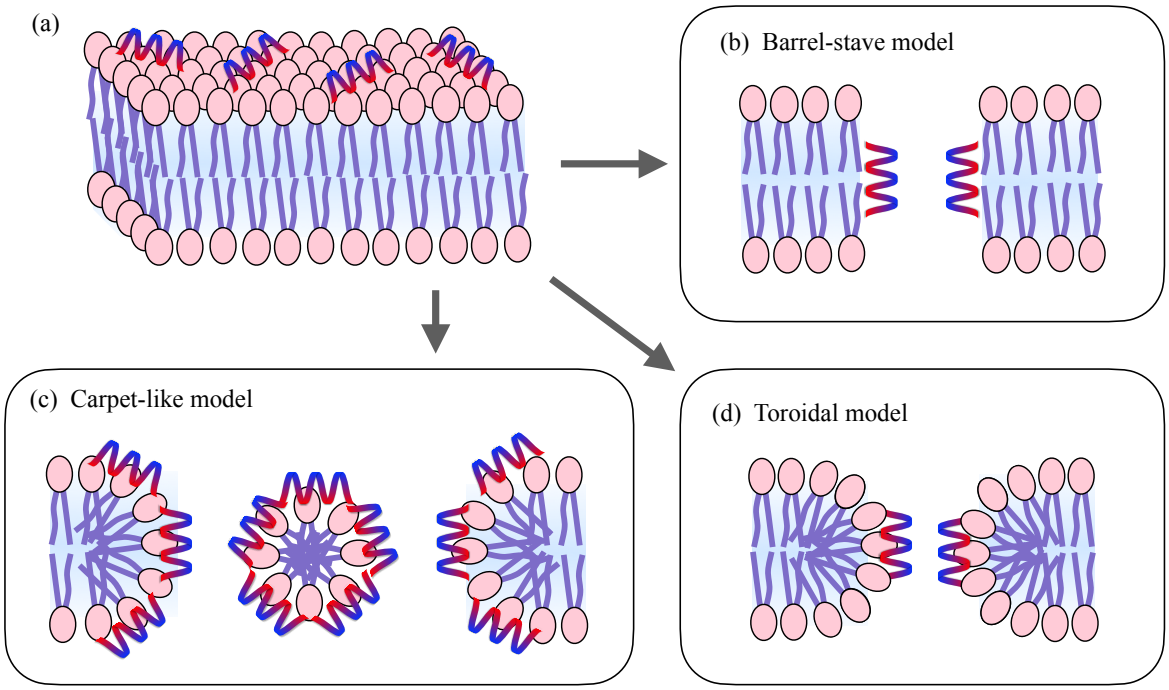

Figure 1.3: Three representative models of a pore-forming mechanism by AMPs on the cellular membrane are presented. (a) Prior to pore formation steps, the concentration of antimicrobial peptide (AMP) does not exceed the threshold $(P/L)^*$. (b) Barrel-stave model: AMPs are inserted perpendicular to the lipid bilayer and generate channels between the interior and exterior environment. (c) Carpet-like model: AMPs destroy the cell membrane in a detergent-like manner. (d) Toroidal model: AMPs are vertically inserted into the bilayer, and phospholipid bends like the ring to create pores. This diagram is adopted from the paper [102].

bind and create pores. [78] Here, the amphipathic peptide is oriented perpendicular such that the hydrophobic domain of the peptide interacts with the hydrophobic core of the lipid bilayer, and the hydrophilic region faces the aqueous channel of the pore. These peptides are arranged parallel to the phospholipid chains while remaining perpendicular to the bilayer plane. This morphology creates pores and channels simultaneously, resulting in cytoplasmic outflow. In addition, as the number of peptide units increases, the number of pores can also increase, leading to cell collapse and death. [54]

Carpet-like model: In this model, the AMPs are aligned parallel to the phospholipid

bilayer. The hydrophobic portion of the peptide aligns with the cell membrane, and the hydrophilic portion faces the solution. After the membrane is completely covered by the peptides like a carpet, pores are formed in a detergent-like manner, [65] which eventually causes the membrane to rupture. This model is illustrated in Fig. 1.2.3 (c). One example using the given mechanism is human cathelicidin LL-37. [17, 79]

Toroidal Pore model: The toroidal pore model lies somewhere between the carpet and barrel-stave pore mechanisms, also known as the wormhole model, and it is shown in Fig. 1.2.3 (d).[27] This mechanism is typically well studied using the α-helical peptides. Initially, peptides are orientated parallel to the surface of the membrane. Then once a threshold concentration of peptides has reached, the peptides vertically get embedded in the cell membrane and bend to form a ring hole of the pore. [57, 58] Similar to the previous model, it ultimately leads to cell disruption. The typical examples of the given mechanisms are commonly exhibited in magainin 2, lacticin Q, and arenicin. [42]

1.2.4 Bound peptide to lipid ratio (P/L)

When AMPs come into contact with cells, they do not immediately trigger cell rupture. Instead, it progressively binds to the surface of the membrane as the concentration of AMP gradually increases. The creation of pores on the surface membrane begins once the threshold limit of the AMP concentrations exceeds in the solution. As a result, it is crucial to determine the values of the molar ratio of bound peptides to lipids for regulating cell death. Thus, we denote (P/L) as a molar ratio of bound peptides to lipids. [43, 48]

To further illustrate this mechanism, we subdivided it into two states: the S (surface bound) state and the I (inserted) state. [44, 48] The S state refers to the state in which the (P/L) (the molar ratio of bound peptides to lipids) is smaller than the $(P/L)^*$ (a threshold value required for a membrane rupture). At this stage, helical peptides are bound to the surface and oriented parallel to the plane of the membrane, thinning the membrane, and no pores have formed yet. In the I state, (P/L) exceeds $(P/L)^*$ resulting in peptide insertion into the membrane oriented parallel to the membrane, and pores appear that promote the cell rupture and lysis. [43, 48]

1.2.5 Measurements of AMP effectiveness

There are two good indicators that we can quantitatively evaluate the effectiveness of AMP. Minimum inhibitory concentrations (MICs) and minimum hemolytic concentrations

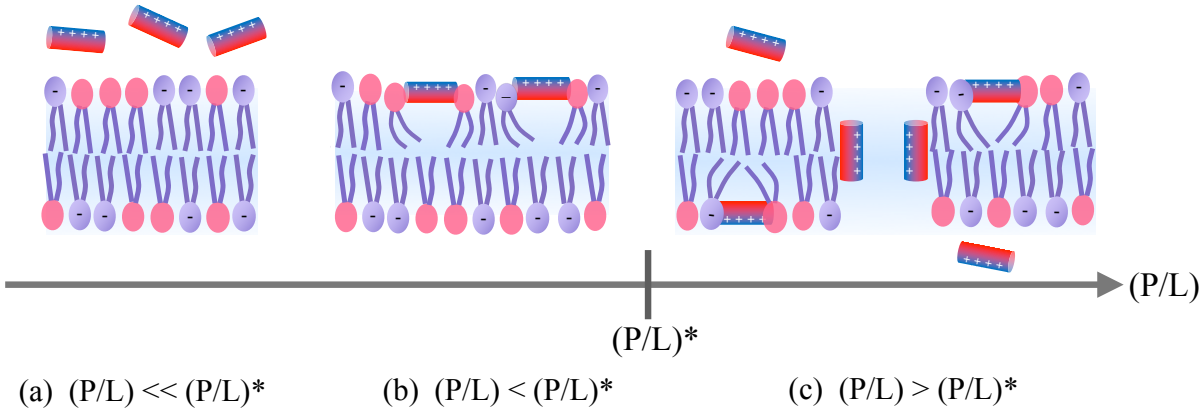

Figure 1.4: Pore formation in membranes. AMPs are represented by cylinder, with the red portion being hydrophobic and the blue portion representing the hydrophilic portion of the AMP. (a) $(P/L) << (P/L)*$ case: The molar ratio of bound peptides to lipids ((P/L)) is significantly less than the $(P/L)*$. The cell membrane morphology remains unchanged. (b) $(P/L) < (P/L)*$ case: (P/L) remains smaller than the $(P/L)*$, and peptide begins getting inserted into phospholipids, resulting in thinning effects. (c) $(P/L) > (P/L)*$ case: (P/L) exceeds the threshold value $(P/L)^*$ and pores are created. This diagram is adapted with permission from ref. [48].(Copyright 2006 American Chemical Society.)

(MHCs) are two important measurements of AMPs activity. Minimum inhibitory concentrations (MICs) refer to the lowest peptide concentration that inhibits the observable growth of microorganisms such as bacteria. [4] It is a good reference when comparing the performance of various antibacterial substances. A lower MIC indicates a better ability to inhibit bacterial growth, which is beneficial for treatment. In contrast, according to Greber et al. [32], minimal hemolytic concentrations (MHCs) were defined as the lowest peptide concentrations that cause 10% hemolysis for human red blood cells. Therefore, having a high MHC is ideal from a human perspective and poses less harm to humans.

Minimum hemolytic concentrations (MHCs) and minimum inhibitory concentrations (MICs) are the important indicators considered throughout the paper. It represents the effectiveness of AMPs in killing the host cells (MHCs) and the bacterial cells (MICs). The range of concentrations typically lies between (MIC < working concentration of AMPS < MHC). Additionally, the ratio between the two (MHC/MIC) is known as the therapeutic index and provides a good reference for the selectivity of a given AMP. In general, a high therapeutic index represents a high degree of AMP selectivity.

1.3 Physical Background

When charged objects are exposed to an ionic solution, they interact with the surrounding ions. The electrostatic double-layer theory explains this behavior and accounts for the interaction between charged objects exposed to ionic solution.

1.3.1 Electric double layer

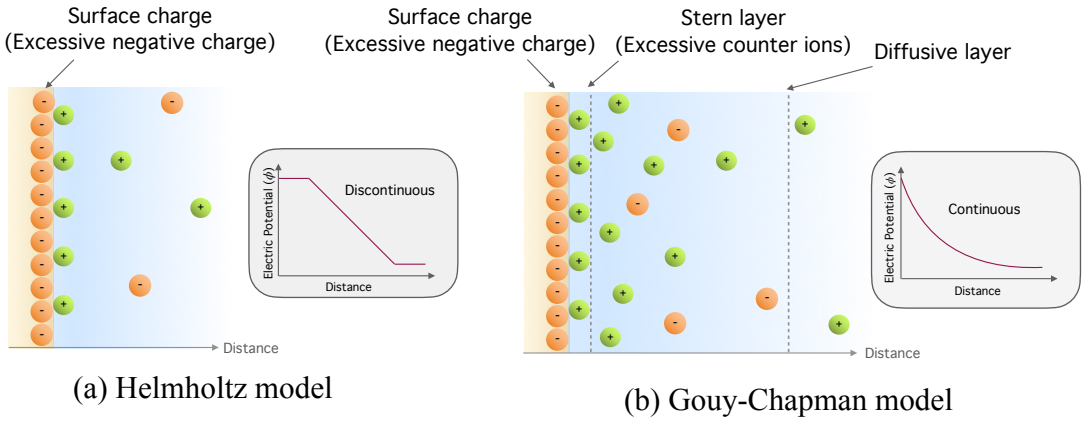

Figure 1.5: Schematic diagram of the electric double layer. The orange circle represents the negative charge, and the green circle represents the positive charge (counterions). (a) Helmholtz model: A simplified discontinuous model. (b) Gouy-Chapman model: Continuous model including the diffusive layer. The diagram is reproduce with the permission by "Wiley Materials" from ref. [1]

The membrane generates an electric field around it and draws counterions (ions with the opposite charge to that of the membrane surface) to the surface. This type of structure is referred to as an electric double layer, typically observed when a charged surface is exposed to a solution containing mobile ions. In general, the electric double layer is separated into three sections: (1) Surface charge, (2) Stern layer (3) Diffusive layer. [68] First, the surface charge represents the interface of an object where the positive or negative (often negative) ions get absorbed. The second layer refers to the stern layer, in which the counterions get attracted to the interface of the object due to electrostatic forces, and counterions get tightly bound to the surface. Finally, the diffusive layer is formed by loosely-bound ions.

The higher concentrations of counterions tend to loosely attract the free ions generating the thermal and electrical forces. [68]

This electric double layer can be solved mathematically, allowing us to derive the electrostatic free energy. The first model of the electric double layer was attributed to the Helmholtz theory. The model accounted for the counterions binding to the surface to neutralize the surface charge, just like the plate capacitor. However, the drawback to the model was that it was oversimplified, which did not capture the ion thermal fluctuation and failed to calculate the capacitance of the layer. [1] To further complement the model, Louis Georges Gouy and David Chapman came up with a better description. The Gouy-Chapman model described that the ions create a diffusive layer as ions get farther away from the surface and successfully illustrates the main properties of the double layer in the continuous model. [31, 11, 30] Furthermore, Debye-Huckle found an analytical solution in the spherical case, which allowed us to calculate the ion distribution and potential around the surface. [18]

1.3.2 Electrostatic free energy derivation

Poisson-Boltzmann Equation

Starting with the Poisson equation, we can derive the electrostatic free energy of the charged surface and the electrical potential. [40, 1] In general, the Poisson equation describes the relationship between the electrostatic potential ψ and the charge density ρ, which is written as,

$$\nabla^2\psi = \frac{\rho}{\epsilon\epsilon_0}, \tag{1.1}$$

where ϵ_0 represents the dielectric constant and ϵ permittivity. When ions are distributed in the solution, we can write the ionic concentration using the Boltzmann distribution. Let c_0 be the bulk concentration of an ion of species with charge Ze and e being the elementary charge of the single electron, and according to the Boltzmann distribution, the concentration of charged potential is written as,

$$c = c_0 \sum_i e^{-Z_i e\psi/KT}. \tag{1.2}$$

Here, $Z = \pm 1$ and therefore, Eq. 1.2 can be expanded as $c = c_0(e^{-Ze\psi/k_BT} - e^{Ze\psi/k_BT})$. This ion concentration can be applied to the local charge density, which is described as,

$$\rho = ec_0(e^{-Ze\psi/k_BT} - e^{Ze\psi/k_BT}) \tag{1.3}$$

If we recall the Poisson equation (Eq. 1.1), we can re-write it in the following form,

$$\nabla^2\psi = \frac{ec_0}{\epsilon\epsilon_0}(e^{-Ze\psi/k_BT} - e^{Ze\psi/k_BT}), \tag{1.4}$$

This equation can be further simplified with a high or low potential case. In the case of the low potential (here, the low potential strictly means $Ze|\psi|/k_BT \ll 1$), we expand the exponential, e.g.($e^x \approx 1 + x + \frac{x^2}{2!} + \cdots$) and obtain

$$\nabla^2\psi = \left(1 + \frac{Ze\psi}{k_BT} - 1 + \frac{Ze\psi}{k_BT} + \cdots\right) \approx \frac{2c_0e^2}{\epsilon\epsilon_0 k_BT}\psi. \tag{1.5}$$

This is called the linearized Poisson-Boltzmann equation and the general solution is found as

$$\psi = C_1e^{-\kappa x} + C_2e^{\kappa x}. \tag{1.6}$$

Here, C_1 and C_2 are constants that can be determined after applying the boundary conditions of a surface potential. Here, κ is defined as,

$$\kappa = \sqrt{\frac{2c_0e^2}{\epsilon\epsilon_0 k_BT}}, \tag{1.7}$$

which is also known as the Debye length. The charged potential surface shows how much the ions in the solution have been screened. To solve the above general solution (Eq. 1.6), we need to apply the boundary condition. The conditions states that when the potential is at the surface, the potential equals the surface potential $\psi(x = 0) = \psi_0$, and when the potential is far from the surface potential disappears, $\psi(x = \infty) = 0$. This leads to the $C_2 = 0$ and $C_1 = \psi_0$, which the general solutions reduced down to $\psi = \psi_0e^{-\kappa x}$ in the low potential case.

To find the electrostatic free energy of a charged object, we return to the original Poisson equation and start from the Eq. 1.4. For simplification purposes in our calculation, we want to reduce the dimensions of the potential by substituting $y = \frac{Ze\psi}{k_BT}$. After the substitution and expansion of the Laplace operator, the equation is reduced down to,

$$\frac{d^2y}{dx^2} = \frac{c_0e^2}{\epsilon\epsilon_0 k_BT}(e^y - e^{-y}) = \frac{2c_0e^2}{\epsilon\epsilon_0 k_BT}\frac{(e^y - e^{-y})}{2} = \kappa^2 \sinh y \tag{1.8}$$

To solve the following differential equation, we multiply $2\frac{dy}{dx}$ on both side and take the

integral as follows:

$$2\left(\frac{dy}{dx}\right)\frac{d^2y}{dx^2} = 2\left(\frac{dy}{dx}\right)\kappa^2 \sinh y \tag{1.9}$$

$$2\frac{d}{dx}\left(\frac{dy}{dx}\right)^2 = 2\left(\frac{dy}{dx}\right)\kappa^2 \sinh y \tag{1.10}$$

$$\int \frac{d}{dx}\left(\frac{dy}{dx}\right)^2 dx = 2\kappa^2 \int \left(\frac{dy}{dx}\right)\sinh y\, dx \tag{1.11}$$

$$\left(\frac{dy}{dx}\right)^2 = 2\kappa^2 \int \sinh y\, dy = 2\kappa^2 \cosh y + C_1 \tag{1.12}$$

C_1 here indicates the integration constant and determined by the factors of boundary conditions, which is found to be $C_1 = -2\kappa^2$; this leads to,

$$\left(\frac{dy}{dx}\right)^2 = 2\kappa^2(\cosh y - 1) \Rightarrow \left(\frac{dy}{dx}\right) = -\kappa\sqrt{2(\cosh y - 1)} \tag{1.13}$$

After applying the trigonometry rules, it can be written as,

$$\left(\frac{dy}{dx}\right) = -2\kappa(\sinh \frac{y}{2}) \tag{1.14}$$

The following Eq. 1.14 comes in handy later for deriving the charge density. Next, we can go on and find the total charge in the electric double layer.

Grahame equation

Grahame equation has been derived from the Gouy–Chapman theory to further explain the relationship between the charge density σ and electrically neutral potential ψ_0. [1] In general, the total charge density, which is the sum of all the charge densities in the area, is written as,

$$\sigma = -\int_0^\infty \rho\, dx \tag{1.15}$$

Utilizing the original Poisson equation and by the fact that the potential converges to the zero at large distance, the Eq.1.15 is written as,

$$\sigma = -\int_0^\infty \epsilon\epsilon_0 \left(\frac{d\psi}{dx}\right)^2 dx = \epsilon\epsilon_0 \frac{d\psi}{dx}\Big|_{x=0} \tag{1.16}$$

If we recall Eq.1.14, we can revert to the potential term which $\frac{dy}{dx} = \frac{e}{k_B T}\frac{d\psi}{dx}$ then,

$$\frac{d\psi}{dx} = \frac{k_B T}{e}\frac{dy}{dx} = -\frac{k_B T}{e} 2\kappa \sinh\left(\frac{e\psi}{2k_B T}\right) \tag{1.17}$$

After the rearrangement in the equation, this finally returns our desired form of the Grahame equation:

$$\sigma = \sqrt{8c_0\epsilon\epsilon_0 k_B T}\sinh\left(\frac{e\psi}{2k_B T}\right) \tag{1.18}$$

Or we can rearrange eq. 1.18 in terms of the surface potential:

$$\psi_0 = \frac{2k_B T}{e}\sinh^{-1}\left(\sigma\sqrt{\frac{1}{8c_0\epsilon\epsilon_0 k_B T}}\right) \tag{1.19}$$

Potential and electrostatic free energy

Now that the surface potential is found, we can utilize Eq. 1.19 to obtain the Gibbs free energy. The differential equation of Helmholtz free energy of the charged systems is written as:

$$dF = -S\,dT + \Pi\,dA + \psi\,dq \tag{1.20}$$

Here, we assume that the system is in the constant temperature (T) and a constant area (A). This condition makes the differential term dT and dA disappear; it reduces to:

$$dF = \psi\,dq \tag{1.21}$$

This represents the contribution of the electrostatic free energy per mole of lipids. After the integration,

$$F_{el,L} = \int_{q=0}^{e} \psi_0\,dq = A_L \int_{\sigma=0}^{\sigma'} \psi_0\,d\sigma \tag{1.22}$$

where A_L represents membrane as a two-dimension system under conditions of the constant area of A_L. Here, using Eq. 1.19 we find

$$F_{el,L} = A_L \int_{\sigma=0}^{\sigma'} \frac{2k_BT}{e} \sinh^{-1}\left(\sigma\sqrt{\frac{1}{8c_0\epsilon\epsilon_0 k_BT}}\right) d\sigma \tag{1.23}$$

$$= A_L \left(\sigma\psi_0 - 4\epsilon\epsilon_0 \left(\frac{k_BT}{e}\right)^2 \kappa \left[\cosh\left(\frac{e\psi_0}{2k_BT}\right) - 1\right]\right) \tag{1.24}$$

This expression is the electrostatic contribution to the free energy dependent on the area per lipids and the ionic strength. [40, 1]

1.4 Thesis overview

The remainder of the thesis is organized as follows. In chapter 2, we presented a biophysical model of peptide activity and selectivity in homogeneous and heterogeneous mixtures of bacteria and host cells. The model clarified how the presence of host cells and peptide trapping influence peptide selectivity and how competitive selectivity differs from non-competitive selectivity. In chapter 3, we introduced a model of interactions between AMPs and the bacterial membrane in electrolyte solutions containing salt ions. In this work, we discussed how binding affinity changes with monovalent cation variations. In chapter 4, we explored the theoretical model of the interactions between LPS and AMPs. Through the analysis, we identify the relative significance of various factors such as brush-peptide interactions, the electrostatic interactions between peptides and LPS headgroups, and brush lengths. Finally, chapter 5 concludes with a brief overview of the previous chapters, including further discussions on future work for improvement.

Chapter 2

Modeling Selectivity of Antimicrobial Peptides: Membrane Selectivity Versus Cell Selectivity

This chapter will be submitted to the journal in the following form.

Modeling selectivity of antimicrobial peptides: membrane selectivity versus cell selectivity

Suemin Lee[1], Bethany R. Schefter[1], Sattar Taheri-Araghi[2], and Bae-Yeun Ha[1]
[1] *Department of Physics and Astronomy, University of Waterloo, Ontario N2L 3G1, Canada*
[2] *Department of Physics, University of California San Diego, La Jolla, CA 92093, USA*

Antimicrobial peptides (AMPs), naturally-occurring peptide antibiotics, are known to attack bacteria selectively over the host cells. They often act through physical mechanisms (e.g., forming pores in membranes) and thus are advantageous over conventional antibiotics that reply on specific (chirality-dependent) interactions. This has spurred much effort in utilizing optimized (more selective) AMPs as new peptide antibiotics. The cell (bacteria versus host cells) selectivity of these peptides depends on various factors such as their binding affinity for cell membranes, peptide trapping in cells, peptide coverages on cell membranes required for membrane rupture, and cell densities. Here, we present a physical model of peptide selectivity, which shows this dependence quantitatively and thus assists with the correct interpretation of selectivity measurements. The model suggests a rather nontrivial dependence of the selectivity on the presence of host cells and peptide trapping; these factors or effects can enhance or reduce the selectivity depending on how cell densities are chosen. It also clarifies how the cell selectivity of AMPs differs from their membrane selectivity.

I. INTRODUCTION

Antimicrobial peptides (AMPs) are microbe-killing molecules deployed in the host defense of living organisms (e.g., animals, plants, and human).[1,2] They are relatively short, typically consisting of 20-50 amino acids. In the bulk, they often resemble random coils but in a lipidic environment, they assume compact, amphiphilic structures (e.g., α helices). AMPs are mostly cationic and thus utilize the unique 'design feature' of microbial membranes[1], enriched with anionic lipids[1–3]. They preferentially bind to and rupture microbial membranes over host cell membranes, which are composed of neutral lipids. Once they gain entry into the cytoplasm, they can target key intracellular components (e.g., DNA and proteins), leading to intra-cellular killing of microbes[1,2].

There has been much interest in developing enhanced AMPs as potent peptide antibiotics, especially for fighting drug-resistant bacteria. Membrane-perturbing AMPs are advantageous. They act via physical mechanisms such as pore formation in membranes, which bacteria cannot easily avoid. Developing bacterial resistance against these peptides would involve a 'costly' solution of membrane redesigning[1], even though pathogens can, in principle, evolve antimicrobial resistance[4,5]. In addition to rupturing bacterial membranes, they act as metabolic inhibitors[1,2] and/or immunomodulators[6]. The therapeutic potential of these multitasking molecules deserves much consideration[7].

Cationic AMPs can single out bacteria through their stronger binding affinity for the bacterial membranes. The resulting selectivity can be quantified by the ratio of two concentrations: the minimum hemolytic concentration (MHC) and the minimum inhibitory concentration (MIC). The larger the ratio MHC/MIC is for a given peptide, the more selective the peptide is. In a sizeable range of peptide concentration ($\sim \mu$M) between MIC and MHC, the peptide is active against bacteria while leaving the host cells unharmed.

The selectivity of AMPs is influenced by a number of factors such as their binding affinity for cell membranes, peptide trapping in (dead) cells[8–10], a peptide coverage on cell membranes required for membrane rupture[11–13], and cell densities **refs**. Let P/L denote the molar ratio of bound peptides to lipids. At the MIC or MHC, P/L reaches a threshold value, P/L^*. The value of P/L^* depends on the type of peptide and lipid[11–13] and is typically larger for membranes containing lipids with smaller headgroups such as phosphatidylethanolamine (PE) as in bacterial membranes. At P/L^*, each cell consumes a certain number of peptides with some of the peptides trapped in the cell[8–10]. This implies that the MIC or the MHC increases with increasing cell density; the ratio MHC/MIC is cell-density dependent. The cell-density dependence is often referred to as an *inoculum* effect[8–10] and is known to enhance population survivability[10].

A point related to the cell density dependence of peptide selectivity is that peptide selectivity also depends on the way it is measured[14–16]. For instance, it can be obtained by combining MIC and MHC measured separately from bacteria-only and host-cell-only solutions, respectively; in this work, the resulting selectivity is referred to as "non-competitive" selectivity. More realistically, it can be measured from a mixture of both types of cells: competitive selectivity. In this case, the presence of host cells raises the MIC and influences the ratio MHC/MIC.[9,14,17] These two approaches generally lead to different levels of selectivity. How the selectivity should be measured has to reflect the biological setting of infected sites (e.g., the degree of infection).

According to what is discussed above, peptide selectivity not only reflects peptide's intrinsic properties such as peptide charge and hydrophobicity, but it also depends on external parameters such as cell densities. Does this mean that the selectivity should be measured for a wide range of cell selectivities and various combinations of host cell and bacterial cell densities? Recent modeling efforts,

however, suggest that these two aspects (intrinsic and extrinsic) are well separated[14,16]. With an appropriate model, one can figure out the selectivity with varying cell densities, once it is known at a low cell-density limit. Furthermore, in the past, model lipid membranes, mimicking cell membranes, were often used for AMP experiments[11–13,18]. How does the resulting selectivity differ from the one measured for cells? Peptide trapping is one of the determining factors in the latter but is insignificant in the former.

Recently, we have examined theoretically peptide selectivity under various conditions and clarified the effects of peptide trapping on the selectivity, MHC/MIC.[14] This effort is relevant in the presence of an excess amount of host cells or for a homogeneous solution of either bacteria or host cells. Here, we extend this effort and map out various scenarios regarding the activity and selectivity of AMPs, which can be used to interpret selectivity measurements or to assist with our endeavor in finding optimized peptides (see Ref.[16] for earlier effort).

The results reported in this work, which are relevant for melittin-like peptides, suggest a rather nontrivial dependence of the selectivity on the presence of host cells, peptide trapping, and cell density. These effects or factors can enhance or reduce the selectivity depending on how the densities of host cells and bacteria are chosen. In most cases, they work in favor of the host cells, enhancing the selectivity. The presence of an excess amount of host cells (5×10^9 cells/mL) as in whole blood, however, can raise the MIC more than 10-fold, proportionally with the density of bacterial cells. The resulting MIC still falls in a low-μM range as long as the bacterial cell density is somewhat less than 5×10^7 cells/mL.

Let $C_{\rm B}$ and $C_{\rm H}$ be the density of bacteria and host cells, respectively, and $N_{\rm p}$ the number of peptides trapped in a cell. As we raise $C_{\rm B}$ and $C_{\rm H}$ coherently so that $C_{\rm B} = C_{\rm H}$, the selectivity also increases in both non-competitive and competitive cases. In the presence of an excess amount of host cells, the selectivity decreases with increasing $C_{\rm B}$ in both cases, more so for larger $N_{\rm p}$. In contrast, when $C_{\rm B} = 5 \times 10^4$ cells/mL is chosen, it increases with increasing $C_{\rm H}$. Compared to the competitive one, the non-competitive selectivity can be overestimated by more than 2 orders of magnitude, depending on how $C_{\rm B}$ and $C_{\rm H}$ are chosen.

We also clarify how the cell selectivity of AMPs differs from their membrane selectivity. While the selectivity based on model membranes is typically larger than the corresponding cell selectivity, the difference between competitive and non-competitive selectivity is generally larger in the latter. Except for some differences, membrane selectivity and cell selectivity of AMPs are qualitatively similar to each other. The former can provide useful information about the latter and may assist with our strategy for optimizing peptide selectivity. It is however important to use properly-chosen membrane parameters such as the surface area of the membrane as well as biologically-relevant membrane densities. Finally, we test and justify the approximate equations describing peptide activity and selectivity we have recently introduced.[14]

In this work, we will focus our effort on presenting a selectivity model in a pedagogical but yet systematic manner. A detailed account of earlier experiments will be skipped, since it can be found in a number of recent papers (see for instance, Refs.[8–10]). In our consideration, the only difference between model membranes and cells comes from peptide trapping in the latter. We will often use membrane densities and cell densities interchangeably; also MICs and MHCs refer to peptide concentration beyond which membranes are ruptured, whether they are model membranes or cell membranes.

This paper is organized as follows: In Sec. II, we present a simple picture of how the activity and selectivity of AMPs vary with cell densities for a non-competitive and competitive medium. Sec. III introduces a Langmuir model of peptide binding. Sec. IV summaries the results for peptide activity and selectivity as a function of cell density; the effect of peptide trapping is highlighted.

II. CELL AND MEMBRANE SELECTIVITY OF ANTIMICROBIAL PEPTIDES

In this section, we present a pedagogical approach to peptide activity and selectivity, which shows how peptide selectivity depends on cell densities. We start with a homogeneous system of either bacterial or host cells, referred to as a noncompetitive case, and turn to a mixture of both types of cells, referred to as a competitive case.

Before proceeding further, we introduce a few key parameters relevant for peptide activity and selectivity. A key "extrinsic" parameter is the concentration of peptides, denoted as $C_{\rm p}$; so is the cell density, $C_{\rm cell}$[8,10,15,16]. The surface area of each cell, $A_{\rm cell}$, matters[15]: doubling $A_{\rm cell}$ for given $C_{\rm cell}$ is equivalent to doubling $C_{\rm cell}$ for given $A_{\rm cell}$. The peptide selectivity arises primarily from different binding energies for bacterial and host-cell membranes, denoted as $w_{\rm B}$ and $w_{\rm H}$, respectively[1,14–16]. Membrane rupture occurs in an all-or-none $C_{\rm cell}$-dependent manner[11,12,19]. Let P/L be the molar ratio of membrane-bound peptides to lipids. At a certain value of $C_{\rm p}$, i.e., $C_{\rm p}^*$, P/L reaches a threshold value required for membrane rupture, $(P/L)^*$[11–13,18]; $C_{\rm p}^*$ is either MIC or MHC. Finally, $N_{\rm p}$ denotes the number of trapped peptides per cell. This needs to be taken with caution. Below $C_{\rm p}^*$, we assume that $N_{\rm p} = 0$. In this case, penetration of peptides into a cell is expected to be a rare event, since it involves overcoming a large free energy barrier for crossing an otherwise intact cell membrane. At $C_{\rm p}^*$, half of the cell membranes are ruptured. Thus, $N_{\rm p}$ can be interpreted as the number of peptides trapped in each dead cell. Alternatively, it can be considered as the "average" number of peptides trapped per cell at $C_{\rm p}^*$: $N_{\rm p}^*$. Here, we employ this definition of $N_{\rm p}$, which is half of the number of trapped peptides in a dead cell. Beyond $C_{\rm p}^*$, $N_{\rm p}$

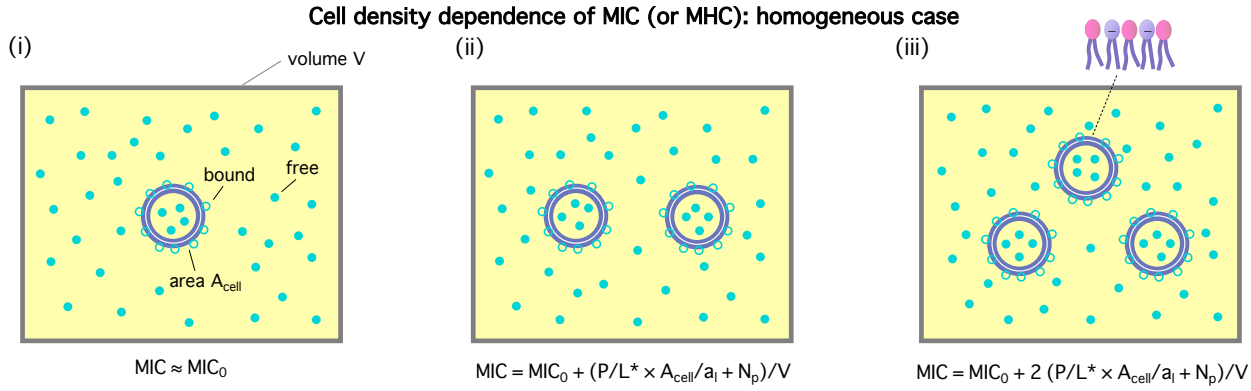

FIG. 1. Cell-density dependence of $C_{\rm p}^*$, i.e., either MIC or MHC: homogeneous or noncompetitive case. Cells are represented by two concentric circles and peptides by filled (free) or unfilled circles (bound). As the peptide concentration $C_{\rm p}$ increase, their surface coverage P/L (molar ratio of peptides to lipids) also increases and eventually reaches a thereshold P/L^* at $C_{\rm p}^*$. Even in the single cell limit shown in (i), $C_{\rm p}^* > 0$, because of the entropy of peptides, which favors unbinding. Imagine introducing a second cell in (i), converting the system into the one in (ii). The number of peptides the first cell consumed is equal to $(P/L^* \times A_{\rm cell}/a_l + N_{\rm p})$, where a_l is the area of each lipid. In order to remain at P/L^*, an extra number of peptides should be supplied. The required number of peptides is equal to this number. This will raise $C_{\rm p}^*$ by $(P/L^* \times A_{\rm cell}/a_l + N_{\rm p})/V$, where V is the volume of the system: $C_{\rm p}^*(2\text{ cells}) = C_{\rm p}^*(1\text{ cell}) + (P/L^* \times A_{\rm cell}/a_l + N_{\rm p})/V$. The progression from (i)-(iii) shows that $C_{\rm p}^* = C_{\rm p}^*(1\text{ cell}) + (N_{\rm cell} - 1) \times (P/L^* \times A_{\rm cell}/a_l + N_{\rm p})/V \approx C_{\rm p}^*(1\text{ cell}) + (P/L^* \times A_{\rm cell}/a_l + N_{\rm p}) \times C_{\rm cell}$. When applied to bacteria, this equation become $\mathrm{MIC}(C_{\rm cell}) = \mathrm{MIC}_0 + (P/L^* \times A_{\rm cell}/a_l + N_{\rm p})\, C_{\rm cell}$, where MIC_0 is MIC in the low-cell density limit: $C_{\rm cell} \to 0$. The slope of this relation, $(P/L^* \times A_{\rm cell}/a_l + N_{\rm p})$, is the total amount of peptides consumed per cell at $P/L = P/L^*$; the 'y'-axis intercept, $(\mathrm{MIC})_0$, is set by the interaction of peptides with membranes among others. It is worth noting that MIC_0 is sensitive to the peptide parameters (e.g., peptide charge and hydrophobicity) but $(P/L^* \times A_{\rm cell}/a_l + N_{\rm p})$ is not. This suggests that MICs (MHCs as well) is less sensitive to peptide parameters at high cell densities; so is the ratio MHC/MIC or peptide selectivity. Figure adapted with permission from Ref.[15]. Copyright 2015 American Chemical Society; Reproduced with modifications from Ref.[16] with permission from the Royal Society of Chemistry.

can be larger than $N_{\rm p}^*$. But we ignore the possible weak dependence of $N_{\rm p}$ on $C_{\rm p}$ (see subsec. II B for further discussion). As a result, for $C_{\rm p} \geq C_{\rm p}^*$, we use $N_{\rm p}$ and $N_{\rm p}^*$ interchangeably.

A. Homogeneous case

Fig. 1 illustrates how $C_{\rm p}^*$ depends on cell density $C_{\rm cell}$ in a homogeneous or noncompetitive case, consisting of one cell type (e.g., bacteria). Here, two concentric circles represent cells (membrane bilayers enclosing cells), whereas small circles stand for peptides; if filled ones are free or trapped, unfilled ones are membrane-bound. The fraction of bound peptides is controlled by the balance between entropy and energy. At a low peptide concentration, peptides are mostly free, because of a large entropic penalty for binding; even at a single-cell limit (Fig. 1(i)), a certain amount of peptides is needed in order for some fraction of them to decorate the cell surface. As the peptide concentration $C_{\rm p}$ increases, the balance is swayed toward energy, which favors binding. As a result, the surface coverage of peptides P/L (molar ratio of bound peptides to lipids) also increases. Eventually, $C_{\rm p}$ reaches $C_{\rm p}^*$ (either MIC or MHC), at which $P/L = P/L^*$. Even in the single cell limit shown in (i), $C_{\rm p}^* > 0$.

As the cell density increases, different cells compete for peptides. Even though the binding is driven by energy, this competition is entropic in origin and does not involve cell-cell interactions. This is responsible for the cell-density dependence of $C_{\rm p}^*$. It can be worked out progressively as shown in Fig. 1. Now imagine introducing a second cell in Fig. 1(i), converting the system into the one in (ii). Because of the presence of the first cell, there will be less peptides for the second one: at $C_{\rm p} = C_{\rm p}^*$, the number of peptides the first cell consumed is equal to $\left[(P/L)^* \times A_{\rm cell}/a_l + N_{\rm p}\right]$, where a_l is the area of each lipid and $A_{\rm cell}$ the surface area of each cell. The presence of a second cell in (ii) is equivalent to removing $\left[(P/L)^* \times A_{\rm cell}/a_l + N_{\rm p}\right]$ in (i); (i) is at $C_{\rm p}^*$. In order to remain at P/L^*, an extra number of peptides should be supplied. The required number of peptides is equal to $\left[(P/L)^* \times A_{\rm cell}/a_l + N_{\rm p}\right]$. This will raise $C_{\rm p}^*$ by $\left[(P/L)^* \times A_{\rm cell}/a_l + N_{\rm p}\right]/V$, where V is the volume of the system:

$$C_{\rm p}^*(2\text{ cells}) = C_{\rm p}^*(1\text{ cell}) + \left[\left(\frac{P}{L}\right)^* \frac{A_{\rm cell}}{a_l} + N_{\rm p}\right] \frac{1}{V}. \quad (1)$$

Here, $C_{\rm p}^*(1\text{ cell})$ is either MIC or MHC in the single-cell or low-cell-density limit.

The progression from (i)-(iii) shows how this analysis

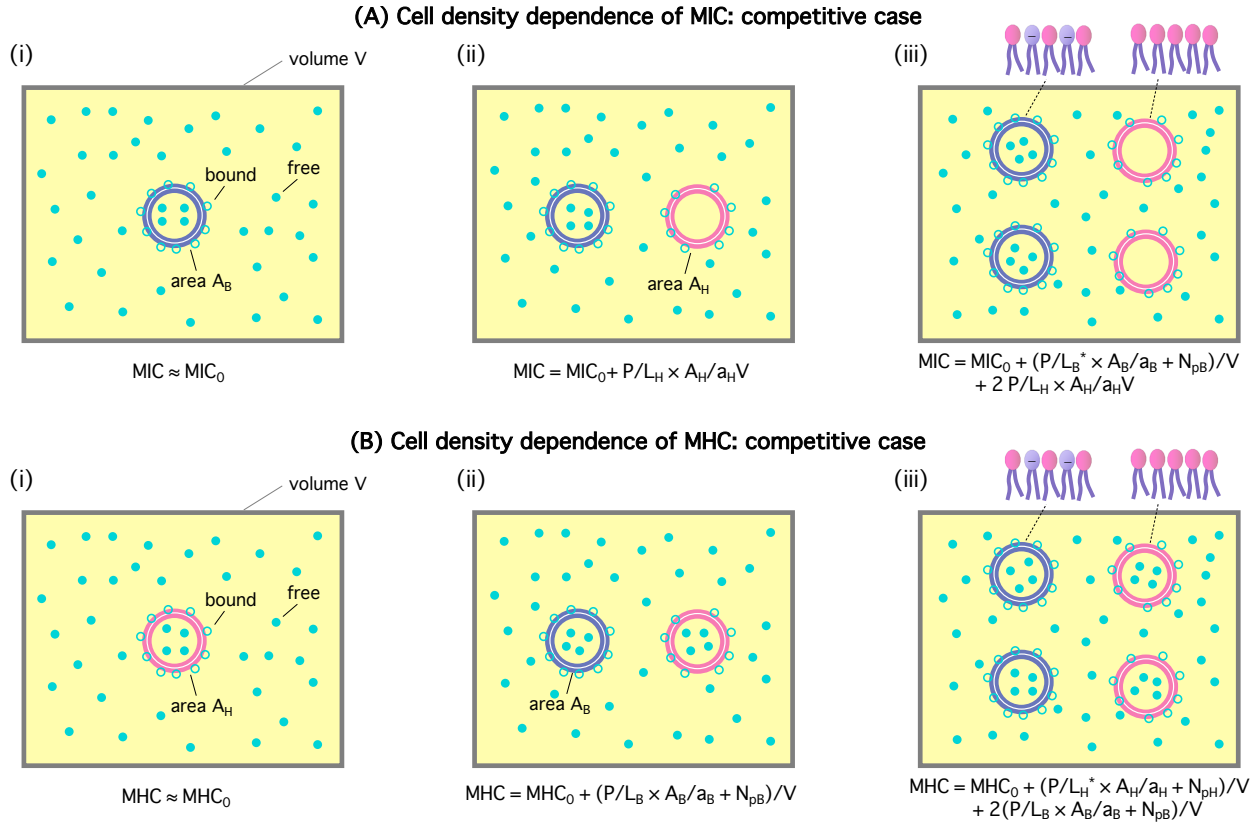

FIG. 2. Cell-density dependence of MIC (A) and MHC (B): competitive case. Cells are represented by two concentric circles and peptides by filled (free or trapped) or unfilled circles (membrane-bound); if the blue circles represent bacterial cells, the pink ones stand for host cells. Let $A_{\rm cell} = A_{\rm B}$ or $A_{\rm H}$ be the bacterial or host cell surface area, respectively; $a_{\rm B}$ and $a_{\rm H}$ the lipid headgroup area of the bacterial or host-cell membranes, respectively; $N_{\rm pB}$ and $N_{\rm pH}$ the number of trapped peptides in each bacterial and host cell, respectively; $(P/L)_{\rm B}$ and $(P/L)_{\rm H}$ are the molar ratio of bound peptides to lipids on the bacterial and host-cell membranes, respectively. (A) The progression from (i)-(iii) suggests that $\mathrm{MIC}(C_{\rm cell}) = (\mathrm{MIC})_0 + [A_{\rm B}/a_{\rm B} \times (P/L)^*_{\rm B} + N_{\rm pB}]\, C_{\rm B} + A_{\rm H}/a_{\rm H} \times (P/L)_{\rm H} C_{\rm H}$. (B) Using a similar line of reasoning, we arrive at $\mathrm{MHC}(C_{\rm cell}) = (\mathrm{MHC})_0 + [A_{\rm H}/a_{\rm H} \times (P/L)^*_{\rm H} + N_{\rm pH}]\, C_{\rm H} + [A_{\rm B}/a_{\rm B} \times (P/L)_{\rm B} + N_{\rm pB}]\, C_{\rm B}$. If $C_{\rm H} \gg C_{\rm B}$, these equations can be simplified as $\mathrm{MIC}(C_{\rm cell}) \approx (\mathrm{MIC})_0 + A_{\rm H}/a_{\rm B} \times (P/L)_{\rm H} C_{\rm H}$ and $\mathrm{MHC}(C_{\rm cell}) \approx (\mathrm{MHC})_0 + [A_{\rm H}/a_{\rm H} \times (P/L)^*_{\rm H} + N_{\rm pH}]\, C_{\rm H}$. In this case, the ratio MHC/MIC becomes independent of $C_{\rm B}$, as $C_{\rm H} \to \infty$ (while $C_{\rm B}$ is held fixed). Imagine combining two data sets of data: one set for bacteria only and one set for host cells only. If $C_{\rm H} \gg C_{\rm B}$, MHC/MIC $\to \infty$ as $C_{\rm H} \to \infty$. This limiting behavior in the homogeneous case is exactly opposite to the one obtained for the corresponding competitive case. It explains how the selectivity can be excessively overestimated, if homogenous solutions are used; it is more so if model membranes are used, since peptide trapping tends to increase the selectivity in the heterogeneous case, but not in the corresponding homogeneous case. Figure adapted with permission from Ref.[15]. Copyright 2015 American Chemical Society; Reproduced with modifications from Ref.[16] with permission from the Royal Society of Chemistry.

can be extended to the $N_{\rm cell}$-cell case:

$$C_{\rm p}^* = C_{\rm p}^*(1\text{ cell}) + \left[\left(\frac{P}{L}\right)^* \frac{A_{\rm cell}}{a_l} + N_{\rm p}\right] \frac{(N_{\rm cell}-1)}{V}$$
$$\approx C_{\rm p}^*(1\text{ cell}) + \left[\left(\frac{P}{L}\right)^* \frac{A_{\rm cell}}{a_l} + N_{\rm p}\right] C_{\rm cell}, \qquad (2)$$

where the second equality holds if $N_{\rm cell} \gg 1$, as is often the case. This equation can be applied to a homogeneous system of either bacteria or host cells. To distinguish between the two cell types, the subscript 'B' and 'H' will be used in place of the subscript 'cell'. For instance, $C_{\rm B}$ is the bacterial cell density; $A_{\rm B}$ is the bacterial cell surface area; $a_{\rm B}$ and $a_{\rm H}$ are the lipid headgroup area of bacterial and host-cell membranes, respectively; similarly, we can interpret $w_{\rm B}$, $w_{\rm H}$, $N_{\rm pB}$, $N_{\rm pH}$, $(P/L)^*_{\rm B}$, and $(P/L)^*_{\rm H}$

Eq. 2 becomes

$$\mathrm{MIC}(C_\mathrm{B}) = \mathrm{MIC}_0 + \left[\left(\frac{P}{L}\right)^*_\mathrm{B}\frac{A_\mathrm{B}}{a_\mathrm{B}} + N_\mathrm{pB}\right]C_\mathrm{B} = \mathrm{MIC}_0 + \left[\frac{\mathrm{MIC}_0 v_\mathrm{p}}{\left(\mathrm{MIC}_0 v_\mathrm{p} + e^{w_\mathrm{B}/k_\mathrm{B}T}\right)}\frac{A_\mathrm{B}}{A_\mathrm{p}} + N_\mathrm{pB}\right]C_\mathrm{B} \tag{3a}$$

$$\mathrm{MHC}(C_\mathrm{H}) = \mathrm{MHC}_0 + \left[\left(\frac{P}{L}\right)^*_\mathrm{H}\frac{A_\mathrm{H}}{a_\mathrm{H}} + N_\mathrm{pH}\right]C_\mathrm{H} = \mathrm{MHC}_0 + \left[\frac{\mathrm{MHC}_0 v_\mathrm{p}}{\left(\mathrm{MHC}_0 v_\mathrm{p} + e^{w_\mathrm{H}/k_\mathrm{B}T}\right)}\frac{A_\mathrm{H}}{A_\mathrm{p}} + N_\mathrm{pH}\right]C_\mathrm{H}. \tag{3b}$$

Here MIC_0 and MHC_0 are, respectively, the MIC and MHC in the low-cell density limit: $C_\mathrm{p}(C_\mathrm{cell} \to 0) \approx C^*_\mathrm{p}(1\text{ cell})$. In the second equality, we used an equation (Eq. 15) obtained in Sec. III to eliminate P/L^* in favor of MIC_0 or MHC_0, which are experimentally more accessible parameters[8–10].

Eq. 3 can be viewed as a function of cell density. Both MIC and MHC increase linearly with the cell density. The slope of the relation in Eq. 3, $[(P/L)^* A_\mathrm{cell}/a_l + N_\mathrm{p}]$, is the total number of peptides consumed per cell at $P/L = (P/L)^*$; the 'y'-axis intercept, either MIC_0 or MHC_0, is set by the interaction of peptides with membranes among others (see Sec. III). It is worth noting that the y-intercept is sensitive to the peptide parameters (e.g., peptide charge and hydrophobicity) but the slope is not as sensitive (recall that the slope is just the number of peptides consumed per cell at C^*_p). The value of P/L^* reflects membrane curvature (peptide parameters as well). It is larger for PE (phosphatidylethanolamine)-containing (e.g., bacterial) membranes, which tend to develop a negative curvature. This, however, does not change P/L^* by an order of magnitude. For the peptide melittin, for instance, $(P/L)^*_\mathrm{B} \approx 0.02$ and $(P/L)^*_\mathrm{H} \approx 0.01$[11–13].

Because of the cell-density dependence, MICs or MHCs are less sensitive to peptide parameters at high cell densities[15,16]; so is the ratio MHC/MIC or peptide selectivity. Imagine combining MHC and MIC values obtained separately for homogeneous solutions. The ratio MHC/MIC increases with C_H: the larger C_H is, the larger the selectivity is. As evidenced below, this does not correctly represent the selectivity in a biological-relevant medium (e.g., a mixture of host cells and bacteria) but tends to overestimate it.

B. Competitive case

The homogeneous-case analysis in Fig. 1 can be extended to a mixture of bacterial and host cells, referred to as a competitive case, as shown in Fig. 2. If the concentric circles in blue represent bacterial cells, the pink ones stand for host cells. Recall that $A_\mathrm{cell} = A_\mathrm{B}$ or A_H is the bacterial or host cell surface area, respectively. Fig. 2(i) shows a single bacterial cell at the MIC. The introduction of a host cell in (ii) will reduce the amount of peptides for the bacterial cell. The extra number of peptides to maintain C_p at the MIC is equal to $[(P/L)_\mathrm{H} \times A_\mathrm{H}/a_\mathrm{H} + N_\mathrm{pH}]$; similarly, in (iii), the number of peptides that should be added is $\left[(P/L)^*_\mathrm{B} \times A_\mathrm{B}/a_\mathrm{B} + N_\mathrm{pB}\right] + 2\left[(P/L)_\mathrm{H} \times A_\mathrm{H}/a_\mathrm{H}\right]$.

The progression from (i)-(iii) suggests that

$$\mathrm{MIC}(C_\mathrm{B}, C_\mathrm{H}) = \mathrm{MIC}_0 + \left[\left(\frac{P}{L}\right)^*_\mathrm{B}\frac{A_\mathrm{B}}{a_\mathrm{B}} + N^*_\mathrm{pB}\right]C_\mathrm{B} + \left(\frac{P}{L}\right)_\mathrm{H}\frac{A_\mathrm{H}}{a_\mathrm{H}}C_\mathrm{H} \tag{4a}$$

$$\mathrm{MHC}(C_\mathrm{B}, C_\mathrm{H}) \stackrel{?}{=} \mathrm{MHC}_0 + \left[\left(\frac{P}{L}\right)^*_\mathrm{H}\frac{A_\mathrm{H}}{a_\mathrm{H}} + N_\mathrm{pH}\right]C_\mathrm{H} + \left[\left(\frac{P}{L}\right)_\mathrm{B}\frac{A_\mathrm{B}}{a_\mathrm{B}} + N_\mathrm{pB}\right]C_\mathrm{B}. \tag{4b}$$

Similarly to what is done with Eq. 3, using Eq. 15, one can eliminate P/L^* in favor of MIC_0 or MHC_0:

$$\mathrm{MIC}(C_\mathrm{B}, C_\mathrm{H}) = \mathrm{MIC}_0 + \left[\frac{\mathrm{MIC}_0 v_\mathrm{p}}{\left(\mathrm{MIC}_0 v_\mathrm{p} + e^{w_\mathrm{B}/k_\mathrm{B}T}\right)}\frac{A_\mathrm{B}}{A_\mathrm{p}} + N_\mathrm{pB}\right]C_\mathrm{B} + \frac{\mathrm{MHC}_0 v_\mathrm{p}}{\left(\mathrm{MHC}_0 v_\mathrm{p} + e^{w_\mathrm{H}/k_\mathrm{B}T}\right)}\frac{A_\mathrm{H}}{A_\mathrm{p}}C_\mathrm{H} \tag{5a}$$

$$\mathrm{MHC}(C_\mathrm{B}, C_\mathrm{H}) = \mathrm{MHC}_0 + \left[\frac{\mathrm{MHC}_0 v_\mathrm{p}}{\left(\mathrm{MHC}_0 v_\mathrm{p} + e^{w_\mathrm{H}/k_\mathrm{B}T}\right)}\frac{A_\mathrm{H}}{A_\mathrm{p}} + N_\mathrm{pH}\right]C_\mathrm{H} + \left[\frac{\mathrm{MIC}_0 v_\mathrm{p}}{\left(\mathrm{MIC}_0 v_\mathrm{p} + e^{w_\mathrm{B}/k_\mathrm{B}T}\right)}\frac{A_\mathrm{B}}{A_\mathrm{p}} + N_\mathrm{pB}\right]C_\mathrm{B}. \tag{5b}$$

If N_p is set to zero as for model membranes, the second equation in Eq. 4 or Eq. 5 can be obtained from the first one by swapping the role of bacteria with that of host cells. Here $(P/L)_\mathrm{H}$ in Eq. 4a is the surface cover-

age of peptides on the host cells evaluated at $C_p = \text{MIC}$, whereas $(P/L)_B$ in Eq. 4b is the surface coverage of peptides on bacteria evaluated at $C_p = \text{MHC}$.

Note that these two lines of equations in Eq. 4 or Eq. 5 are not symmetric with respect to the exchange in role between host cells and bacteria for the obvious reason: as C_p increases, the MIC will be reached first. This explains why the last term in Eq. 4a or Eq. 5a does not contain N_{pH}. In other words, $(P/L)_H < (P/L)^*_H$ in Eq. 4a. In contrast, $(P/L)_B > (P/L)^*_B$ in Eq. 4b. As a result, over a sizeable C_p range, the peptide under consideration is active against bacteria only and is thus selective.

Also, Eq. 4b and Eq. 5b need to be understood with caution. Beyond $(P/L)^*_B$, some of bound peptides start to rupture the membranes by forming pores, for instance. The last term in these equations may be interpreted as the total amount of bound peptides whether on the membrane surface or in pores. As a result, w_B needs to be interpreted accordingly. As it turns out, the term inside [...] in Eq. 5b is dominated by N_p (see below). Furthermore, w_H in Eq. 5a is not constant but can vary with $(P/L)_H$. The main source of this dependence is the electrostatic interaction between bound peptides. But this dependence is generally weak, since the distance between bound peptides for $P/L \le (P/L)^* \approx 0.01$ is typically larger than the Debye screening length, r_D, beyond which the electrostatic interaction is exponentially screened. At $(P/L)^* = 0.01$, the typical distance between the adjacent peptides is $\approx \sqrt{100 \times 70}$Å ≈ 80Å. This is appreciably larger than the screening length under physiological conditions (e.g., in the presence of 100 mM of monovalent salts): $r_D \approx 10$Å. Finally, in Eq. 4a, N_{pB} is the number of trapped peptides in each cell above the MIC. The value of this parameter will eventually be determined by chemical equilibrium between trapped peptides and those on the membrane or in the bulk. The energetics of this is unknown and can be influenced by a number of factors such as peptide's interaction with cellular components and crowding in the cell. In our consideration, we ignore this complexity and approximate N_{pB} in Eq. 4b by N^*_{pB}.

It is worth noting that Eqs. 3 and 4 are a special case of the following relations:

$$C_p = \frac{1}{v_p} \cdot \frac{\frac{A_p}{a_B}\left(\frac{P}{L}\right)_B}{1 - \frac{A_p}{a_B}\left(\frac{P}{L}\right)_B} e^{w_B/k_BT} + \left[\left(\frac{P}{L}\right)_B \frac{A_B}{a_B} + N_{pB}\right] C_B + \left(\frac{P}{L}\right)_H \frac{A_H}{a_H} C_H \tag{6a}$$

$$= \frac{1}{v_p} \cdot \frac{\frac{A_p}{a_H}\left(\frac{P}{L}\right)_H}{1 - \frac{A_p}{a_H}\left(\frac{P}{L}\right)_H} e^{w_H/k_BT} + \left[\left(\frac{P}{L}\right)_H \frac{A_H}{a_H} + N_{pH}\right] C_H + \left[\left(\frac{P}{L}\right)_B \frac{A_B}{a_B} + N_{pB}\right] C_B. \tag{6b}$$

Here, N_p is a function of P/L and is generally different from N^*_p; $N_p = N^*_p$ for $P/L = (P/L)^*$ and $N_p = 0$ for $P/L < (P/L)^*$. The first term in each line is inspired by Eq. 14; w_B and w_H are, respectively, the binding energy of a given peptide on bacterial and host-cell membranes (see Sec. III for details). If evaluated at $(P/L)_B = (P/L)^*_B$, the first term on the right hand side of Eq. 6(a) is MIC_0; the first term in Eq. 6(b) can be interpreted similarly. Strictly speaking, both w_B and w_H have a weak dependence on P/L. At the relevant range of P/L around P/L^*, however, this dependence can be neglected as discussed above.

For given values of C_p and cell densities (C_B and C_H), the two equations in Eq. 6 can be solved simultaneously for P/L: $(P/L)_B$ and $(P/L)_H$. Initially, we set $N_p = 0$ and increase C_p gradually from zero. At some value of C_p, i.e., $C^*_p = \text{MIC}$, $(P/L)_B$ will reach $(P/L)^*_B$. We then increase C_p further until $(P/L)_H = (P/L)^*_H$. The resulting C_p is the MHC. In this step, N_{pB} in the last term of Eq. 6b needs to be set to an appropriately-chosen value. For practical purposes, however, this extra complication can be ignored, since it will not change the MHC in any significant way. To understand this, recall that $(P/L)_B (A_B/a_B) \ll N_{pB}$. As a result, P/L evaluated with $N_p = 0$ can approximate the P/L term inside [...] in Eq. 6.

It is worth noting that the values of MIC_0, MHC_0, N_{pB}, and N_{pH} can be obtained from noncompetitive measurements. If these values are fed into Eq. 5 (or Eq. 3), the cell-density dependence of peptide selectivity can, in principle, be mapped out. The term in front of C_B or C_H in Eq. 4 and Eq. 5 (i.e., the one inside [...] in Eq. 4 or Eq. 5, respectively) can be interpreted as the total number of peptides consumed per cell; recall N^*_p is the value of N_p at C^*_p (e.g., MIC); $(P/L)_H$ in Eq. 4a is the surface coverage of peptides on the host-cell membranes at $C_p = \text{MIC}$. As indicated below Eq. 4, it is assumed that $\text{MHC}_0 > \text{MIC}_0$: peptides are selective, i.e., at the MIC, host cells remain intact. As a result, these relations are not fully symmetric with respect to the exchange between the subscripts 'B' and 'H'. Finally, note that the term $[(P/L)_B (A_B/a_B) + N_{pB}]$ in Eq. 4b is larger than [...] in Eq. 4a, since the former is evaluated at a larger value of C_p.

It will be instructive to compare the two terms inside [...] in Eq. 4 or Eq. 5: the number of membrane-bound peptides and the number of adsorbed peptides per cell. For this consideration, we invoke some simplification: a cell viewed as a sack of molecules enclosed by a membrane bilayer. For *E. coli* as a representative bacterium, $A_B \approx 12\,\mu\text{m}^2$, which is twice the area of each layer (either inner or outer) in the cytoplasmic membrane. Since $a_B \approx$

$a_H \approx 70\,\text{Å}^2$, $A_B/a_B \approx 1.7 \times 10^7$. For the peptide melittin, $(P/L)^*_B \approx 0.02$ and $(P/L)^*_H \approx 0.01$.[11–13] We thus find $(P/L)^*_B\,(A_B/a_B) \approx 3.4 \times 10^5$. This number is much smaller than $N_{pB} \approx 10^7$-10^8.[10] For the outer *E. coli* membrane, $(P/L)^*_B$ is several fold larger,[18,20] but this does not change the picture. For human red blood cells as representative host cells, $A_H \approx 17A_B$ and $A_H/a_H \approx 2.9 \times 10^8$. As a result, we obtain $(P/L)^*_H(A_H/a_H) \approx 2.9 \times 10^6$, which is smaller than $N_{pH} \approx 10^7$.[8,9] The main source of inoculum effects is the trapping of peptides inside dead cells (i.e., at or above $(P/L)^*$).

The analysis above implies that only the last term in Eq. 4a or Eq. 5a has an explicit dependence on the binding energy w_H for given MIC_0 and MHC_0. As a result, both the MIC and the MHC in Eqs. 4 and 3 are not sensitive to w_B for a fixed value of MIC_0. Also, the MIC in Eq. 4a can be sensitive to w_H, whereas the MHC in Eq. 4b is not. For the homogeneous case in Eq. 3, none of the MIC and the MHC is "explicitly" sensitive to w_B or w_H. For this reason, we favor Eq. 5 over Eq. 4. This consideration suggests that a realistic value of w_H is needed to estimate the MIC in Eq. 5a.

Furthermore, one can show that the trapping of peptides inside a cell will not change $C^*_p(1\,\text{cell})$, i.e., either $(MIC)_0$ or $(MHC)_0$. This quantity is dictated by cell's susceptibility against a given peptide, i.e., it is intrinsic to the type of cell and peptide. Otherwise it would reflect such external parameters as cell density. But this contradicts the meaning of $C^*_p(1\,\text{cell})$. Indeed, peptide trapping in a cell reduces the amount of peptides for the cell surface. In the single-cell limit, however, this will not change the bulk peptide concentration in any significant way. Thus the effect of peptide trapping on C^*_p is insignificant (see Sec. III for additional details).

Because of peptide trapping in cells (the main inoculum effect), C^*_p will increase more rapidly with C_{cell}. It makes steeper the slope of a C^*_p curve versus C_{cell}. Otherwise, the general features of our analysis in subsec. II A and II B remain relevant, e.g., an excessive overestimation of peptide selectivity in a noncompetitive environment, if the cell density is much higher for host cells.

C. Limiting cases

It proves instructive to take some mathematical limits and simplify Eq. 4 or Eq. 5. First, consider the case $C_B = C_H$. In the low cell-density limit, i.e., $C_B = C_H \to 0$, the MIC and MHC in Eq. 4 reduce to MIC_0 and MHC_0, respectively, as there is no competition between different cells (or membranes). As a result, the distinction between the competitive and noncompetitive cases disappears in this limit.

In the high-cell-density case, for simplicity, let's assume that $A_B = A_H$ and $N_p = 0$, as is often the case for lipid bilayers, and $a_B = a_H$ ($\approx 70\text{Å}^2$), which is a good approximation. (If $A_H \neq A_B$, this analysis is applicable to the case: $A_BC_B = A_HC_H$.) The competitive selectivity, MHC/MIC, becomes cell-density independent: $\text{MHC/MIC} \approx [(P/L)_B + (P/L)^*_H] \,/\, [(P/L)^*_B + (P/L)_H] \gtrsim 1$. To understand the origin of the inequality, note that $(P/L)_B$ in the numerator is larger than $(P/L)^*_B$ and $(P/L)_H$ in the denominator is smaller than $(P/L)^*_H$, because of stronger binding affinity of peptides for bacterial cell membranes. Thus MHC/MIC in this limit will get saturated at some constant larger than 1.

In the noncompetitive case, however, the ratio MHC/MIC approaches the following constant: $(P/L)^*_H/(P/L)^*_B$. The threshold P/L is better known for lipid bilayers mimicking cell membranes than for cell membranes. As noted in subsec. II A, because of the presence of PE (phosphatidylethanolamine) in bacterial cell-membrane mimics, $(P/L)^*_B$ somewhat larger than $(P/L)^*_H$. In the large cell-density limit in the noncompetitive case, we thus have $\text{MHC/MIC} \lesssim 1$. There is a noticeable difference between the competitive and noncompetitive cases in the large cell-density limit; the selectivity is higher in the former case.

If $C_H \gg C_B$, Eq. 4 can be simplified as $\text{MIC} \approx (\text{MIC})_0 + A_H/a_H \times (P/L)_H C_H$ and $\text{MHC} \approx (\text{MHC})_0 + A_H/a_H \times (P/L)^*_H C_H$. Note that the MIC in this case is much larger than the MIC for the corresponding bacteria-only case and the MHC here is approximately equal to the MHC for the corresponding host-cell-only case, as illustrated in Fig. 3. Accordingly, the ratio MHC/MIC is roughly independent of C_B and approaches a constant of order 1, as $C_H \to \infty$ (while C_B is held fixed).

Imagine combining two sets of data: one set for bacteria only and one set for host cells only, i.e., two homogeneous cases in Eq. 3. Second, if $C_H \gg C_B$, $\text{MHC/MIC} \to \infty$ as $C_H \to \infty$. This limiting behavior in the homogeneous case is opposite to the one obtained for the corresponding competitive case (see Fig. 3). It explains how the selectivity can be excessively overestimated.

When $N_p \neq 0$ and $A_B \neq A_H$, the analysis above should reflect this. But the difference is often quantitative rather than qualitative, as discussed in Sec. IV.

A full analysis of Eq. 4 or Eq. 5 is involved, since it requires the determination of $(P/L)_B$ and $(P/L)_H$ with varying C_p and identify the value of C_p at which $(P/L)_B = (P/L)^*_B$ or $(P/L)_H = (P/L)^*_H$. In some relevant limits, we can use Eq. 4 to map out a few scenarios regarding peptide selectivity. In the competitive case, if $C_H \gg C_B$ as in whole blood, Eq. 4 can be approximated as

$$\text{MIC}(C_B, C_H) \approx (\text{MIC})_0 + \left(\frac{P}{L}\right)_H \frac{A_H}{a_H} C_H \tag{7a}$$

$$\text{MHC}(C_B, C_H) \approx (\text{MHC})_0 + \left[\left(\frac{P}{L}\right)^*_H \frac{A_H}{a_H} + N^*_{pH}\right] C_H. \tag{7b}$$

Here $(P/L)_H$ is to be evaluated at $C_p = \text{MIC}$. Chemical equilibrium between free and bound peptides (see Eq. 13

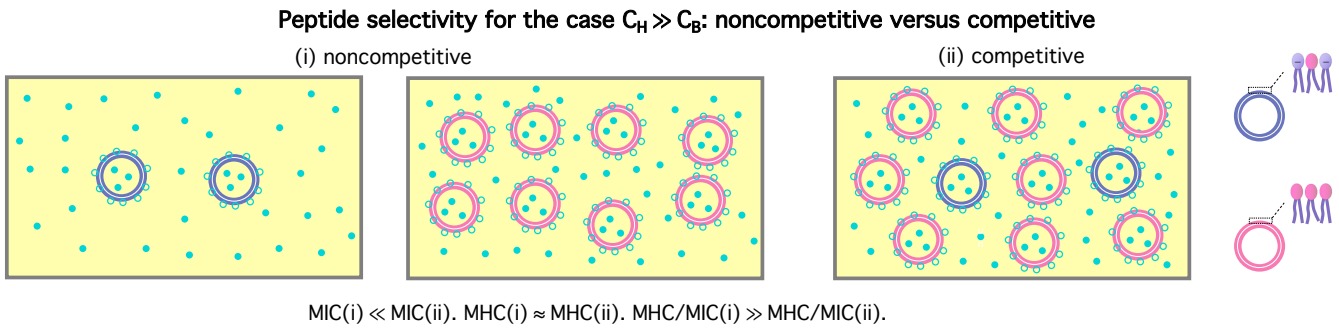

FIG. 3. Peptide selectivity for a noncompetitive (homogeneous) (i) versus competitive (heterogeneous) case (ii). It is assumed that $C_{\rm H} \gg C_{\rm B}$. In this case, whether the selectivity is measured noncompetitively (i) or competitively (ii) has a profound impact on the selectivity. It can be excessively overestimated in the noncompetitive case (i) with reference to the corresponding competitive case (ii), since the MIC is much larger for the latter case. The opposite is true if $C_{\rm H} \ll C_{\rm B}$. Figure adapted with permission from Ref.[15]. Copyright 2015 American Chemical Society; Reproduced with modifications from Ref.[16] with permission from the Royal Society of Chemistry.

in Sec. III) leads to

$$\mathrm{MIC}(C_{\rm B}, C_{\rm H}) \approx \left(\frac{P}{L}\right)_{\rm H} \frac{A_{\rm H}}{a_{\rm H}} C_{\rm H} + \frac{1}{v_{\rm p}} \cdot \frac{\frac{A_{\rm p}}{a_{\rm H}} \left(\frac{P}{L}\right)_{\rm H}}{1 - \frac{A_{\rm p}}{a_{\rm H}} \left(\frac{P}{L}\right)_{\rm H}} e^{w_{\rm H}/k_{\rm B}T}, \tag{8}$$

where $w_{\rm H}$ is the binding energy of a peptide on the host-cell membrane (see Sec. III). This can be used to eliminate $(P/L)_{\rm H}$ in Eq. 7(a); similarly $(P/L)^*_{\rm H}$ can be eliminated in favor of MHC_0:

$$\mathrm{MIC}(C_{\rm B}, C_{\rm H}) \approx \mathrm{MIC}_0 + \frac{\mathrm{MIC}_0 v_{\rm p}}{\left(\mathrm{MIC}_0 v_{\rm p} + e^{w_{\rm H}/k_{\rm B}T}\right)} \frac{A_{\rm H}}{A_{\rm p}} C_{\rm H} \tag{9a}$$

$$\mathrm{MHC}(C_{\rm B}, C_{\rm H}) \approx \mathrm{MHC}_0 + \left[\frac{\mathrm{MHC}_0 v_{\rm p}}{\left(\mathrm{MHC}_0 v_{\rm p} + e^{w_{\rm H}/k_{\rm B}T}\right)} \frac{A_{\rm H}}{A_{\rm p}} + N^*_{\rm pH}\right] C_{\rm H}. \tag{9b}$$

The MIC expression in this equation is strikingly different from the one in the homogeneous case in Eq. 3(a). Similarly to our earlier analysis in subsec. II B and in Fig. 3, for $C_{\rm H} \gg C_{\rm B}$, the competitive MIC is much larger than the noncompetitive one. This results in much smaller selectivity in the competitive case.

For the case $C_{\rm H} \gg C_{\rm B}$, the ratio MHC/MIC become

$$\frac{\mathrm{MHC}}{\mathrm{MIC}} \approx \frac{\mathrm{MHC}_0 + \left[\left(\frac{P}{L}\right)^*_{\rm H} \frac{A_{\rm H}}{a_{\rm H}} + N^*_{\rm pH}\right] C_{\rm H}}{\mathrm{MIC}_0 + \frac{\mathrm{MIC}_0 v_{\rm p}}{\left(\mathrm{MIC}_0 v_{\rm p} + e^{w_{\rm H}/k_{\rm B}T}\right)} \frac{A_{\rm H}}{A_{\rm p}} C_{\rm H}} = \frac{\mathrm{MHC}_0 + \left[\frac{\mathrm{MHC}_0 v_{\rm p}}{\left(\mathrm{MHC}_0 v_{\rm p} + e^{w_{\rm H}/k_{\rm B}T}\right)} \frac{A_{\rm H}}{A_{\rm p}} + N^*_{\rm pH}\right] C_{\rm H}}{\mathrm{MIC}_0 + \frac{\mathrm{MIC}_0 v_{\rm p}}{\left(\mathrm{MIC}_0 v_{\rm p} + e^{w_{\rm H}/k_{\rm B}T}\right)} \frac{A_{\rm H}}{A_{\rm p}} C_{\rm H}}. \tag{10}$$

This implies that peptide trapping in host cells enhances peptide selectivity. Compared to the case $N^*_{\rm pH} \approx 0$, more peptides will be needed in order for $(P/L)_{\rm B}$ to reach $(P/L)^*_{\rm B}$ for $N^*_{\rm pH} \gg 1$. Since the second term inside [...] in the numerator of Eq. 10 is larger than the first term roughly by an order of magnitude, the effect of peptide trapping is about 10-fold.

So far, we have used a simple biophysical picture to explore how peptide selectivity depends on cell densities and on the way it is measured (i.e., competitive versus noncompetitive). The y-intercepts, MIC_0 and MHC_0, may be considered as fitting parameters. They can be related to more microscopic parameters. In the next section, we recapture the main results in this section; we then relate MIC_0 and MHC_0 to the biophysical parameters of peptides and membranes.

III. LANGMUIR BINDING MODEL

In this section, using a Langmuir-type model for molecular binding[21], we derive the main results presented in Sec. II and relate MIC_0 and MHC_0 to the biophysical parameters of peptides and membranes. Note that such a model was already considered recently[15,16]. Here, we recapture the essence of this consideration and generalize it to include peptide trapping in a cell. It suffices to focus on the homogeneous case, since the dependence of peptide activity on cell densities in the competitive case is already obvious from Eq. 4 or Eq. 5.

In this model, peptides are either "free" (in the bulk) or "bound"; bound peptides are further classified as adsorbed to the cell surface or trapped inside a cell (see Fig. 1). Initially, peptide binding occurs on the outer membrane layer or the outmost one in the case of Gram-negative bacteria. Adsorbed peptides will be eventually symmetrically distributed between the two layers after or even prior to membrane rupture[22,23] For simplicity, we ignore peptide trapping below C_{p}^* within typical experimental time scales. Indeed, it was shown that a large amount of trapped peptides were observed in dead bacterial cells, not dividing cells[10]. At and beyond C_{p}^*, the amount of bound peptides is determined by chemical equilibrium between free and bound.

Let w and u be the adsorption and trapping energy, respectively. The value of w is typically more negative for bacterial membranes containing a large fraction of anionic lipids. It is worth noting that w is an effective parameter in which the effect of lipid demixing and peptide-peptide interactions on the membrane surface are subsumed (see Ref.[16] for details). Similarly, u takes into account the interactions of a peptide with intracellular components as well as their mutual interactions inside the cell; it is also influenced by molecular crowding in the cell[24,25].

Let C_{p} be the total concentration of peptides whether free or bound, σ_{p} [$= (P/L)/a_l$] the planar density of adsorbed peptides and A_{p} the area occupied by a bound peptide; n_{p} the density of trapped peptides and v_{p} the volume of each peptide; $n_{\mathrm{p}} = 0$ for $P/L < P/L^*$ and $n_{\mathrm{p}} = N_{\mathrm{p}}/V_{\mathrm{cell}}$ for $P/L = P/L^*$, where V_{cell} is the volume of each cell. In our Langmuir model, the chemical potential of bound peptides μ_{bound} at and above P/L^* can readily be obtained as

$$\frac{\mu_{\mathrm{bound}}}{k_{\mathrm{B}}T} = \frac{w}{k_{\mathrm{B}}T} + \ln\left(\frac{\sigma_{\mathrm{p}}A_{\mathrm{p}}}{1-\sigma_{\mathrm{p}}A_{\mathrm{p}}}\right) = \frac{u}{k_{\mathrm{B}}T} + \ln\left(\frac{n_{\mathrm{p}}v_{\mathrm{p}}}{1-n_{\mathrm{p}}v_{\mathrm{p}}}\right). \tag{11}$$

Here and below, k_{B} is the Boltzmann constant and T the temperature. The log term is related to the number of ways in which bound peptides are distributed on the membrane surface or inside the cell. The second equality holds in chemical equilibrium between adsorbed and trapped peptides.

The chemical potential of free peptides is

$$\frac{\mu_{\mathrm{free}}}{k_{\mathrm{B}}T} = \ln\left\{\left[C_{\mathrm{p}} - C_{\mathrm{cell}}\left(\sigma_{\mathrm{p}}A_{\mathrm{cell}} + n_{\mathrm{p}}V_{\mathrm{cell}}\right)\right]v_{\mathrm{p}}\right\}. \tag{12}$$

Note that the expression inside [...] is the concentration of free peptides and the term inside (...) is the inoculum size; recall that A_{cell} is the cell surface area and V_{cell} denotes the volume of the cell.

By equating the two chemical potentials in Eqs. 11 and 12, we obtain

$$C_{\mathrm{p}} = \frac{1}{v_{\mathrm{p}}}\cdot\frac{\frac{A_{\mathrm{p}}}{a_l}\left(\frac{P}{L}\right)}{1-\frac{A_{\mathrm{p}}}{a_l}\left(\frac{P}{L}\right)}e^{w/k_{\mathrm{B}}T} + \left[\frac{A_{\mathrm{cell}}}{a_l}\left(\frac{P}{L}\right) + n_{\mathrm{p}}V_{\mathrm{cell}}\right]C_{\mathrm{cell}} \tag{13a}$$

$$= \frac{1}{v_{\mathrm{p}}}\cdot\frac{n_{\mathrm{p}}v_{\mathrm{p}}}{1-n_{\mathrm{p}}v_{\mathrm{p}}}e^{u/k_{\mathrm{B}}T} + \left[\frac{A_{\mathrm{cell}}}{a_l}\left(\frac{P}{L}\right) + n_{\mathrm{p}}V_{\mathrm{cell}}\right]C_{\mathrm{cell}}. \tag{13b}$$

In this final expression, we eliminated σ_{p} in favor of P/L via the relation $\sigma_{\mathrm{p}}a_l = P/L$ (with a_l as the lipid head-group area). In the absence of peptide trapping in cells (or below C_{p}^*), Eq. 13(a) with $n_{\mathrm{p}} = 0$ describes chemical equilibrium between free and adsorbed peptides; Eq. 13(b) becomes irrelevant.

At C_{p}^*, i.e., either MIC or MHC,

$$C_{\mathrm{p}}^* = \frac{1}{v_{\mathrm{p}}}\cdot\frac{\frac{A_{\mathrm{p}}}{a_l}\left(\frac{P}{L}\right)^*}{1-\frac{A_{\mathrm{p}}}{a_l}\left(\frac{P}{L}\right)^*}e^{w/k_{\mathrm{B}}T} + \left[\frac{A_{\mathrm{cell}}}{a_l}\left(\frac{P}{L}\right)^* + n_{\mathrm{p}}^*V_{\mathrm{cell}}\right]C_{\mathrm{cell}} \tag{14a}$$

$$= \frac{1}{v_{\mathrm{p}}}\cdot\frac{n_{\mathrm{p}}^*v_{\mathrm{p}}}{1-n_{\mathrm{p}}^*v_{\mathrm{p}}}e^{u/k_{\mathrm{B}}T} + \left[\frac{A_{\mathrm{cell}}}{a_l}\left(\frac{P}{L}\right)^* + n_{\mathrm{p}}^*V_{\mathrm{cell}}\right]C_{\mathrm{cell}}. \tag{14b}$$

Here $n_{\mathrm{p}}^*V_{\mathrm{cell}} = N_{\mathrm{p}}^*$ can be interpreted as the total number of peptides trapped in each cell at $C_{\mathrm{p}} = C_{\mathrm{p}}^*$.

The relation in Eq. 14 shows how $C_{\rm p}^*$ varies with $C_{\rm cell}$ for a given w value: $C_{\rm p}^*$ is insensitive to $C_{\rm cell}$ for $C_{\rm cell} \approx 0$ but it increases approximately linearly with $C_{\rm cell}$ for a sufficiently large $C_{\rm cell}$. Comparison between Eq. 14 and Eq. 3 leads to the following relation

$$\mathrm{MIC}_0 = \frac{1}{v_{\rm p}} \cdot \frac{\frac{A_{\rm p}}{a_{\rm B}} \left(\frac{P}{L}\right)^*_{\rm B}}{1 - \frac{A_{\rm p}}{a_{\rm B}} \left(\frac{P}{L}\right)^*_{\rm B}} e^{w_{\rm B}/k_{\rm B}T} = \frac{n^*_{\rm pB}}{1 - n^*_{\rm pB} v_{\rm p}} e^{u_{\rm B}/k_{\rm B}T} \tag{15a}$$

$$\mathrm{MHC}_0 = \frac{1}{v_{\rm p}} \cdot \frac{\frac{A_{\rm p}}{a_{\rm H}} \left(\frac{P}{L}\right)^*_{\rm H}}{1 - \frac{A_{\rm p}}{a_{\rm H}} \left(\frac{P}{L}\right)^*_{\rm H}} e^{w_{\rm H}/k_{\rm B}T} = \frac{n^*_{\rm pH}}{1 - n^*_{\rm pH} v_{\rm p}} e^{u_{\rm H}/k_{\rm B}T}. \tag{15b}$$

Here the subscript 'B' and 'H' refer to bacteria and host cells, respectively. Both MIC_0 and MHC_0 are exponentially sensitive to w or u but they are not as sensitive to other quantities. This energy scale is the main determinant of peptide selectivity. The results in Eq. 15 can be used in Eq. 4 (competitive) or in Eq. 3 (noncompetitive).

It is worth mentioning that we will not attempt to solve Eq. 13 for $n_{\rm p}$, partly because the energetics involved in peptide trapping (i.e., u) is not well known. Instead, we will use suitable values of $n_{\rm p}V_{\rm cell} = N_{\rm p} \approx N_{\rm p}^*$, the number of peptides trapped in each cell, inspired by recent experiments[8–10]. With this simplification, Eq. 13 can readily be extended to the competitive case shown in Fig. 2. The cell-density dependence of $C_{\rm p}$ is obvious in light of the discussion in subsec. II B; one can readily write down Eq. 6.

IV. RESULTS

In this section, we present the results for peptide activity and selectivity obtained for model membranes (subsec. IV A) and cells (subsec. IV B). Recall that the main difference between the two comes from peptide trapping in the latter case. As evidenced below, MIC_0 and MHC_0 are chosen differently for the two cases. If calculated values of these quantities are used for model membranes, they are chosen appropriately for cells. For instance, the value $\mathrm{MIC}_0 = 5\,\mu$M that we use is to reflect recent experiments[10].

A. Membrane selectivity

Following Sec. II, we first present our results for peptide activity and selectivity without taking into account peptide trapping using peptide parameters relevant for the peptide melittin[15,16]: peptide charge $Q = 5$ (?), $(P/L)^*_{\rm B} = 1/48$, $(P/L)_{\rm H} = 1/99$,[11–13] $v_{\rm p} = 33^3$Å^3, and $A_{\rm p} = 400$Å^2[15,16]. For this peptide, w was mapped out for model membranes, mimicking bacterial and host-cell membranes: $w_{\rm B} = -16.6 k_{\rm B}T$ and $w_{\rm H} = -6.72 k_{\rm B}T$.[16] Also, $a_{\rm B} = 74$Å^2 (a_l for bacterial membranes), $a_{\rm H} = 71$Å^2 (a_l for bacterial membranes)[11–13], $A_{\rm B} = 1.2 \times 10^9$Å^2 $= 12\mu$m^2 (as for *E. coli*, and $A_{\rm H} = A_{\rm B}$ or $A_{\rm H} = 17A_{\rm B}$ as for human red blood cells[15]. Note here that this value of $A_{\rm B}$ is two times the surface area of *E. coli* ($\approx 6\mu$m^2)[26]. This is to reflect the symmetrical binding of peptides on the inner and outer layers of the cytoplasmic membrane. Finally we set $N_{\rm p} = 0$ as expected for model membranes.

We have solved Eq. 3 for the noncompetitive case and Eq. 4 for the competitive case (both together with Eq. 15). This is equivalent to solving Eq. 6 for P/L at and found $C_{\rm p}$ at which P/L is equal to P/L^*, as discussed below Eq. 6. In Fig. 4, the resulting $C_{\rm p}^*$, either MIC or MHC, as well as the ratio MHC/MIC are shown as a function of cell density. When $C_{\rm H}$ ($C_{\rm B}$) is held fixed, the x axis represents $C_{\rm B}$ ($C_{\rm H}$); for the case $C_{\rm H} = C_{\rm B}$, it indicates both $C_{\rm H}$ and $C_{\rm B}$. If the competitive cases are represented by dashed lines with filled symbols, the noncompetitive ones are described by solid lines with open symbols.

As shown in Fig. 4(A) and (B), both MICs and MHCs increase with increasing cell density ($C_{\rm H}$ or $C_{\rm B}$), as suggested by Eqs. 3 and 4. For $A_{\rm H} = 17A_{\rm B}$, the presence of a large amount of host-cell membranes ($C_{\rm H} = 5 \times 10^9$ cells/mL) raises the MIC by an order of magnitude as long as $C_{\rm B} \lesssim 5 \times 10^5$ cells/mL; for $A_{\rm H} = A_{\rm B}$, however, its impact on the MIC appears to be minor. There is no essential difference between the three cases in (A): (i) $C_{\rm H} = C_{\rm B}$, $A_{\rm H} = A_{\rm B}$, (ii) $C_{\rm H} = 0$, $A_{\rm H} = A_{\rm B}$, and (iii) $C_{\rm H} = C_{\rm B}$, $A_{\rm H} = 17A_{\rm B}$ (labelled as (i), (ii), (iii), respectively, in the legend); in these cases, the MIC is insensitive to the presence of host-cell membranes or the value of $A_{\rm H}$. As $C_{\rm B}$ increases, the MIC curves eventually collapse onto each other. In this case, it is dominated by the $C_{\rm B}$-dependent term in Eq. 4a or Eq. 5a.

As shown in 4(B), in the presence of a large amount of host-cell membranes ($C_{\rm H} = 5 \times 10^9$ cells/mL), the MHC obtained with $A_{\rm H} = 17A_{\rm B}$ is about ten-fold larger, as long as $C_{\rm B} \lesssim 10^8$ cells/mL. There is no essential difference between the MHC curves obtained with (i) $C_{\rm H} = C_{\rm B}, A_{\rm H} = A_{\rm B}$, (ii) $C_{\rm B} = 0, A_{\rm H} = 17A_{\rm B}$, and (iii) $C_{\rm B} = 5 \times 10^5$ cells/mL, $A_{\rm H} = 17A_{\rm B}$ (labelled as (i), (ii), and (iii), respectively, in the legend). The similarity between (ii) and (iii) means that the presence of 5×10^4 cells/mL of bacterial cell membranes does not have any noticeable impact on the MHC; at a low $C_{\rm H}$ range, the MHC is dominated by MHC_0. The similar-

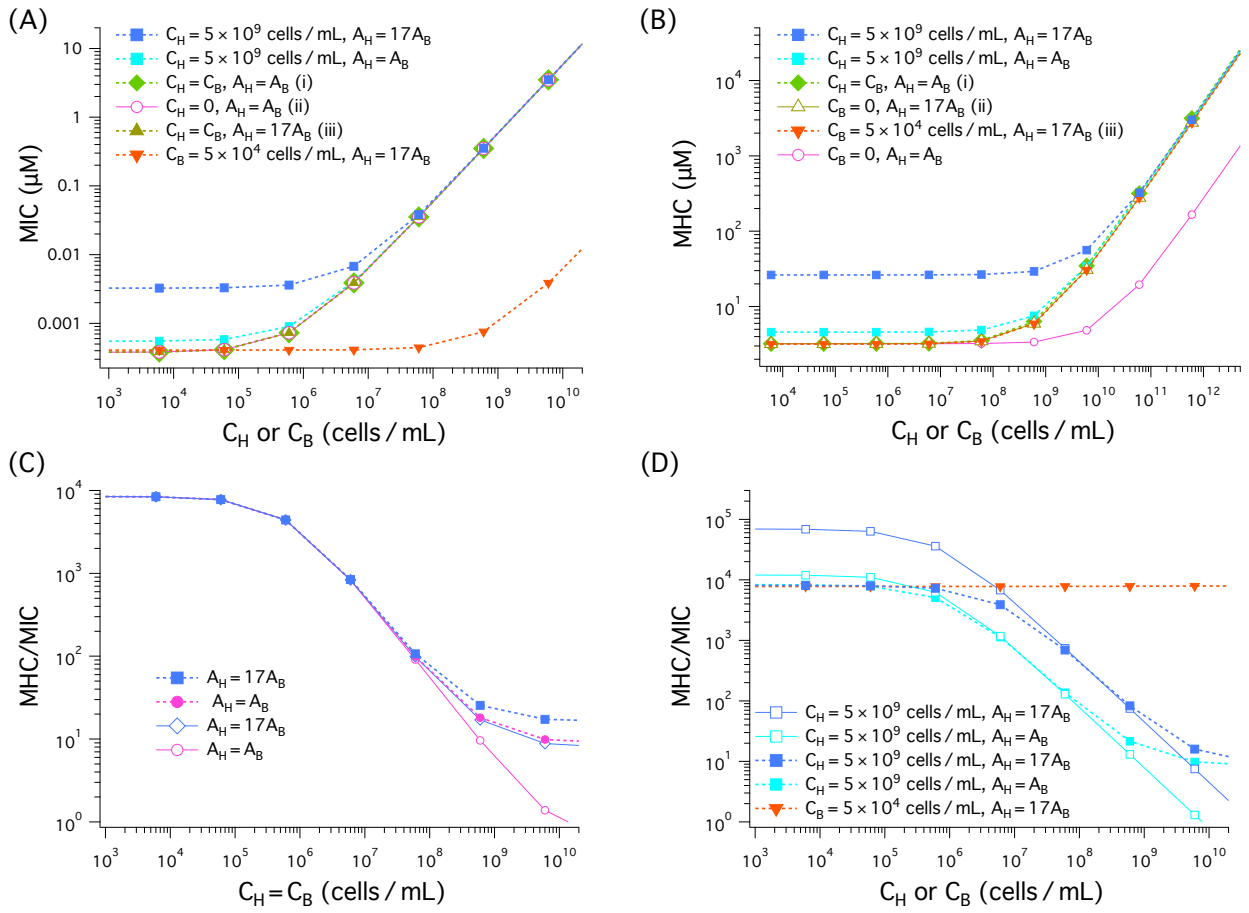

FIG. 4. Cell (membrane)-density dependence of MIC, MHC, and MHC/MIC for the noncompetitive and competitive cases, represented by solid lines with unfilled symbols and dashed lines with filled symbols, respectively. When $C_{\rm H}$ ($C_{\rm B}$) is held fixed, the 'x' axis should be interpreted as $C_{\rm B}$ ($C_{\rm H}$); for the case $C_{\rm H} = C_{\rm B}$, it stands for both $C_{\rm H}$ and $C_{\rm B}$. We have chosen the parameter as follows: the peptide charge $Q = 5$ (as for melittin); the bacterial cell surface area $A_{\rm B} = 12\,\mu{\rm m}^2$ (suitable for *E. coli*); the host cell surface area $A_{\rm H} = A_{\rm B}$ and $A_{\rm H} = 200\,\mu{\rm m}^2 \approx 17 \times A_{\rm B}$ (as for human red blood cells); $a_{\rm B} = 71\,{\rm \AA}^2$ and $a_{\rm H} = 74\,{\rm \AA}^2$; $P/L_{\rm B}^* = 1/48$ and $P/L_{\rm H}^* = 1/99$[11–13]; $v_{\rm p} = 33^3\,{\rm \AA}^3$, and $A_{\rm p} = 400{\rm \AA}^2$[15,16]; $w_{\rm B} = -16.6\,k_{\rm B}T$ and $w_{\rm H} = -6.72\,k_{\rm B}T$[16] as for the peptide melittin. (A)-(B) In all cases, both MICs and MHCs increase with increasing cell (membrane) density ($C_{\rm H}$ or $C_{\rm B}$), as expected from Eq. 4a or Eq. 5a. Also, the presence of a large amount of hot-cell membranes ($C_{\rm H} = 5 \times 10^9$ cells/mL) raises both the MIC and the MIC as long as $C_{\rm H} \gg C_{\rm B}$ – almost by an order of magnitude for the case $A_{\rm H} = 17A_{\rm B}$. There is no essential difference between the three cases labelled as (i), (ii), and (iii) in the legend in (A): the presence of an equal amount of host-cell membranes ($C_{\rm H} = C_{\rm B}$) does not influence the MIC in any noticeable way. Similarly, the curves labelled as (i), (ii), and (iii) tend to collapse onto each other in (B), as if the presence of an equal amount of bacterial membranes ($C_{\rm H} = C_{\rm B}$) does not seem to have any noticeable impact on the MHC. But this is a coincidence. Indeed, for $A_{\rm H} = A_{\rm B}$, the non-competitive MHC curve deviates from and fall below these curves. The selectivity, as measured by MHC/MIC, in (C) decreases as the membrane density increases; in both competitive and noncompetitive cases, we chose $C_{\rm H} = C_{\rm B}$. The difference between the competitive and noncompetitive cases becomes obvious when the cell density is $\gtrsim 10^8$ cells/mL, in which the selectivity is higher for the former case. Also the selectivity is higher for the larger $A_{\rm H}$ case as long as $C_{\rm B} = C_{\rm H} \gtrsim 10^8$ cells/mL. In (D), except for the red dashed curve, $C_{\rm H} = 5 \times 10^9$ cells/mL but $C_{\rm B}$ varies. Similarly to what the graphs in (C) suggests, the selectivity in (D) decreases as $C_{\rm B}$ decreases. Compared to the competitive case represented by the blue dashed curve with filled squares, the corresponding noncompetitive case overestimates the selectivity by about one order of magnitude at a low $C_{\rm B}$ range of $C_{\rm B} \lesssim 10^5$ cells/mL. Also shown is the red dashed line with inverted triangles obtained with $C_{\rm B} = 5 \times 10^4$ cells/mL. This curve is nearly flat in the $C_{\rm H}$ range shown.

ity between (i) and (ii) (or (iii)) is, however, a coincidence. Indeed, with different parameter choices, the two cases deviate from each other[15]. As one way to see this, imagine increasing the value of $A_{\rm H}$ in (ii). The corresponding curve will shift to the right. Finally, the MHC obtained with $C_{\rm B} = 0$ and $A_{\rm H} = A_{\rm B}$ falls below the other curves, e.g., the curve representing the case (ii), as long as $C_{\rm H} \gtrsim 10^8$cells/mL. This is well aligned with the $A_{\rm H}$

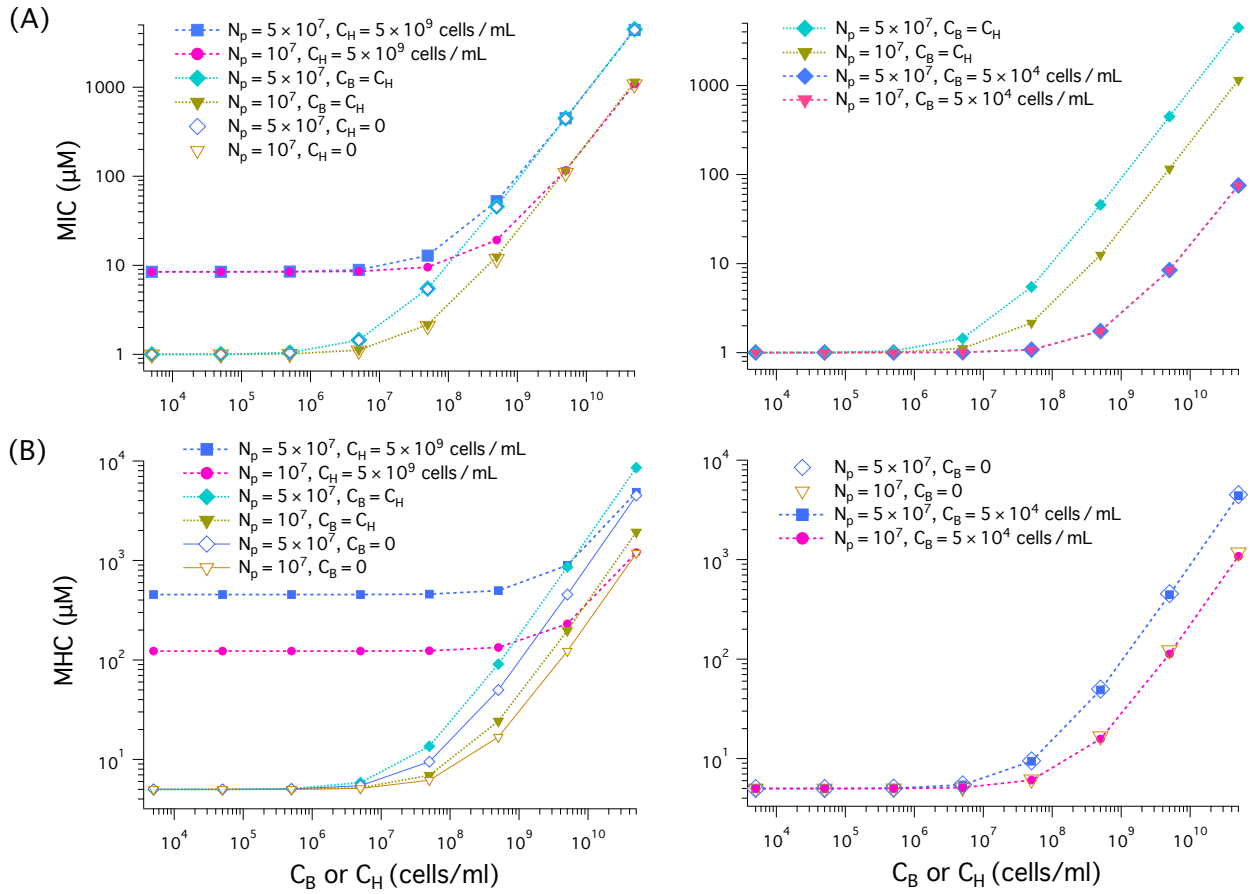

FIG. 5. Cell-density dependence of MIC (A) and MHC (B) for the noncompetitive and competitive cases, represented by unfilled symbols (or solid lines with unfilled symbols) and dashed or dotted lines with filled symbols, respectively. When C_H (C_B) is held fixed, the 'x' axis represents C_B (C_H); for the case $C_H = C_B$, it indicates both C_H and C_B (the results for this case are included in all the graphs). We have chosen the parameters as follows: $\mathrm{MIC}_0 = 1\,\mu$M and $\mathrm{MHC}_0 = 5\,\mu$M; $w_B = -16.6\,k_BT$ and $w_H = -6.72\,k_BT$; the peptide charge $Q = 5$ (as for melittin); the bacterial cell surface area $A_B = 12\,\mu\mathrm{m}^2$ (suitable for *E. coli*); the host cell surface area $A_H = 200\,\mu\mathrm{m}^2 \approx 17 \times A_B$ (as for human red blood cells); the lipid headgroup area $a_B = 71\,\text{Å}^2$ and $a_H = 74\,\text{Å}^2$. In all cases shown in (A) and (B), both the MIC and MHC increase with increasing cell density (C_H or C_B), as expected from Eq. 4(a) and (b). (A) (Left) The presence of host cells increases the MIC, more so for larger N_p, as long as $C_B \lesssim 5\times10^8$ cells/mL; for this, compare the two curves obtained with $C_H = 5\times10^9$ cells/mL and $C_H = 0$. The MIC remains $\lesssim 10\,\mu$M if $C_B \lesssim 5\times10^7$ cells/mL. If $C_B \gtrsim 5\times10^8$ cells/mL, the presence of host cells does not have a significant impact on the MIC; in this case, peptide trapping in bacterial cells is a determining factor. For the same value of N_p, different curves representing different values of C_H collapse onto each other for sufficiently large C_B: $C_B \gtrsim 5\times10^8$ cells/mL. In all cases, the MIC increases more rapidly with C_B for larger N_p. There is no noticeable difference between the two cases: $C_B = C_H$ and $C_H = 0$ for given N_p. In this case, the main source of inoculum effects is the trapping of peptides in bacterial cells. (A) (Right) The results obtained with $C_B = 5\times10^4$ cells/mL (the two bottom curves) indicate that the MIC increases "slowly" with C_H (see Eq. 4). At the MIC, host cells are below the MHC. As a result, the binding of peptides to the host-cell membrane is responsible for the increase of MIC with C_H. This also explains why there is no essential difference between the two cases: $C_B = C_H$ and $C_H = 0$ for given N_p. (B) (Left) When $C_H = 5\times10^9$ cells/mL, the MHC is large and remains roughly flat as C_B increases up to $C_B = 10^9$ cells/mL. It is obviously larger for the larger N_p case (squares or diamonds); it can be two orders of magnitude larger than MHC_0. In all other cases, the MHC increases with increasing cell densities: either C_B or C_H. Also the MHC is larger for the competitive case $C_B = C_H$ compared to the corresponding non-competitive case $C_B = 0$: at the MHC, the bacterial cells are above the MIC and the resulting peptide trapping in the bacterial cells raises the MHC. (B) (Right) The presence of a small concentration of bacteria (i.e., $C_B = 5\times10^4$ cells/mL) does not alter the MHC in any significant way. Also the MHC increases faster with C_H or C_B for larger N_p, as expected from Eq. 4(b). The competitive curve obtained with $C_B = C_H$ is similar to the corresponding noncompetitive one obtained with $C_B = 0$.

dependence of the MHC in Eq. 4b or Eq. 5b.

The MIC and MHC results in Fig. 4(A) and (B) suggest that the presence of bacterial membranes influences MHCs more effectively than the presence of host cell membranes influences MICs. For this, compare the two curves obtained with (i) $C_H = C_B, A_H = A_B$ and (ii) $C_H = 0, A_H = A_B$ in (A) as well as those obtained with (i) $C_H = C_B, A_H = A_B$ and $C_B = 0, A_H = A_B$ in (B). This difference can be attributed to the stronger binding of peptides to bacterial membranes.

In the competitive case with an excessive amount of host cells ($C_H = 5 \times 10^9$ cells/mL), however, MICs in (A) and MHCs in (B) are much larger than in the other cases as long as $C_B \ll C_H$. This is consistent with what Eq. 4 or Eq. 5 suggests: the presence of a large amount of host cells increases both MICs and MHCs. Also the MIC or the MHC is generally larger for $A_H = 17A_B$ than for $A_H = A_B$, as long as $C_H \gtrsim C_B$. As discussed in Sec. II, increasing A_H is equivalent to increasing C_H. This explains the observation of larger MHCs for larger A_H.

The ratio MHC/MIC measures peptide selectivity. Our results for this ratio are shown in Fig. 4(C) and (D). In (C), $C_B = C_H$; in (D), except for the red dashed line, $C_H = 5 \times 10^9$ cells/mL but C_B is allowed to vary. In all cases, the selectivity decreases (or remains flat), as the cell density increases as discussed in Sec. II. In (C), the difference between the competitive and noncompetitive cases for $A_H = A_B$ becomes obvious when the cell density is $\gtrsim 10^8$ cells/mL, in which the selectivity is higher for the former case. This is correlated with the observation that MHCs are higher for the competitive case in this range of cell density as shown in Fig. 4(B). Also, the selectivity is higher for the larger A_H case.

The competitive case in (D), except for the red dashed line, contains a large amount of host cells ($C_H = 5 \times 10^9$ cells/mL) as well as bacterial cells with variable C_B. In the noncompetitive measurement, MHCs obtained with the choice $C_H = 5 \times 10^9$ cells/mL were combined with MICs. Similarly to what the graphs in (C) suggests, the selectivity in (D) decreases as the density C_B decreases. However, the selectivity in the noncompetitive case is overestimated compared to the corresponding competitive case, as long as $C_B \lesssim 10^7$-10^8 cells/mL $\ll C_H$. For the large A_H case, it is overestimated by up to an order of magnitude.

This finding is well aligned with the view that the selectivity measured in a noncompetitive manner (with $C_H \gg C_B$) can be an experimental illusion.[27] The results in (D) also clear up possible confusions. Even in the presence of a large amount of host cells, the selectivity measured in a competitive environment is not an experimental artifact. It just reflects correctly the cell-density dependence of the selectivity, presented in Sec. II.

B. Cell selectivity: inoculum effects

We have also solved Eq. 5 or equivalently Eq. 4 with realistic choices of N_p and mapped out various scenarios for peptide activity and selectivity. One of the challenges in this effort is that the parameters in these equations are not well known for real cells. In particular, w_B for Gram-negative bacteria should take into account the peptide interaction with their outer membrane (OM), among others; recall that this is an effective parameter, in which microscopic details (e.g., peptide charge, peptide interaction with the OM) are subsumed. This quantity has only recently been mapped out theoretically for the interaction of melittin-like peptides with model membranes[16]. For the reasons explained in Sec. II, the dependence of peptide activity on w_B is reflected mainly through MIC_0. Furthermore, the MIC and the MHC in the homogeneous case in Eq. 3 do not depend sensitively on w_B or w_H for given MIC_0 and MHC_0.

Here we do not attempt to calculate the effective binding energy w (either w_B or w_H) for real cells and use it in the computation of MIC_0 and MHC_0. Instead, we start with conveniently-chosen but biophysically-relevant values of MIC_0 and MHC_0: $\mathrm{MIC}_0 = 1\,\mu$M and $\mathrm{MHC}_0 = 5\,\mu$M. For simplicity, the number of trapped peptides N_p is chosen to be the same for bacteria and host cells: $N_p = 0, 10^7, 5 \times 10^7$. Otherwise, we choose the same parameters used in Fig. 4: the bacterial cell surface area $A_B = 12\,\mu\mathrm{m}^2$ (suitable for *E. coli*); the host cell surface area $A_H = 200\,\mu\mathrm{m}^2 \approx 17 \times A_B$ (as for human red blood cells); $a_B = 71\,\text{Å}^2$ and $a_H = 74\,\text{Å}^2$; $w_B = -16.6\,k_BT$ and $w_H = -6.72\,k_BT$.

Fig. 5 displays the results for MIC (A) and MHC (B) for the noncompetitive and competitive cases, represented by solid lines with unfilled symbols or unfilled symbols and dashed lines with filled symbols, respectively. As in Fig. 4, when C_H (C_B) is held fixed, the 'x' axis represents C_B (C_H); for the case $C_H = C_B$, it stands for both C_H and C_B.

In all cases shown in Fig. 5(A)-(B), both MICs and MHCs increase with increasing cell density (C_H or C_B), similarly to what is shown for model membranes in Fig. 4. This is a natural consequence of the cell-density dependence shown in Eq. 5 (or Eq. 4). As indicated in the graph on the left in Fig. 6(A), the presence of an excess amount of host cells raises the MIC, more so for larger N_p as long as $C_B \lesssim 5 \times 10^8$ cells/mL; for this, compare the two top curves obtained with $C_H = 5 \times 10^9$ cells/mL and $C_H = 0$. Nevertheless, the MIC remains somewhat smaller than $10\,\mu$M if $C_B \lesssim 5 \times 10^7$ cells/mL. When $C_B \gtrsim 5 \times 10^8$ cells/mL, the presence of host cells does not have a significant impact on the MIC; in this case, peptide trapping in bacterial cells is a determining factor. For the same value of N_p, different curves representing different values of C_H collapse onto each other for sufficiently large C_B: $C_B \gtrsim 5 \times 10^8$ cells/mL. In all cases, the MIC increases more rapidly with C_B for larger N_p. In contrast, the results obtained with $C_B = 5 \times 10^4$ cells/mL,

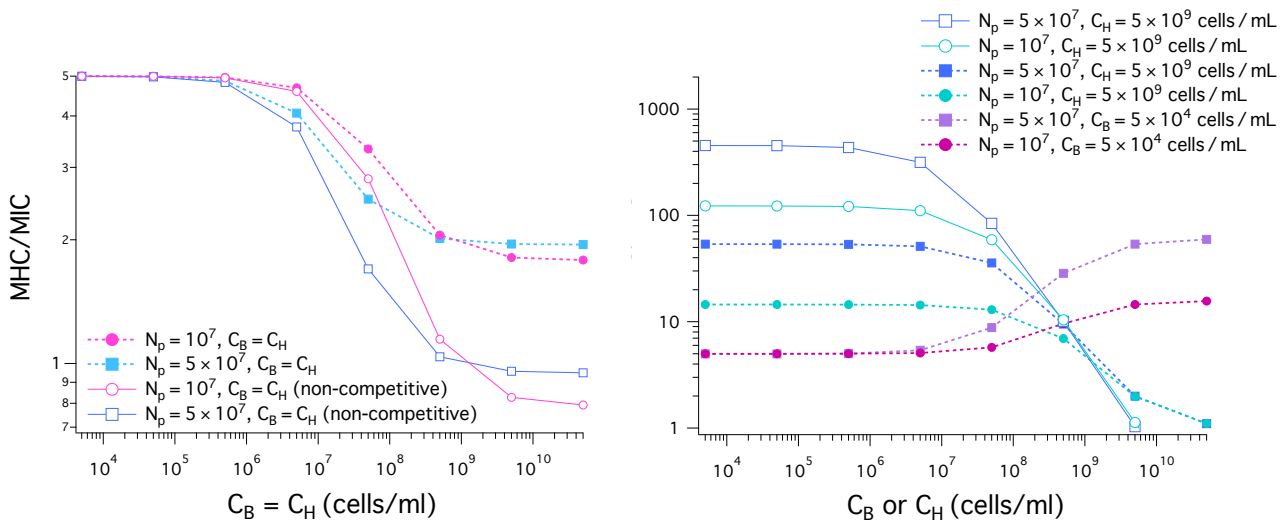

FIG. 6. Cell-density dependence of MHC/MIC for the noncompetitive and competitive cases, represented by solid lines with unfilled symbols and dashed lines with filled symbols, respectively. When C_H (C_B) is held fixed, the 'x' axis represents C_B (C_H); for the case $C_H = C_B$, it stands for both C_H and C_B. We have chosen the same parameters as in Fig. 5: $MIC_0 = 1\,\mu M$ and $MHC_0 = 5\,\mu M$; $w_B = -16.6\,k_BT$ and $w_H = -6.72\,k_BT$ as for melittin; the peptide charge $Q = 5$ (as for melittin); the bacterial cell surface area $A_B = 12\,\mu m^2$ (suitable for *E. coli*); the host cell surface area $A_H = 200\,\mu m^2 \approx 17\times A_B$ (as for human red blood cells); $a_B = 71\,Å^2$ and $a_H = 74\,Å^2$. (Left) In all cases shown, $C_H = C_B$. The selectivity, MHC/MIC, decreases as the cell density increases. It is larger for the competitive case (filled symbols), more so for larger $C_H = C_B$. For $C_H = C_B \lesssim 10^9$ cell/mL, the selectivity is somewhat larger when N_p is smaller; in this case, peptide trapping works in bacteria's favor by increasing the MIC. (Right) This graph shows how peptide selectivity depends on cell densities. The selectivity obtained with $C_H = 5\times10^9$ cells/mL decreases with increasing C_B. In this case, peptide trapping enhances the selectivity for $C_B \lesssim 10^9$ cells/mL (competitive) or $C_B \lesssim 10^8$ cells/mL (non-competitive) but does not seem to have a noticeable impact outside this range. In contrast, it increases with C_H in the presence of $C_B = 5\times10^4$ cells/mL. With the parameter choices used, the non-competitive selectivity can be an order of magnitude larger than the corresponding competitive one. Depending on how the selectivity is measured, it can be two or three order of magnitude different; for this, compare the blue and purple curves.

plotted in the graph in the right, indicate that the MIC increases "slowly" with C_H (see Eq. 4). At the MIC, host cells are below the MHC. As a result, the binding of peptides to the host-cell membrane is responsible for the slow increase of MIC with C_H, i.e., a weak inoculum effect. (For comparison purposes, we included the competitive curves obtained with $C_H = C_B$ in both graphs in Fig. 5.)

Fig. 5(B) shows how the MHC varies as a function of cell density: C_B or C_H. As shown in the left graph, when $C_H = 5\times10^9$ cells/mL, the MHC is large and remains roughly flat as C_B increases up to $C_B = 10^9$ cells/mL. This is consistent with Eq. 4b or Eq. 5b, which suggests that the MHC is roughly independent of C_B, as long as C_H is sufficiently larger than C_B. The MHC is obviously larger for the larger N_p case (squares or diamonds). In all other cases, the MHC increases with increasing cell density: C_B or C_H. Finally, there is no essential difference between the two cases: $C_B = C_H$ (competitive) and $C_B = 0$ (non-competitive).

As shown in the graph on the right in Fig. 5, the presence of a small concentration of bacteria (i.e., $C_B = 5\times10^4$ cells/mL) does not alter the MHC in any significant way. Similarly to the other cases shown on the left in Fig. 5(B), the MHC obtained with $C_B = 5\times10^4$ cells/mL increases faster with C_H or C_B for larger N_p, as expected from Eq. 4b or Eq. 5b.

Fig. 6 shows the results for MHC/MIC. In the graph on the left, we have chosen $C_H = C_B$. If the dashed lines with filled symbols represent competitive selectivity, the solid lines with unfilled symbols describe noncompetitive selectivity; in the latter case, MHCs and MICs, obtained for host-cell only and bacteria-only solutions, respectively, are combined into MHC/MIC. In all cases shown, the selectivity, MHC/MIC, decreases from the initial value MHC_0/MIC_0 as the cell density increases. It is larger for the competitive case (filled symbols) than for the non-competitive case so that the difference between the two cases is more pronounced for larger $C_H = C_B$. For $C_H = C_B \lesssim 10^9$ cell/mL, the selectivity is somewhat larger when N_p is smaller; in this case, peptide trapping works in bacteria's favor by increasing the MIC.

As shown in the graph on the right in Fig. 6, the selectivity obtained with $C_H = 5\times10^9$ cells/mL decreases with increasing C_B. In this case, peptide trapping enhances the selectivity for $C_B \lesssim 10^9$ cells/mL (competitive) or $C_B \lesssim 10^8$ cells/mL (non-competitive) but does not seem to have a noticeable impact outside this range.

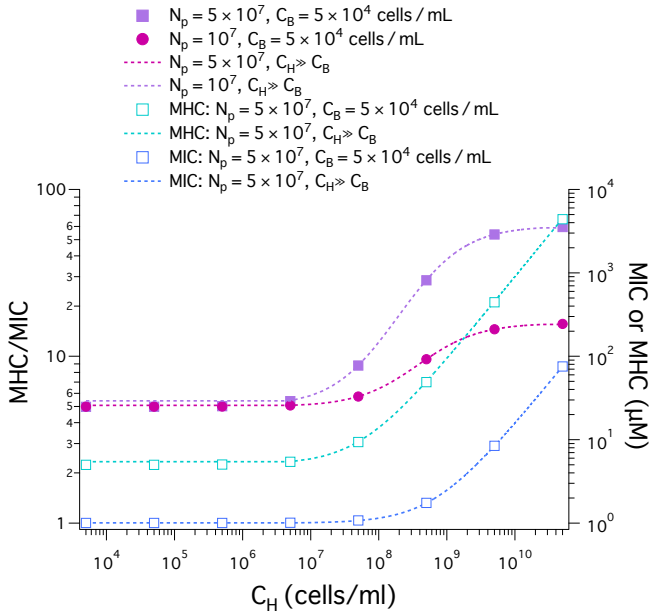

FIG. 7. Comparison between full-analysis and approximate results for MHC/MIC (left axis) and MIC or MHC (right axis). If the former are based on Eq. 4 as in Fig. 6, the latter are obtained from Eq. 9. We have chosen the same peptide-membrane parameters used in Fig. 6: $(\mathrm{MIC})_0 = 1\,\mu$M and $(\mathrm{MHC})_0 = 5\,\mu$M; $w_\mathrm{B} = -16.6\,k_\mathrm{B}T$ and $w_\mathrm{H} = -6.72\,k_\mathrm{B}T$; $A_\mathrm{p} = 400\,\text{Å}^2$; $v_\mathrm{p} = 33^3\,\text{Å}^3$; $A_\mathrm{B} = 1.2\times10^9\,\text{Å}^2$ and $A_\mathrm{H} = 17\times A_\mathrm{B}$; $N_\mathrm{p} = 10^7, 5\times10^7$ (chosen to be the same for bacteria and host cells). If the full-analysis results are represented by filled symbols, the corresponding approximate results are described by dashed lines. The agreement between the two sets of results is excellent, especially for large C_H. For practical purposes, one can use Eq. 9 to examine peptide activity and selectivity as a function of C_H for $C_\mathrm{H} > C_\mathrm{B}$. The results in this figure seem to suggest that the agreement is good even when $C_\mathrm{H} \simeq C_\mathrm{B} = 5\times10^4$ cells/mL.

In contrast, it increases with C_H in the presence of $C_\mathrm{B} = 5\times10^4$ cells/mL. The presence of host cells in the competitive case works in favor of the host cells by enhancing the selectivity, more so for larger N_p. With the parameter choices used, the non-competitive selectivity can be an order of magnitude larger than the corresponding competitive one. Depending on how the selectivity is measured, it can be two or three order of magnitude different; for this, compare the solid line with unfilled squares in blue (non-competitive) and the dashed line with filled squares in purple (competitive).

The picture offered by the graph on the right in Fig. 6 is not only consistent with the earlier observation that the selectivity can be excessively overestimated[27] (see Ref.[14] for a theoretical basis) but also clarifies further how peptide selectivity is influenced by various factors or even the way it is measured: competitive, non-competitive, the presence of host cells, peptide trapping in dead cells, ...

So far, we have focused on analyzing Eq. 5 (or Eq. 4). When C_H is sufficiently large as in whole blood, one can use the approximate results in Eq. 9, which are easier to analyze. It is worth comparing the "full-analysis" results in Fig. 6 with the corresponding approximate results.

In Fig. 7, two sets of results are compared: full-analysis and approximate results for MHC/MIC (left axis) and MIC or MHC (right axis). If the former are based on Eq. 4 as in Fig. 6, the latter are obtained from Eq. 9. We have chosen the same peptide-membrane parameters used in Fig. 6: $(\mathrm{MIC})_0 = 1\,\mu$M and $(\mathrm{MHC})_0 = 5\,\mu$M; $w_\mathrm{B} = -16.6\,k_\mathrm{B}T$ and $w_\mathrm{H} = -6.72\,k_\mathrm{B}T$; $A_\mathrm{p} = 400\,\text{Å}^2$; $v_\mathrm{p} = 33^3\,\text{Å}^3$; $A_\mathrm{B} = 1.2\times10^9\,\text{Å}^2$ and $A_\mathrm{H} = 17\times A_\mathrm{B}$; $N_\mathrm{p} = 10^7, 5\times10^7$ (chosen to be the same for bacteria and host cells). If the full-analysis results are represented by filled symbols, the corresponding approximate results are described by dashed lines. The agreement between the two sets of results is excellent, especially for large C_H. For practical purposes, one can use Eq. 9 to examine peptide activity and selectivity as a function of C_H for $C_\mathrm{H} > C_\mathrm{B}$. The results in this figure seem to suggest that the agreement is good even when $C_\mathrm{H} \simeq C_\mathrm{B} = 5\times10^4$ cells/mL. For $C_\mathrm{B} = 5\times10^4$ cells/mL, the C_B-dependent in Eq. 5 is dominated by MIC_0 or MHC_0.

C. Membrane versus cell selectivity

There are both similarities and differences between membrane selectivity (Fig. 4) and cell selectivity (Fig. 6) of antimicrobial peptides. In both cases, the membrane or cell-density dependence of the selectivity is well manifested. If we set $C_\mathrm{H} = C_\mathrm{B}$, both membrane and cell selectivity decrease with cell density; the latter is somewhat larger except in the low-cell density limit. Similarly, in the presence of 5×10^9 cells/mL of host cells or neutral membranes (mimicking host cell membranes) as in whole blood, the selectivity decreases as C_B increases. In both cases, the selectivity tends to be overestimated in a non-competitive environment with reference to the corresponding competitive case; when $A_\mathrm{H} = A_\mathrm{B}$, however, the difference between competitive and non-competitive selectivity against model membranes appears to be minor, unless $C_\mathrm{B} \gtrsim 10^9$ cells/mL (Fig. 4). When C_B is held fixed at $C_\mathrm{B} = 5\times10^4$ cells/mL, the membrane selectivity remains nearly flat as a function of C_H, whereas the cell selectivity increases up to about 10 folds for $N_\mathrm{p} = 5\times10^7$; if $N_\mathrm{p} = 0$, the selectivity would remain nearly flat (the data not shown).

It is worth noting that the MICs in Fig. 4 are much smaller than the ones in Fig. 5. In contrast, the MHCs in the two figures are comparable. In the case of *E. coli*, the outer membrane enclosing the cell tends to raise MIC_0. In addition, peptide trapping in dead cells is also responsible for the differences between membranes and cells. Nevertheless, the qualitative picture offered from membranes (Fig. 4) is generally consistent with the one obtained for cells.

V. DISCUSSIONS AND CONCLUSIONS

We have presented a biophysical model of peptide activity and selectivity by combining a pedagogical approach with a Langmuir type model. If the former captures the cell-density dependence of peptide activity and selectivity in an intuitively-obvious way, the latter relates peptide binding (or trapping) to an effective binding (or trapping) energy.

Using the model, we have clarified how the presence of host cells and peptide trapping influence peptide selectivity and how competitive selectivity differs from non-competitive selectivity. If the competitive selectivity represents correctly a mixture of bacteria and host cells, the non-competitive one is obtained by combining MICs and MHCs for a homogeneous solution of bacteria and host cells, respectively. In this work, we chose parameters relevant for the peptide melittin. The results based on the model suggest a rather nontrivial dependence of the selectivity on the presence of host cells and peptide trapping; these factors or effects can enhance or reduce the selectivity depending on how the densities of host cells and bacterial cells are chosen. The presence of host cells works in favor of the host cells, but it raises the MIC up to about 10-fold.

When $C_{\rm B} = C_{\rm H}$, the selectivity decreases from the initial value $\mathrm{MHC}_0/\mathrm{MIC}_0$, more so for the non-competitive case; the selectivity is higher for the competitive case and is not sensitive to the choice of $N_{\rm p}$. In the presence of a large amount of host cells ($C_{\rm H} = 5 \times 10^9$ cells/mL), the selectivity decreases with increasing $C_{\rm B}$ in both competitive and non-competitive cases. The non-competitive selectivity can be one-order of magnitude larger than the competitive one. In contrast, when $C_{\rm B} = 5 \times 10^4$ cells/mL, the competitive selectivity increases with $C_{\rm H}$. Depending on how cell densities are chosen, the non-competitive selectivity can be larger than the competitive one by three orders of magnitude; the selectivity can be overly overestimated. Our work also clarifies how the cell selectivity of AMPs differs from their membrane selectivity. While the selectivity based on model membranes is typically larger than the one measured for cells, the difference between competitive and non-competitive selectivity is generally larger in the latter.

The non-trivial dependence of peptide selectivity on various factors or parameters noted above suggests that the selectivity does not just measure the intrinsic properties of peptides but it also reflects the "external" parameters, cell densities, and even the way the selectivity is measured (competitive vs. non-competitive). This is a natural consequence of MICs and MHCs that vary with cell densities: $C_{\rm B}$ and $C_{\rm H}$, the density of bacteria and host cells, respectively. Mapping out possible scenarios of peptide activity and selectivity thus would involve exploring wide ranges of $C_{\rm B}$ and $C_{\rm H}$, which are not easily realized in experiments.

If the involved peptide-membrane parameters are characterized, our model described by Eq. 5 or Eq. 9 (or Eq. 10) can be used as a predictive model. It enables one to calculate MICs, MHCs, and MHC/MIC, as a function of cell densities: $C_{\rm B}$ and $C_{\rm H}$, the density of bacterial and host cells, respectively.

Alternatively, Eq. 3 can be used as a fitting model for analyzing MIC and MHC data obtained in a non-competitive manner: the 'y'-intercept and the 'slope' can be extracted by fitting MIC or MHC data to Eq. 3a or Eq. 3b, respectively. This enables one to determine MIC_0 or MHC_0. Eq. 15 shows how these quantities are related to peptide's binding energy w ($w_{\rm B}$ or $w_{\rm H}$) and $(P/L)^*$ ($(P/L)^*_{\rm B}$ or $(P/L)^*_{\rm H}$). It is worth noting that P/L^* has been measured for various model membranes[11–13] as well as for cells[18]. Once P/L^* is known, MIC_0 and MHC_0 can be converted into $w_{\rm B}$ and $w_{\rm H}$, respectively. Conversely, if w is known, $(P/L)^*$ can be estimated. If all this information is used in the 'slope,' the value of $N_{\rm p}$ can be extracted.

The information from the homogeneous analysis above can be used in Eq. 9 and Eq. 10, which represent competitive cases. Accordingly, one can quantify peptide selectivity for a biologically relevant setting, which reflects the degree and location of infection. For instance, $C_{\rm B}$ ranges from 1 colony-forming unit (CFU/mL) (in blood stream, where $C_{\rm H} \approx 5 \times 10^9$cells/mL) to 10^9 CFU/mL (in soft tissue or peritonea) (see a recent review[8] and relevant references therein).

VI. ACKNOWLEDGEMENT

This work was supported by NSERC (Canada).

[1] M. Zasloff, "Antimicrobial peptides of multicellular organisms," Nature **415**, 389-395 (2002).

[2] K. A. Brogden, "Antimicrobial peptides: pore formers or metabolic inhibitors in bacteria?" Nat. Rev. Microbiol. **3**, 238-250 (2005).

[3] R. M. Epand and R. F. Epand, Biophysical Analysis of Membrane-Targeting Antimicrobial Peptides: Membrane Properties and the Design of Peptides Specifically Targeting Gram-negative Bacteria, in *Antimicrobial peptides discovery, design and novel therapeutic strategies*, ed. G. Wang, Cabi, 2010.

[4] Perron GG, Zasloff M, Bell G. Experimental evolution of resistance to an antimicrobial peptide. Proc R Soc B. (2006) 273: 251-256. doi: 10.1098/rspb.2005.3301

[5] Peschel A, Sahl HG. The co-evolution of host cationic antimicrobial peptides and microbial resistance. Nat Rev Microbiol. (2006) 4: 529-536. doi: 10.1038/nrmicro1441

[6] Hancock, R. E., Haney, E. F., and Gill, E. E. (2016). The immunology of host defence peptides: beyond antimicrobial activity. Nat. Rev. Immunol. 16, 321-334.

[7] Mookherjee N, Anderson MA, Haagsman HP, Davidson DJ. Antimicrobial host defence peptides: functions and clinical potential. Nat Rev Drug Discov. (2020) 19:311?32. doi: 10.1038/s41573-019-0058-8

[8] F. Savini, S. Bobone, D. Roversi, M. L. Mangoni, and L. Stella, "From liposomes to cells: Filling the gap between physicochemical and microbiological studies of the activity and selectivity of host-defense peptides," Peptide Science **110**, e24041–1-14 (2018).

[9] F. Savini, V. Luca, A. Bocedi, R. Massoud, Y. Park, M. L. Mangoni, and L. Stella, Cell-Density Dependence of Host-Defense Peptide Activity and Selectivity in the Presence of Host Cells, ACS Chem. Biol. 2017, 12, 52-56.

[10] M. Snoussi, J. P. Talledo, N.-A. D. Rosario, S. Mohammadi, B.-Y. Ha, A. Košmrlj, S. Taheri-Araghi, "Heterogeneous absorption of antimicrobial peptide LL37 in *Escherichia coli* cells enhances population survivability," **7**, *eLife*, e38174 (2018).

[11] Huang, H. W. Molecular mechanism of antimicrobial peptides: The origin of cooperativity. Biochim. Biophys. Acta, Biomembr. 2006, 1758, 1292-1302.

[12] Lee, M.; Hung, W.; Chen, F.; Huang, H. W. Many-Body Effect of Antimicrobial Peptides: On the Correlation Between Lipid's Spontaneous Curvature and Pore Formation. Biophys. J. 2005, 89, 4006-4016.

[13] Lee, M.-T.; Chen, F.-Y.; Huang, H. W. Energetics of Pore Formation Induced by Membrane Active Peptides. Biochemistry 2004, 43, 3590-3599.

[14] B. R. Schefter, S. Nourbakhsh, S. Taheri-Araghi and B.-Y. Ha, "Modeling Cell Selectivity of Antimicrobial Peptides: How Is the Selectivity Influenced by Intracellular Peptide Uptake and Cell Density," Front. Med. Technol. **22**, 626481 (2021).

[15] A. Bagheri, S. Taheri-Araghi, and B.-Y. Ha, "How Cell Concentrations Are Implicated in Cell Selectivity of Antimicrobial Peptides," Langmuir **31**, 8052-8062 (2015).

[16] S. Nourbakhsh, S. Taheri-Araghi, and B.-Y. Ha, "Toward building a physical model for membrane selectivity of antimicrobial peptides: making a quantitative sense of the selectivity," *Soft Matter*, **15**, 7509-7526 (2019).

[17] Starr, C. G., He, J., Wimley, W. C. Host cell interactions are a significant barrier to the clinical utility of peptide antibiotics. ACS Chem. Biol. (2016) 11:3391-9.

[18] Manuel N. Melo, Rafael Ferre and Miguel A. R. B. Castanho. Antimicrobial peptides: linking partition, activity and high membrane-bound concentrations. **7**, 2009, 245-250.

[19] Gregory, S. M.; Cavenaugh, A.; Journigan, V.; Pokorny, A.; Almeida, P. F. F. A Quantitative Model for the All-or-None Permeabilization of Phospholipid Vesicles by the Antimicrobial Peptide Cecropin A. Biophys. J. 2008, 94, 1667-1680.

[20] Ding, L.; Yang, L.; Weiss, T. M.; Waring, A. J.; Lehrer, R. I.; Huang, H. W. Interaction of antimicrobial peptides with lipopolysaccharides. Biochemistry 2003, **42**, 12251-12259.

[21] K. Dill and S. Bromberg, *Molecular Driving Forces: Statistical Thermodynamics in Biology, Chemistry, Physics, and Nanoscience*, 2nd Edt. (Garland Science, 2010).

[22] K. Matsuzaki, O. Murase, N. Fujii and K. Miyajima, "An Antimicrobial Peptide, Magainin 2, Induced Rapid Flip-Flop of Phospholipids Coupled with Pore Formation and Peptide Translocation," Biochemistry, 1995, **34**, 6521-6526.

[23] Lee, M.-T.; Hung, W.-C.; Chen, F.-Y.; Huang, H. W. Mechanism and kinetics of pore formation in membranes by water-soluble amphipathic peptides. Proc. Natl. Acad. Sci. U. S. A. 2008, **105**, 5087.

[24] S. B. Zimmerman and A. P. Minton, "Macromolecular crowding: Biochemical, biophysical, and physiological consequences," Annu. Rev. Biophys. Biomol. Struct. **22**, 27-65 (1993).

[25] H.-X. Zhou, G. Rivas, and A. P. Minton, "Macromolecular crowding and confinement: Biochemical, biophysical, and potential physiological consequences," Annu. Rev. Biophys. 37, 375-397 (2008).

[26] See for instance R. Philips, J. Kondev, J. Theriot, and H. G. Garcia, *Physical Biology of the Cell*, 2nd Edt. (Garland Science, 2013), Chapter 2.

[27] K. Matsuzaki, "Control of cell selectivity of antimicrobial peptides," Biochim. Biophys. Acta, Biomembr. **1788**, 1687-1692 (2009).

Chapter 3

Antimicrobial Peptides Activities: Salt dependence

3.1 Introduction

Electrostatic interactions are an important driving force for AMPs to exhibit cell selectivity. In general, changes in salt concentration affect electrostatic interactions. In fact, there are circumstances in which changes in salt concentration affect humans. For instance, salt concentrations in humans are normally constant, but hospitalized patients tend to have abnormal sodium levels. [52] Moreover, when foods get spoiled, the salt concentration in the product changes. [42] Due to these issues, other studies [29, 14, 67] have raised the problem that salt sensitivity impacts the activity of AMPs. Despite its significance in practice, the salt dependence of peptide activity has not been well understood. Recently, Taheri's group [87] measured MICs at various salt concentrations. Based on this, we introduced a theoretical model to calculate the binding affinity between the AMPs and the charged membranes and compared it with experimental data.

In an effort to understand the interactions between a charged membrane and AMPs, we first began by constructing a theoretical model and computed MICs with varying salt concentration. We then further compare the MICs against experimental results. Experimental MIC was measured for *E.coli* as a representative bacterium and the antimicrobial peptides LL-37. This chapter is structured as follows: In Sec. 3.2, we present our theoretical model that illustrates the interactions between the peptides and the bacterial cell membrane in an electrolyte solution containing monovalent cations such as Na^+. In Sec. 3.3, we analyzed the results for MICs. Finally, we further compared our theoretical results with the

experimental MICs from the Taheri lab [87].

3.2 Theoretical Model and Method

In this work, unlike the earlier model presented by Nourbakhsh et al. [63], we ignored lipid demixing induced by peptide binding for simplicity. Here, we begin by computing the total binding free energy between AMPs and charged cell membranes. We then map the free energy onto a binding energy as assumed in the Langmuir model introduced in Chap. 2.

3.2.1 Binding energy on salt (NaCl) concentration variations

A key quantity in our modeling is the total binding free energy between AMPs and a cell membrane. This binding free energy comprises three main elements: electrostatic energy, hydrophobic energy, and entropic free energy.

$$F_{\text{total}} = \sigma_p F_{\text{int}} + F_{\text{ent}} \tag{3.1}$$

Here, the interaction free energy term F_{int} is defined as $F_{\text{int}} = \Delta F_{el} + \epsilon$, which contains both the electrostatic energy (ΔF_{el}) and the hydrophobic energy (ϵ). In the last term on the right-hand side of Eq. 3.1, F_{ent} denotes the entropic free energy. Hydrophobic energy is set as the constant value between -8 and -14k_BT. The electrostatic energy (ΔF_{el}) involves several contributions, and here, we examine how each element affects the system.

Electrostatic Energy: The electrostatic energy is described as the interaction between the charged surface and charged peptides, with reference to the case where the peptides are far from a membrane [39, 41]:

$$\Delta F_{el} = F_{el}^{s} - F_{el}^{s}(0) - F_{el}^{L}. \tag{3.2}$$

Here, F_{el}^{s} represents the electrostatic free energy of bound peptides on the charged surface, and the remaining terms describe unbound peptides. The bound free energy term F_{el}^{s} can be determined by solving the non-linear Poisson-Boltzmann equation. Through the derivation found in the introduction Sec. 1.3.2, we take the final result of Eq. 1.24, i.e., [1]

$$F_{el}^{s} = \mathcal{A}_p \left(\sigma_{\text{net}} \Psi_0 - (4\epsilon\epsilon_0) \left(\frac{k_B T}{2} \right)^2 \kappa \left[\cosh \left(\frac{e\Psi_0}{2k_B T} \right) - 1 \right] \right). \tag{3.3}$$

Here, it is useful to introduce the Bjerrum length (l_B) defined as

$$l_B = \frac{e^2}{4\pi\epsilon_0\epsilon_r k_B T}, \tag{3.4}$$

where e is the electric charge, ϵ_0 is the permittivity of free space, and ϵ_r is the dielectric constant of water. Using l_B, the screening length (κ^{-1}) can be expressed as $\kappa = \sqrt{4\pi l_B n_{\text{total}}}$, where n_{total} is the total concentration of cations and anions in the solution. Now, using the l_B, Eq. 3.3 is then rewritten as

$$F_{el}^{s} = \mathcal{A}_p \left(\sigma_{\text{net}} \Psi_0 - \frac{\kappa}{\pi l_{\text{B}}} \left[\cosh\left(\frac{\Psi_0}{2} \right) - 1 \right] \right). \tag{3.5}$$

Here, the net charge density of the membrane is defined as $\sigma_{\text{net}} = Q/\mathcal{A}_p - f_A/a_l$ with f_A being the fraction of anionic lipids, a_l the area per lipid molecule, Q the charge of the peptide, and $\mathcal{A}_p$ being the surface area per bound peptide. Typically for LL-37 peptides, the effective charge is known to be $Q = 6$. Furthermore, the surface potential, derived as $\Psi_0 = 2\sinh^{-1}\left(\frac{2\pi l_{\text{B}}\sigma_{\text{net}}}{\kappa}\right)$, depends on the concentration of NaCl.

In the absence of peptide binding, the surface charge density is $\sigma_0 = -\frac{f_A}{a_l}$ and the surface charge potential is $\Psi_0^* = 2\sinh^{-1}\left(\frac{2\pi l_{\text{B}}\sigma_0}{\kappa}\right)$. This leads to

$$F_{el}^{s}(0) = \mathcal{A}_p \left(\sigma_0 \Psi_0^* - \frac{\kappa}{\pi l_{\text{B}}} \left[\cosh\left(\frac{\Psi_0^*}{2} \right) - 1 \right] \right). \tag{3.6}$$

Finally, assuming that the free peptides are spherical in structure the free energy in units of $k_B T$ of the peptide in a bulk is [39],

$$F_{el}^{L} = \frac{Z^2\, l_B\, 2\pi}{r_0(1 + \kappa r_0)}, \tag{3.7}$$

with r_0 being the radius of peptide ($r_0 = 15\mathring{A}$).

Entropy: The entropic free energy of bound peptides per $k_B T$ with reference to the bulk reads

$$F_{\text{ent}} = \sigma_p \ln\left(\frac{\sigma_p A_p}{n_p v_p} \right) - \sigma_p. \tag{3.8}$$

Here, σ_p represents the charge density of bound peptides, where $\sigma_p = \left(\frac{P}{L}\right)/a_0$. Furthermore, A_p is the physical area of the peptide set as $A_p = 400\mathring{A}^2$, the bulk concentration of the peptides n_p, and the volume of the peptides in the bulk chosen as $v_p = 33\mathring{A}^3$.

This outlines all the aspects required to calculate the electrostatic free energy. After substituting all the elements into Eq. 3.1, we calculated the total binding free energy between peptides and a membrane by taking two distinctive approaches.

Direct substitution method

In the first approach, we defined the total binding free energy as the sum of the electrostatic free energy ΔF_{el} (Eq. 3.2) and the hydrophobic energy ϵ, expressed as $\Delta F_{\text{total}} = \Delta F_{el} + \epsilon$. This total binding free energy (ΔF_{el}) was directly used as the binding energy (w_b) to compute the MIC. We adjusted the parameter values to reflect the experimental setup and to mimic the inner or outer membrane cell membrane. The choices of parameter values are described in each figure's caption.

Minimization method

In the second approach, we utilized the total binding free energy in Eq. 3.1 to derive the binding energy (w_b). Here, we minimize the total binding free energy in Eq. 3.1 with respect to the surface charge density of the peptide $\sigma_p = (P/L)/a_0$, where a_0 represents the surface area per lipid. As we vary the bulk concentration of peptides (C_p), we can find (P/L). Then we select the bulk concentration of peptides (C_p^*) at which the (P/L) becomes $(P/L)^*$ for the inner or outer membranes. The resulting values of bulk concentration of peptides (C_p^*) at the $(P/L)^*$, cell density (C_{cell}) and threshold value $(P/L)*$ enable us to calculate the binding energy (w_b) as follows:

$$W_B^*/k_bT = \ln\left(\left(C_p^* - \frac{A_B}{a_l}\left(\frac{P}{L}\right)^* C_{\text{cell}}\right) v_p \frac{\left(1 - \left(\frac{P}{L}\right)^* \frac{A_p}{a_l}\right)}{\left(\frac{P}{L}\right)^* \frac{A_p}{a_l}}\right) \tag{3.9}$$

Here, A_B is the surface area of a bacteria cell, and a_l represents the area per lipid. This binding energy derivation is analogous to the one introduced by Nourbakhsh et al. [63].

3.2.2 Mapping to Langmuir model

Section 3.2.1 introduced a procedure for finding the binding energy using two different approaches. To complete the theoretical model, we use the binding energy (w_b) in the

Langmuir model, introduced in Chap. 2. Since our interest lies in examining AMP activity against bacteria, we computed MICs. We take the MIC model of non-competitive and no peptide trapping cases from Chap. 2 written as:

$$\mathrm{MIC}\,(C_p^*) = \frac{A_{cell}}{a_l}\left(\frac{P}{L}\right)^* C_{\mathrm{cell}} + \mathrm{MIC}_0 \tag{3.10}$$

$$\mathrm{MIC}_0 = \frac{1}{v_p}\frac{\frac{A_p}{a_l}\left(\frac{P}{L}\right)^*}{1-\frac{A_p}{a_l}\left(\frac{P}{L}\right)^*} e^{w_b^*/k_BT} \tag{3.11}$$

All variables presented in Eq. 3.10 are the same as in Chap. 2, except for the threshold $(P/L)^*$. In Chap. 2, it was assumed that AMPs bind to the inner membrane. As a result, we selected the threshold value for the inner membrane of the bacterial cell to be $(P/L)^*_{\mathrm{B}} = 1/48$. [49, 44] However, the threshold value for the outer membrane should be much higher. Thus, we updated the threshold value suitable for the outer membrane by adopting the methods presented in the paper [76]. Following this approach, we found $(P/L)^* = 0.13$ by setting the reference Debye length to be $\kappa = 0.1\mathring{A}$ and the binding energy to be $w_B = -11.7k_BT$ at $\mathrm{MIC}_0 = 1.2\mu\mathrm{M}$. According to the study by Lai et al., [22], the threshold value for antimicrobial peptide LL37 is in the range between 0.1 and 0.2 at which the outer membrane is permeabilized. Thus, our estimate of $(P/L)^* = 0.13$ falls in this range. For generalization purposes in this model, we chose $(P/L)^* = 0.1$ to be the outer membrane threshold value.

3.2.3 Comparison with the Experimental Data

We compared the theoretical model against the experimental measurements [87]. These experimental data, however, need to be taken with caution. They only reveal the estimated MICs as a function of the Na^+ ion concentration. They do not explain which part of the lipid bilayer ruptures initially by AMPs. In order to comprehend the experimental data correctly, we applied two sets of parameters relevant for either inner or outer bacterial cell membranes. The theoretical model was then compared to the experimental results to evaluate which one better fits the data.

3.3 Results and Discussions

First, we applied our proposed methods (i.e., direct substitution method and minimization method) to find how peptide binding changes with respect to change in salt concentration. Then, we obtained the MIC results from our theoretical model. Through comparison of the MICs from the theory and experimental measurements, we described the interaction between AMPs and the outer and inner membranes of *E. coli*.

3.3.1 Direct substitution method

In the first direct substitution method, the total free energy was defined as the sum of the electrostatic free energy (ΔF_{el}) and the hydrophobic energy (ϵ), denoted as $\Delta F_{\text{total}} = \Delta F_{el} + \epsilon$. Here, the total free energy ΔF_{total} serves as the binding energy (w_b). w_b was calculated by changing the Na^+ concentration and the results are shown in Fig. 3.1 (a). According to Fig. 3.1 (a), as the Na^+ concentration increases in the solution, the magnitude of the binding energy (w_b) decreased. This suggests the electrostatic interaction between the membrane and the peptide gets reduced significantly as the concentration of Na^+ increases. This is because it is screened more effectively by the surrounding ions.

Furthermore, MICs were calculated using the binding energy (w_b) and mapped to the Langmuir model. As shown in Fig. 3.1 (b), MIC increases with the increasing Na^+ concentration. This effect is associated with the binding energy. As the binding energy decreases, the binding affinity of AMPs towards the cell membrane decreases. As a result, more peptides are required to rupture the bacterial cell membrane; thus, it increases the MIC. Additionally, Fig. 3.1 (b) represents that the theory and the experiments are a good agreement with each other.

3.3.2 Minimization method

Furthermore, we applied the second (i.e., minimization) approach to obtain the binding energy and MICs. To find the binding energy, we first computed the molar ratio of bound peptides to lipids (P/L) by minimizing the total binding free energy of Eq. 3.1 with respect to the planar density of bound peptides σ_p. Since we define $\sigma_p = (\frac{P}{L})/a_0$, we can calculate (P/L) while increasing the bulk concentration of peptide (C_p). The following result is presented in Fig. 3.3 (a), and the various color plots in the figure depict the different Na^+ concentrations. By selecting the bulk concentration of peptides (C_p^*) at which the (P/L) becomes $(P/L)^* = 0.1$ for the outer membrane, we derived the binding energy using Eq. 3.9

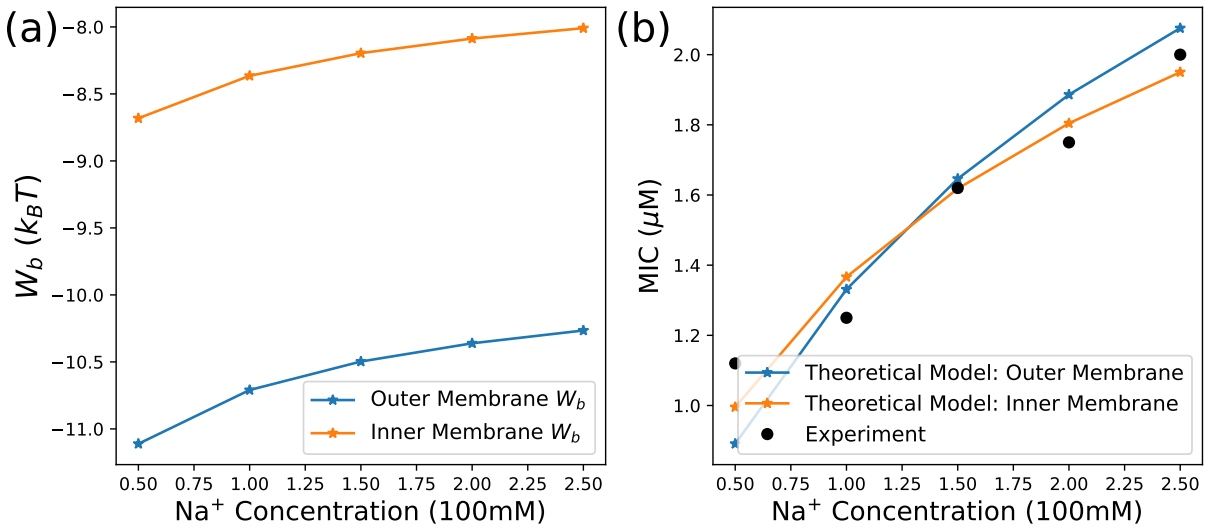

Figure 3.1: MIC results were generated by following the first direct substitution approach. The first direct substitution method takes the total free energy as a summation between the electrostatic free energy (ΔF_{el}) and the hydrophobic energy (ϵ), represented as $\Delta F_{\text{total}} = \Delta F_{el} + \epsilon$. (a) Binding energy ($w_b$) calculated as a function of sodium concentration variations (Na^+). The following parameters were chosen to model the outer membrane (presented with a blue curve): f_A = 1 (Fraction of anionic lipids), ϵ = -10 k_BT (Hydrophobic Energy), $\mathcal{A}_p$=194$\mathring{A}^2$ (Total area of lipid), Q=6 (peptide charge). The following parameters were selected to model the inner membrane (presented with an orange curve): f_A = 0.4 (Fraction of anionic lipids), ϵ = -7.25 k_BT (Hydrophobic Energy), $\mathcal{A}_p$=472$\mathring{A}^2$ (Total area of lipid), Q=6 (peptide charge). (b) MIC results for theoretical and experimental data. Theoretical MIC results were generated using the binding energies (w_b) found in subplot (a) and mapped into the Langmuir model. Threshold values were selected for the outer and inner membrane of the membrane, $(P/L)^*$ = 0.1 and $(P/L)^*$ = 0.02, respectively.

as shown in the Fig. 3.3 (b). Subsequently, the MIC values were obtained by utilizing w_b from Fig. 3.3 (b). Using this model, we were able to compute the MICs as a function of Na^+ concentration in the solution, as presented in Fig. 3.3 (c).

Following this method, however, the fit results for the outer and inner membranes were not optimal compared to the experimental ones. When the binding energy was calculated using the appropriate parameters relevant for the outer membrane, the binding energy was

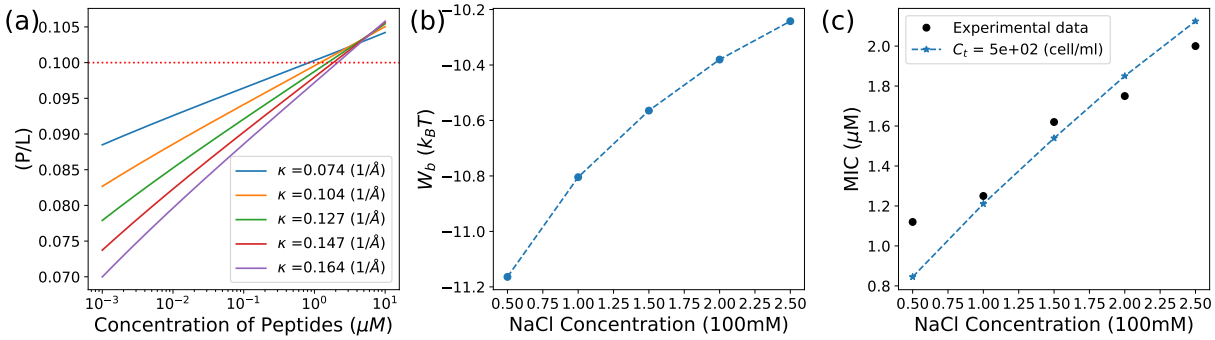

Figure 3.2: MIC results were generated by following the second (i.e., minimization) approach suitable for the outer membrane. (a) The molar ratio of bound peptides to lipids (P/L) plotted against the bulk concentrations of the peptides. (P/L) was computed by minimizing the total free energy with respect to the planar density of bound peptides (σ_p) at various salt concentrations, with peptide concentrations being the control variable. To find the best fit results in the outer membrane, the parameters were chosen as the follows: $f_A = 0.586$ (Fraction of anionic lipids), ϵ = -8 k_BT (Hydrophobic Energy), $(P/L)^* = 0.1$ (threshold value), Q=6 (peptide charge). (b) Binding energy (w_b) calculated with respect to variations in Na^+ concentration. (c) MIC results for theoretical and experimental data. Theoretical MIC results were generated using the binding energies (w_b) found in subplot (a) and mapped into the Langmuir model. As for the threshold values, $(P/L)^* = 0.1$ was selected to model the outer membrane.

observed to be large negative, ranging from -35 to $-27k_BT$, as shown in Fig. 3.3 (b). Due to the strong binding energy, this resulted in small MICs, which were inconsistent with the experiment, even at the high cell density of $C_{\text{cell}} = 5 \times 10^8$cells/ml. In contrast, the results were more promising after modifying the parameter values to be $f_A = 0.587$ and $\epsilon = -8k_bT$. The comparative results between the experiment and the newly fitted parameters of the theoretical model showed good agreement, as presented in Fig. 3.2 (c). Despite the agreement between the experiment and the newly fitted theoretical model, it is not entirely clear if the selected parameter values of the hydrophobic energy (ϵ) and the anionic lipid fraction (f_A) accurately describe the outer membrane. Nevertheless, the MIC results calculated using the minimization method and the outer membrane parameters are consistent with the experiment.

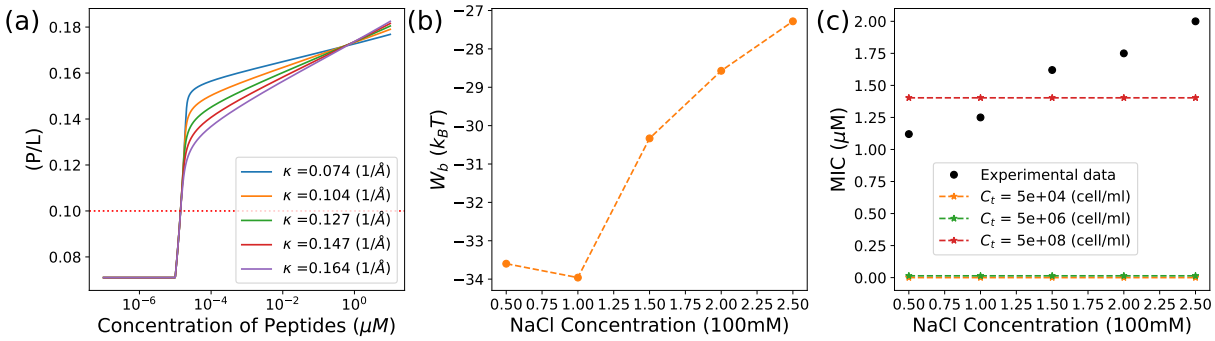

Figure 3.3: MIC results were generated by following the second minimization approach and fitting into the outer membrane. (a) The molar ratio of bound peptides to lipids (P/L) plotted against the bulk concentrations of the peptides. (P/L) was computed by minimizing the total free energy with respect to the charge density of the peptides (σ_p) at various salt concentrations, with peptide concentrations being the control variable. The ideal parameters for the outer membranes (as in the Fig. 3.1), were chosen as the follows: f_A = 1 (Fraction of anionic lipids), ϵ = -10 k_BT (Hydrophobic Energy), $(P/L)^*$ = 0.1 (threshold value), Q=6 (peptide charge). (b) Binding energy (w_b) calculated with respect to Na^+ concentration variations. (c) MIC results for theoretical and experimental data. Theoretical MIC results were generated using the binding energies (w_b) found in subplot (a) and mapped into the Langmuir model. As for the threshold values, $(P/L)^* = 0.1$ was selected to model the outer membrane.

3.3.3 Comparison with the Experimental Data

We took the experimental measurements and compared them with theoretical results using two different approaches. Figure 3.4 (a) was generated using the direct substitution approach and showed good agreement between the experiment and the theory in both inner and outer membrane cases. In contrast, Fig. 3.4 (b), generated using the minimization approach and only allowed to fit the outer membrane. This analysis supports the idea that fitting our theoretical model in terms of the outer membrane is suitable. It also suggests that the outer membrane rupture plays a significant role than the inner membrane in cell death driven by AMPs. If a given hypothesis is true, (P/L) should be greater in the inner membrane. The detailed calculation is not included in this section; however, through a computational check, it was verified that the inner membrane of (P/L) at MIC far exceeds the $(P/L)^* = 1/48$ threshold. This confirmed that the rupture of the AMPs caused by the outer membrane is more significant than the inner membrane.

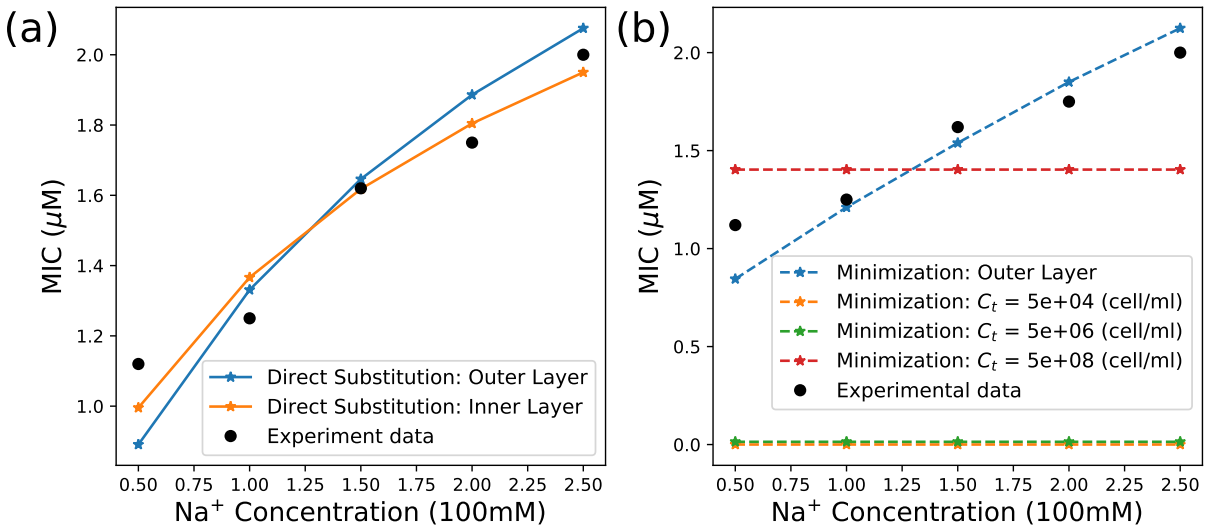

Figure 3.4: Comparisons between the experiments and theoretical results for MICs under salt concentration variations. (a) A first direct substitution method was used to produce a model result for both the inner and outer membrane binding of AMPs. The list of chosen parameters to fit the outer layers of the membrane is as follows: $f_A = 1$ (Fraction of anionic lipids), ϵ = -10 k_BT (Hydrophobic Energy), $\mathcal{A}_p$=194$\mathring{A}$ (Total area of lipid), and $(P/L)^* = 0.1$ (threshold value). The selection of the parameters to suit the inner membrane is as follows: $f_A = 0.4$ (Fraction of anionic lipids), ϵ = -7.25 k_BT (Hydrophobic Energy), $\mathcal{A}_p$=472$\mathring{A}$ (Total area of lipid), and $(P/L)^* = 0.02$ (threshold value) (b) A second minimization method was used to produce the result. The blue curve is the optimal fitting result calculated with the following parameters: $f_A = 0.586$ (Fraction of anionic lipids), ϵ = -8 k_BT (Hydrophobic Energy), $(P/L)^* = 0.1$ (threshold value). The remaining color curves do not show optimal fitting even at the high cell density limit of $C_t = 5 \times 10^8$ cells/ml. The following parameters are used to calculate the remaining curves: $f_A = 1$ (Fraction of anionic lipids), ϵ = -10 k_BT (Hydrophobic Energy), and $(P/L)^* = 0.1$ (threshold value).

In this study, we focused on examining the effect of binding affinity between AMPs and cells under variations in Na^+ ion concentration. In practice, however, the implications of divalent ions are considered more significant than the Na^+ ion. For instance, other studies [59, 60] have highlighted that Mg^{2+} ions play a competitive role between peptides. This naturally leads to another question of the behavioral changes in the presence of Mg^{2+} ions. Although we attempted to tackle this problem, we were unable to resolve the issue

in a given time frame. A simple way to incorporate the Mg^{2+} ions is as follows. From our second minimization method, the nonlinear PB equations can be replaced with a linearized PB equation (i.e., the renormalized Debye Hückel theory). Through this adjustment, the charge density of the peptide can be determined more accurately and further help us find the refined results in MIC.

3.4 Conclusion

In this work, we introduced a theoretical model that explains the interaction between AMPs and charged membranes in solutions containing salt ions. Our model showed that when the presence of salt ions diminished, the binding of AMPs to bacterial cell membranes tended to increase. As a result, MICs decreased. In addition, when the theoretical results were compared to the experiments, we found that the fitting results were more suitable for the outer membrane model. This implied that the rupture of the outer cell membrane plays a more important role in the process of cell rupture, leading to cell death. Furthermore, we anticipate that the additional work of incorporating Mg^{2+} ions into the system will help to improve the model for explaining the interactions between cell membranes and the AMPs in an electrolyte solution.

Chapter 4

Interaction between the Antimicrobial Peptides and the Protective layers of Lipopolysaccharide

4.1 Introduction

Unlike Gram-positive bacteria or eukaryotic cells, Gram-negative bacteria are known to have outer membranes (OMs) and inner membranes. In particular, the outer layer of the outer membrane (OM) is mainly composed of lipopolysaccharide (LPS). [72, 80] This outer LPS layer plays a crucial role as a protective layer against the invasion of toxic materials. [66] In the previous theoretical model introduced by Nourbakhsh et al. [64], they investigated the interaction between AMPs and LPS under various conditions. Here, we extend this effort to examine the protective role of LPS in wider parameter ranges. One suggestive idea is to increase the strength of the attractive energy between the brush and peptides. As we increase the binding affinity between the brush and peptides, more peptides get trapped inside the brush, leaving fewer peptides to bind to the lipid head group region. The first part of this chapter focuses on the effects of peptide-brush interactions on peptide activity. Our attempts will become useful for finding optimized AMPs for fighting Gram-negative bacteria.

Furthermore, numerous studies [59, 60] have noted that the presence of divalent ions in the Gram-negative bacterial environment is crucial for inhibiting the binding of external

sources like AMPs. In the previous Chap. 3, we only explored the impact of Na^+ ions and left out divalent ions. Here, we integrate divalent ions into the system to replicate a more accurate model of the bacteria cell surface and investigate the interaction between AMPs and LPS.

The main goal of this chapter is to clarify how variations in two biologically significant factors influence the interaction of AMPs with bacterial LPS. Initially, we used a theoretical model and examined the consequences of changing peptide-brush attractive energy (ϵ_{att}). In addition, we investigated AMP binding to the membrane in the presence of two types of salt (Na^+ and Mg^{2+}) in the solution. The remaining chapter is structured as follows: In Sec. 4.2, we introduced background materials on the cell surface of Gram-negative bacteria and the theoretical lattice model that describes the interaction between AMPs and LPS layers in an electrolyte solution. In Sec. 4.3, we described the process of adjusting the strength of brush-peptide interactions and the concentration of ions. In Sec. 4.4, we analyzed the interaction between AMP-LPS due to the change in attractive energy (ϵ_{att}) and salt concentration.

4.2 Preliminary

4.2.1 Anti-symmetrical Lipopolysaccharide (LPS)

The LPS layer of Gram-negative bacteria such as *E.coli* helps to prevent the invasions of toxic materials. In this study, we focused on examining the stability of the LPS layer. Generally, LPS contains three major structural domains: phospholipid A, core oligosaccharides, and O antigens, as shown in Fig. 4.1. [72, 95, 80] Lipid A is located in the innermost part of the LPS and anchors the LPS to the OM through its hydrophobic properties from the fatty acid component. It also includes endotoxins responsible for the toxicity of Gram-negative bacteria. [72, 95] The core domain contains oligosaccharide components and is divided into inner and outer parts of the core. The inner core is covalently bound to lipid A and consists of 1-3 keto deoxy octanoate (KDO) residues. The remaining core portion, linked to the O antigen, is the outer core, which consists of hexose residues. Finally, the O antigen is located in the outermost domain and comprises repeating units of oligosaccharides composed of 2-6 sugars. [72, 95]

In the presence of salts such as sodium (Na^+) or magnesium ions (Mg^{+2}), LPS provides the binding sites on the sugar groups of lipid A and the Kdo groups of the inner core to neutralize the negative charge of phosphate groups present on the molecule. [60, 8]

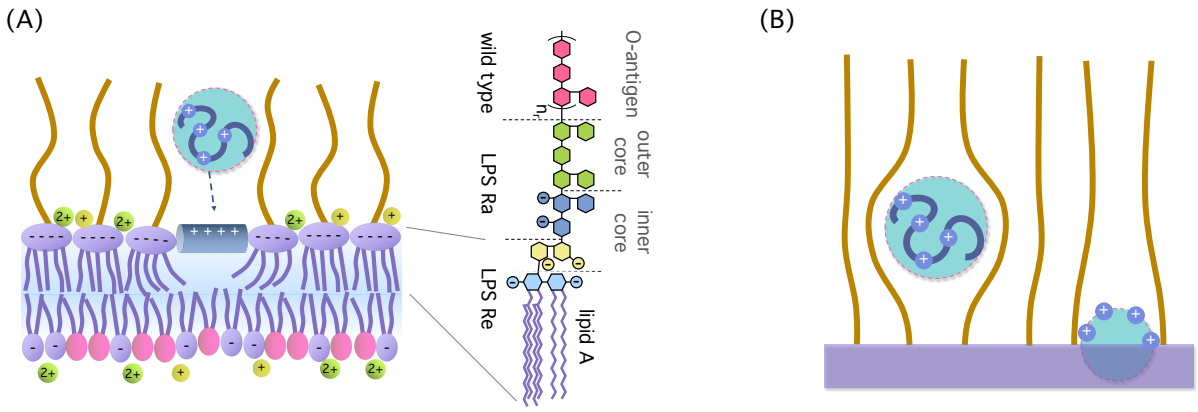

Figure 4.1: Schematic diagram of AMP interfacially bound to Gram-negative bacteria on a LPS layer. (a) Structures of the OM of the Gram-negative bacteria with LPS presented with the molecular details. The left side of the figure represents the bound AMP molecules on the OM. The right-hand side of the LPS layers of each sugar molecule is presented with a hexagon with a different color. For example, the pink hexagon represents the repeating units of O-antigen. In the mid panel, each hexagon represents GluN (glucosamine) colored in light blue, Kdo (2-keto-3-deoxy octanoic acid) in yellow, and heptose in gray blue. (b) Schematics of two different binding modes on the peptides trapped or bound to the LPS layer. The left side of the diagram represents the tertiary binding of the peptide trapped in the brush layer, and the right side represents the primary binding of the peptides, weakly bound to the membrane. This figure is adapted with permission from ref. [64]. (Copyright 2021 American Chemical Society)

Furthermore, LPS provides the same binding sites to the cationic peptides just like the divalent ions. Thus, in the presence of divalent ions, the binding of AMPs decreases due to competition. [59, 60]

4.2.2 Theoretical Model

In this work, instead of using the mean-field method applied in the previous Chap. 3, we adopt the lattice model to find the binding energy between the charged membranes and the AMPs. The major difference between the two comes from the way the binding sites are described. The mean-field approach assumes charged ions are smeared out across the surface. Whereas, in the lattice model, the electrostatic binding sites are discretized into a small square lattice. This allows the model to capture details on the charge discreteness,

ion-pairing, and non-uniform charge effects. [45] In this work, we adopted the model from paper [64]. Here, we elaborate on the major components that contribute to the binding energy.

The first step is to determine the total free energy for the multivariate LPS-peptide-ion system. The total free energy comprises of four components: primary binding energy (F_{pri}), ternary binding energy (F_{ter}), entropic for the free peptides ($E_{\text{p}}^{\text{free}}$) and the free ions ($E_i^{\text{free}}$). Among these components, we add two binding energy terms and subtract the entropy, where the complete form is written as:

$$F_{\text{total}} = F_{\text{pri}} + F_{\text{ter}} - E_{\text{p}}^{\text{free}} - E_i^{\text{free}} \tag{4.1}$$

Here, the binding energy is divided into two terms, i.e., primary binding and tertiary binding. They are distinguished according to the way the AMPs bind with LPS. In the primary binding, the peptide binds to the interface of the membrane. These interfacially bound peptides are expressed as N_{p}. In contrast, in the ternary binding, the peptides get trapped within the LPS brush, and the number of trapped peptides is denoted by NpBA.

Entropy ($E_{\text{p}}^{\text{free}}$ and $E_{\text{i}}^{\text{free}}$)

$$E_{\text{p}}^{\text{free}} = (N_{\text{p}} + N_{\text{pB}}) \ln \left(v_p \left(C_p - C_{\text{cell}} N_p - C_{\text{cell}} N_{\text{pB}}\right)\right) \tag{4.2}$$

$$E_i^{\text{free}} = \sum_{i=1}^{2} N_i \ln \left(\frac{4}{3}\pi r_i^3 C_i\right) \tag{4.3}$$

The entropy of the free peptides ($E_{\text{p}}^{\text{free}}$) is comprised of the chemical potential of the free peptide $\mu_{\text{p}}^{\text{free}} = \ln \left(v_p \left(C_p - C_{\text{cell}} N_p - C_{\text{cell}} N_{\text{pB}}\right)\right)$ and the total number of bound peptides ($N_{\text{p}}+N_{\text{pB}}$). The free ions such as Na^+, and Mg^{2+} of the entropies are expressed $E_{\text{i}}^{\text{free}}$, where the subscripts ($i = 1, 2$) represent the monovalent and divalent cations, respectively. Thses entropies are composed of the chemical potentials of the free ions $\mu_{\text{i}}^{\text{free}} = \ln \left(\frac{4}{3}\pi r_i^3 C_i\right)$ and the total number of ions μ_i^{free}. Each of the C_j terms ($j = p, \text{cell}, i$) represents the bulk concentration of peptides (C_p), cell (C_{cell}) and ionic concentration (C_i ($i = 1, 2$)), respectively.

Binding Energy (Primary: F_{pri} and Ternary: F_{ter})

$$F_{\text{pri}} = F_{\text{el}} + \varepsilon_I N_{\text{p}} + F_{\text{def}} + \Delta F_{\text{brush}}^{\text{prim}} + F_{\text{ent}}^{\text{prim}} \tag{4.4}$$

$$F_{\text{ter}} = \Delta F^{\text{ter}}_{\text{brush}} + F^{\text{ter}}_{\text{ent}} \tag{4.5}$$

Here, the primary binding (F_{pri}) and the ternary binding (F_{ter}) terms include several more contributions. Specifically, the primary binding energy (F_{pri}) presented in Eq. 4.4 are composed of (starting from the first term on the right-hand side of the equation) electrostatic free energy (F_{el}), hydrophobic energy (ε_I), membrane deformation free energy (F_{def}), brush free energy ($\Delta F^{\text{prim}}_{\text{brush}}$), and bound entropic free energy ($F^{\text{prim}}_{\text{ent}}$). Moreover, the terms in Eq. 4.5 of the ternary binding (F_{ter}) refers to brush free energy ($\Delta F^{\text{ter}}_{\text{brush}}$), and bound entropic free energy ($F^{\text{ter}}_{\text{ent}}$). Each component is comprised of other effective energies determined by multiple contributions. In the following section, we break down each component and elaborate on the details.

Electrostatic Free Energy (F_{el}): This electrostatic part of the energy was adapted from papers [64, 82, 45, 46]. According to the approach provided in ref. [82], the electrostatic free energy of the LPS layer, F_{el}, is written as:

$$F_{\text{el}}(N_p, N_1, N_2) = F_{\text{self}} + F_{\text{MF}} + F_{\text{pair}} + F_{\text{lat}} \tag{4.6}$$

This electrostatic energy is typically affected by the three main components of N_p, N_1, and N_2. Here, N_p is the number of peptides bound to the LPS interface, and N_1 and N_2 are the number of monovalent and divalent cations, respectively. The self-energy of bound particles (ions or AMPs) in bulk is denoted as F_{self}, which is constant in a homogeneous medium but changes when it gets close to a dielectric interface. At the mean-field level, F_{MF} depicts the interaction between bound particles. F_{pair} represents the ion-pairing energy between opposing charges. The final term, F_{lat}, describes a lateral correlation between LPS and bound charges.

The **self-free energy of bound particles (F_{self})** is derived from the previous studies [64, 82, 45, 46], with the bound particles being the cations and the peptide written as follows:

$$F_{\text{self}} = \sum_{i=1}^{2} N_i \frac{Z_i^2\, l_B}{2} \left[\frac{\eta}{\delta_i} + \frac{\kappa}{1+\kappa r_i}\right] + N_{\text{p}} \frac{Q\, l_B}{2} \left[\frac{\eta}{\delta_p} + \eta \frac{\mathcal{M}_Q - \mathcal{M}_1}{a^2} + \frac{\kappa}{1+\kappa r_1}\right] \tag{4.7}$$

The bound ion is represented by the first term on the right-hand side of the equation, and the second term describes the peptides. Several factors influence self-energy in this case,

including Bjerrum length (l_B) and Debye length (κ). With both monovalent and divalent ions present in the solution, Debye length is defined as $\kappa = 4\pi l_B 2[n_1 + (1+2)n_2^2]$ and here, the Bjerrum length being $l_B = \frac{e^2}{4\pi\epsilon_r\epsilon_0 k_B T}$. The remaining terms of δ_i or δ_p represent the gap distance between a bound ion or peptides and the LPS charges, respectively. Also, due to the impact of dielectric discontinuities on the LPS surface, we set $\eta = 1$ ($\approx \frac{\epsilon_w - \epsilon_l}{\epsilon_w + \epsilon_l}$). Lastly, $\mathcal{M}_j$ terms are presented to compensate for the electrostatic free energy for the over-counting of Coulomb interaction, and it is defined as, $\mathcal{M}_j(\kappa, a) = \int_{-aj/2}^{+aj/2} dx \int_{-aj/2}^{+aj/2} dy \frac{e^{-\kappa\sqrt{x^2+y^2}}}{x^2+y^2}$.

The **mean-field electrostatic free energy ($F_{\mathbf{MF}}$)** in the papers [64, 82, 45, 46] is calculated as follows:

$$F_{\mathrm{MF}} = \frac{l_B(1+n)}{\tilde{N}_0}\Bigg[\left(\frac{\pi}{\kappa} - \frac{\mathcal{M}_1}{2}\right)(N_0 - N_1 - 2N_2 - QN_{\mathrm{p}})^2 - \frac{\mathcal{M}_Q - \mathcal{M}_1}{2}(QN_{\mathrm{p}} + 2N_2 + QN_{\mathrm{p}})\Bigg] \tag{4.8}$$

Moreover, the **ion-pairing energy ($F_{\mathbf{pair}}$)**, one of the remaining terms of transverse interaction between cations and LPS charges, or the ion-pair interaction from ref. [64, 82, 45, 46] is derived as:

$$F_{\mathrm{pair}} = -l_B\,(1+n)\left(\sum_{i=1}^{2} N_i\frac{Z_i}{\delta_i} + N_{\mathrm{p}}\frac{Q}{\delta_{\mathrm{p}}}\right) \tag{4.9}$$

Finally, the residual **lateral free energy ($F_{\mathbf{lat}}$)**, referred to in the paper. [64, 82, 45, 46] as the lateral correlation free energy, is obtained as:

$$F_{\mathrm{lat}}\tilde{N}_0 \approx 2\frac{N_+ N_-}{\tilde{N}_0}\,\Sigma_{\mathrm{alt}}, \tag{4.10}$$

where Σ_{alt} denotes the electrostatic energy between one lattice site and the rest of the alternatively charged lattice written as:

$$\Sigma_{\mathrm{alt}} = l_B(\Delta_\epsilon + 1)\frac{1}{2}\sum_{i=1}^{\infty}\sum_{j=1}^{i}(-1)^{i+j-1}\frac{e^{-\kappa a\sqrt{i^2+j^2}}}{a\sqrt{i^2+j^2}}\,k(i,j)\,,$$

$$\text{here } k(i,j) = \begin{cases} 4, & \text{if } j = 0 \text{ or } i = j \\ 8, & \text{otherwise} \end{cases}$$

Hydrophobic Energy (ε_I): Hydrophobic energy denoted with the ε_I is attained when the hydrophobic portion of the peptide binds to the interface of the LPS layer, particularly inside the acyl chain region. This interaction between the peptide and the LPS layer associated with the hydrophobic bond extends the original area of the LPS surface and perturbs the lattice regions. Thus, this gives rise to the change in the number of lattice sites as the peptide bonds, which is equal to $\tilde{N}_0 = N_0 + \Omega N_{\mathrm{p}}$. [64]

Membrane Deformation Free Energy ($F_{\mathbf{def}}$): Hydrophobic binding of the peptide to the LPS layer occurs at the expense of membrane deformation as the peptide perturbs the surrounding lipids. Here, F_{def} membrane deformation energy around the threshold value of $(P/L)^*$ in the unit of k_BT is expressed as:

$$F_{\mathrm{def}} = \frac{a_0^2}{2} K_A \frac{(QN_{\mathrm{p}})^2}{N_0}, \tag{4.11}$$

where the K_A represents the area stretch modulus. We take the number of the additional site as ΩN_p, which is created by the peptide-induced membrane expansion. The expansion area per peptide, Ωa_0^2, is known to differ from the cross-section of the peptide.

Brush Free Energy ($\Delta F^{\mathbf{prim}}_{\mathbf{brush}}$, $\Delta F^{\mathbf{ter}}_{\mathbf{brush}}$): The brush-free energy term is the most distinctive component for obtaining the free energy in the LPS layer as opposed to generalized bacteria cells. Others have proposed brush-free energy ($\Delta F_{\mathrm{brush}}$) in a few different research. [85, 34] As discussed in these papers and adopting the views of volume exclusion between the peptides and the LPS monomers caused by the repulsive forces, we take the free energy as in the ref. [64] presented as follows:

$$\Delta F^{\mathrm{prim}}_{\mathrm{brush}} = \beta \left(\frac{\phi^3}{b^3} V_{\mathrm{cyl}} + \frac{\phi^2}{b^2} A_{\mathrm{cyl}} + \frac{\phi}{b^2} A_{\mathrm{cyl}}\, \epsilon_{\mathrm{attr}} \right) \tag{4.12}$$

$$\Delta F^{\mathrm{ter}}_{\mathrm{brush}} = \frac{\phi^3}{b^3} V_{\mathrm{sph}} + \frac{\phi^2}{b^2} A_{\mathrm{sph}} + \frac{\phi}{b^2} A_{\mathrm{sph}}\, \epsilon_{\mathrm{attr}} \tag{4.13}$$

In the following Eq. 4.12 and Eq. 4.13, the brush and the peptide interact with weak attractions of Van der Waals forces or hydrogen bonds that enable to trap the peptide within the brush chain. Specifically, the given formula adopts a scaling method to obtain peptide trapping that considers the weak interaction between the inclusion and the brush chains. Furthermore, the essential control parameter in this brush free energy comes from the interaction per monomer that is in contact with the surface of inclusion, labeled as the ϵ_{att}. The remaining parameters represent the volume and the area of peptides modeled as

cylinder or spherical as specified in the subscript. Lastly, the β term appearing in Eq. 4.12 indicates different binding modes to which peptides interact within the LPS interface.

Bound Entropic Free Energy ($F_{\mathbf{ent}}^{\mathbf{prim}}$, $F_{\mathbf{ent}}^{\mathbf{ter}}$): To compute the entropic free energy, we distinguish between primary and ternary terms and express it as follows:

$$F_{\text{ent}}^{\text{pri}} = \sum_{i=1}^{2} N_i \ln\left(\frac{N_i}{\tilde{N}_0}\right) + N_{\text{p}} \ln\left(\frac{\Omega N_{\text{p}}}{\tilde{N}_0}\right) \tag{4.14}$$

$$+ (\tilde{N}_0 - N_1 - N_2 - \Omega N_{\text{p}}) \ln\left(1 - \frac{N_1 + N_2 + \Omega N_{\text{p}}}{\tilde{N}_0}\right)$$

$$+ \frac{1-\Omega}{\Omega}(\tilde{N}_0 - \Omega N_{\text{p}}) \ln\left(1 - \frac{\Omega N_{\text{p}}}{\tilde{N}_0}\right) - N_{\text{p}} \left(\left(\frac{(4+4/\Omega)^2}{16\pi/\Omega}\right) + 1\right) \tag{4.15}$$

$$- \frac{\tilde{N}_0}{\Omega} \ln\left(1 - \frac{\Omega N_{\text{p}}}{\tilde{N}_0}\right) + \frac{\tilde{N}_0 \left(\frac{(4+4/\Omega)^2}{16\pi/\Omega}\right)}{\Omega(1 - \Omega N_{\text{p}}/\tilde{N}_0)}$$

$$dF_{\text{ent}}^{\text{ter}} = \tilde{N}_0^{\text{ter}} \phi_{\text{p}} \ln \phi_{\text{p}} + (1 - \phi_{\text{p}}) \ln(1 - \phi_{\text{p}}) \tag{4.16}$$

In the $F_{\text{ent}}^{\text{pri}}$, all the bound particles are considered including the peptides and cations of Na^+ and Mg^{2+}. In Eq. 4.14, the first two lines represent the number of ways the particles N_1 Na^+ ions, N_2 Mg^{2+} ions, and N_p peptides can be arranged in the lattice at the binding sites of N_0. The term Ω refers to the number of sites on the LPS surface that each peptide takes up. Whereas Eq. 4.16 explains ternary entropy, which is only associated with the trapped peptides within the brush specified by $\phi_p = \frac{V_p^{\text{sph}} N_{\text{pB}}}{H_{\text{brush}}(N_{\text{p}})[A + \Delta A(N_{\text{p}})]}$. The number of ternary binding sites, represented by $\tilde{N}_0^{\text{ter}}$, is expressed as $\tilde{N}_0^{\text{ter}} = H_{\text{brush}}(N_{\text{p}})[A + \Delta A(N_{\text{p}})]/V_{\text{sph}}$, followed by the ref. [64, 82, 45, 46].

In this section, we did not explicitly specify all the parameter values used in this work. Unless otherwise stated, the majority of the parameters are taken from the original paper [64]. Furthermore, to complete the calculation, we used the free binding energy Eq. 4.1 obtained earlier. From the given Eq. 4.1, we took the minimization approach to find the optimize energy and determine the number of bound particles (N_1,N_2,N_{p},N_{pB}) at the total number of binding sites (N_0). We also applied additional modifications to the model to correctly capture the interaction between bacterial LPS and AMPs.

4.3 Method

4.3.1 Brush-Peptide attractive energy ($|\epsilon_{att}|$) variations

To update the brush-peptide attractive energy ($|\epsilon_{att}|$) in the model, the key is to capture the distinctions between the primary and ternary binding in the LPS. As discussed earlier, the primary binding refers to the peptide bindings to the interface of the LPS, whereas ternary binding indicates the peptide getting trapped within the brush. In the previous study [64], the primary binding was described to have a weak attraction, which was reflected by setting $\beta = 1/2$ in Eq. 4.12. This β parameter describes how much the peptide and the LPS brush interact. However, to remove the weak attractive constraints and observe the effect of the ternary binding, we removed the last term containing ϵ_{att} from Eq. 4.12. Making the following changes makes it easier to pay attention to the attraction between the brush and the peptide. Furthermore, we adjusted the ϵ_{att} parameter, typically greater than $0.1k_BT$ in magnitude.

Furthermore, while increasing the ϵ_{att}, we adjusted the two conditions to observe significant impact: 1. high cell density 2. long brush length. Setting up the high cell density limit reduces the volume occupancy to a fixed number of peptides since the cell density is defined as the 'number of peptides/total number of volumes'. Thus, increasing the cell density is equivalent to decreasing the total volume. This causes AMPs to behave within the constrained volume and makes it easier to capture the behavior. Moreover, extending the length of the brush enables the brush to stretch out further so that AMPs get trapped easily within the brush.

4.3.2 Ionic concentration variations

In previous Chap. 3, we studied the interaction between the AMPs and the cell membranes under Na^+ concentration variation. Here, we incorporate divalent ions to replicate a more realistic model. This model has three control parameters: monovalent, divalent, and peptide concentration. Since we are interested in the behavior of AMP, we control the concentration of ions based on the AMP concentration change. As numerous parameters are associated with the model, we divide it into several cases. First, we fixed the monovalent concentrations at $\approx$ 100mM and controlled the divalent ion concentration. Second, we fixed the divalent ion close to zero and controlled the monovalent concentrations. Finally, we fixed the divalent concentration at 5mM and controlled the monovalent concentrations. This allows us to examine the results in various scenarios.

4.4 Results and Discussions

4.4.1 Brush-Peptide attractive energy ($|\epsilon_{att}|$) variations

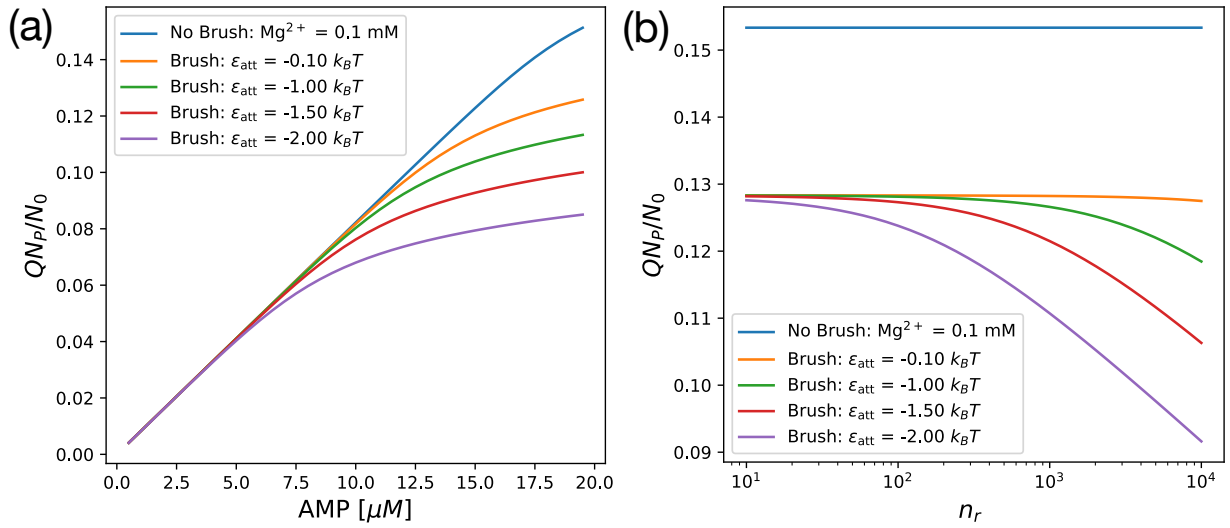

Figure 4.2: (a) The bound peptides to lipid ratio (QN_p/N_0) result with AMPs as the control variate at various attractive energy (ϵ_{att}). The parameters are set as follows: Cell density (C_{cell}) = 1×10^{10}cells/ml, area-stretch modulus (K_A) =200pN/nm, brush length (n_r) = 20000, and Mg^{2+} = 0.1mM. The number of bound peptides (N_p) decreases with an increase in the magnitude of the attractive energy ($|\epsilon_{att}|$). The blue curve represents no brush term ($n_r = 0$) and has the largest binding peptide (N_p) due to the non-interference from the other factors. (b) The bound peptide to lipid ratio (QN_p/N_0) results, with brush length (n_r) being the control variable at various ranges of attractive energy (ϵ_{att}). The parameters are set as follows: Cell density (C_{cell}) = 1×10^{10}cells/ml, AMP concentration (C_p) = 20μM, and Mg^{2+} = 0.1mM. The attractive energy does not affect the number of bound peptides (N_p) at a short brush length. The discrepancy is observed at large brush lengths. The blue curve indicates no brush term ($n_r = 0$) and is set as a reference curve to compare with other results.

Following the method, we computed the molar ratio of bound peptides to lipids (QN_p/N_0) as shown in Fig. 4.2. Unless specified, we apply the same parameters as in the original model without further adjustment.[64] Here, we used cell density (C_{cell}) = 1×10^{10} cells/ml, LPS area-stretch modulus (K_A) =200 pN/nm, brush length (n_r) = 2000, and

$Mg^{2+} = 0.1$mM. Figure 4.2 (a) represents the result of QN_p/N_0 controlled by the concentrations of the AMPs. (Here, the notation for the bound peptides to lipid ratio (QN_p/N_0) differs from the previous chapters but corresponds to the same notion of (P/L)). The results show that the ratio of bound peptides decreased as the magnitude of the attraction energy ($|\epsilon_{att}|$) increased. As expected, the majority of peptides get trapped inside the brush through the ternary binding. Subsequently, a lower amount of peptide gets bound to the LPS interface as $|\epsilon_{att}|$ increases. This result verifies that our hypothesis is indeed true.

One caveat to the Fig. 4.2 (a) is that, the brush length (n_r) was selected to be $n_r = 20,000$, which is physically unreasonable. To gain better insights into the brush length effects, we fixed the AMP concentration and varied the brush length (n_r) at different ϵ_{att} as in Fig. 4.2 (b). The results show that ϵ_{att} does not contribute to the bound peptide ratio at a short brush length and starts to decrease at a large brush length around $n_r = 100$ and large $|\epsilon_{att}|$. To show a clear comparison, we added the no-brush case, represented with the blue curve. In the no-brush case, peptides can easily be bound to the membrane since there is no interference, allowing them to have the largest bound peptide to lipid ratio. Thus, Fig. 4.2 (b) illustrates the effects of the brush length effects. However, it remains questionable on the physically acceptable range. Generally, the frequently repeated unit of n_r falls between 8 and 15. In our Fig. 4.2 (b), this range has substantially less influence. This leaves room for further investigation.

Exploring Fig. 4.2 does not reveal the amount of peptide trapped within the bush. To supplement the descriptions of the idea that less peptide gets bind at the LPS interface, we compared the cross-sectional area of the trapped peptide in the volume with that of the bound peptide at the interface region. The cross-sectional area of the trapped peptide is calculated by the volume fraction of the trapped peptide (ϕ_p) times the brush height (H_{Brush}). The result of our the proposed method is presented in Fig. 4.3 (a), which shows that the ratio increased as the number of peptides increased. Simultaneously, as shown in Fig. 4.3 (b), a shift toward long brush length units increased peptide trapping at large $|\epsilon_{att}|$. This result supplements our hypothesis that fewer peptides get bounds to the LPS interface at a large $|\epsilon_{att}|$.

This work conclusively demonstrated that the change in attractive energy (ϵ_{att}) in the bacterial cell membrane of the LPS affects the activity of the AMPs. Moreover, the behaviors are well captured in an environment with high cell density with extremely long brush length. However, this is still implausible in practice due to physically unrealistic value selections. Although our model cannot be translated into a practical model at this stage, we anticipate that future attempts will resolve the issue and allow us to view more realistic models.

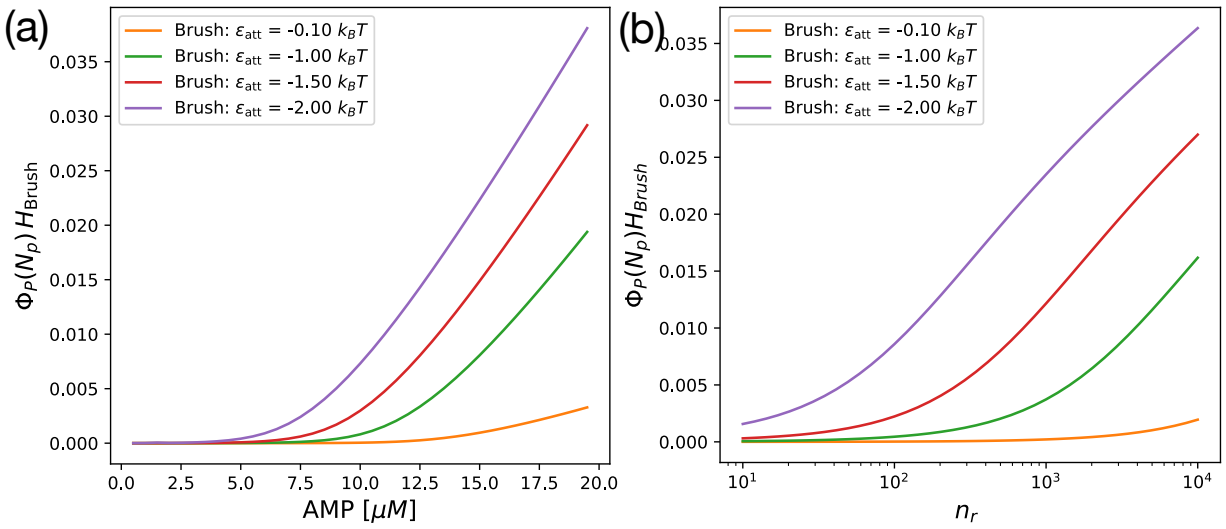

Figure 4.3: (a) The results of the cross-sectional area of the trapped peptide within the brush as a function of AMPs concentrations at various attractive energy ranges (ϵ_{att}). The parameters are set as follows: Cell density (C_{cell}) = 1×10^{10} cells/ml, area-stretch modulus (K_A) =200 pN/nm, brush length (n_r) = 20000, and Mg^{2+} = 0.1mM. It is analogous to Fig. 4.2 (a), but here, the results represent the trapped peptide ratio at a given area. (b) The results of the cross-sectional area of the trapped peptide within the brush as a function of brush length (n_r) at various attractive energy ranges (ϵ_{att}). The parameters are set as follows: Cell density (C_{cell}) = 1×10^{10} cells/ml, AMP concentration (C_p) = 20μM, and Mg^{2+} = 0.1mM. It is analogous to Fig 4.2 (b); instead, the results represent the ratio of trapped peptides at a given area.

4.4.2 Ionic concentration variations

Using the model again, we changed the salt concentration and analyzed the behaviors. First, we fixed Na^+ to 0.1M (=100mM) and adjusted the Mg^{2+} in the range between 1mM to 0.0001mM. This result is presented in the Fig. 4.4 (a) and it is analogous to the ref. [64] idea. As opposed to ref. [64], we reduced Mg^{2+} concentration close to zero (=0.0001mM). As a result, Fig. 4.4(a) showed that the ratio of the number of bound peptides to the total binding sites increased when Mg^{2+} ions concentration decreased. Additionally, the ratio asymptotically converged near 0.175 in the absence of Mg^{2+} ions in the solution. Aside from the peptide binding, Fig. 4.4 (b) and (c) represent the ion binding behavior for Na^+ and Mg^{2+}, respectively. Particularly, Fig. 4.4 (b) showed that when Mg^{2+} ions concentration decreased, Na^+ binding increased. This observation is consistent with the

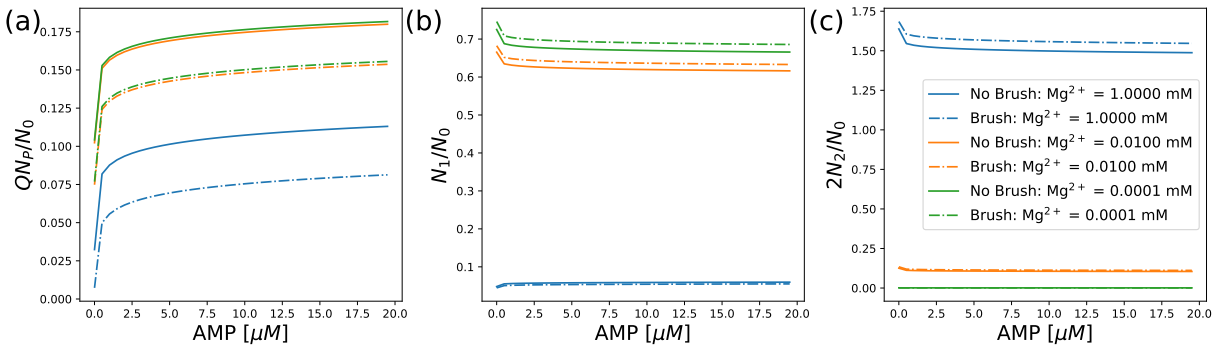

Figure 4.4: The behavioral changes in interfacial-binding peptides and ions (Mg^{2+} and Na^{+}) in response to Mg^{2+} concentration modulation. The solid line depicts the LPS without the brush chain, while the dashed line represents the LPS, including the brush that allows trapping the ions and the peptides. The legend in subplot (c) applies to other subplots (a) and (b). To generate the plot, the choice of the parameters is as follows: Cell density (C_{cell}) = 1×10^5 cells/ml, peptide-brush attraction (ϵ_{att}) = -0.05 k_BT, brush length (n_r) = 15, and Na^{+} = 100mM. (a) The ratio of interfacially bound peptides to total binding sites with AMP being the control variate at various ranges of Mg^{2+} concentration. (b) The ratio of interfacially bound Na^{+} to total binding sites. (c) The ratio of interfacial bound Mg^{2+} to total binding sites.

previous study [64], and it is attributable to the reducing effects of Mg^{2+}. Through this work, we observed that when Mg^{2+} ions decrease close to zero concentration, peptides can easily bind to the interface of the LPS.

In Fig. 4.5, we fixed the Mg^{2+} concentration near zero (=1μM) and altered the Na^{+} in the range between 0.05M and 0.20M. It has similar effects to the previous Chap. 3. As a result of changing salt concentration, Fig. 4.5 (a) showed that the peptide binding diminished with increasing Na^{+} concentrations. This is due to the effects of an increased number of Na^{+} ions. The Na^{+} ions screen the cell membrane and inhibit the binding of the peptides. As a result, the increase in the Na^{+} concentrations reduces peptide binding in the absence of Mg^{2+} ions. Furthermore, Fig. 4.5 (b) and (c) show the behavioral change of Na^{+} and Mg^{2+} ions binding to the surface.

In addition, the more intriguing result appeared as we increased Na^{+} concentrations at a high Mg^{2+} level. As depicted in Fig. 4.5, opposite effects take place, in which the number of bound peptide ratios increased in the abundant Mg^{2+} and when Na^{+} ion concentration increases. This indicated that the screening effects caused by the Na^{+} might have been reduced, and the Mg^{2+} competitiveness could have been diminished. However, it remains

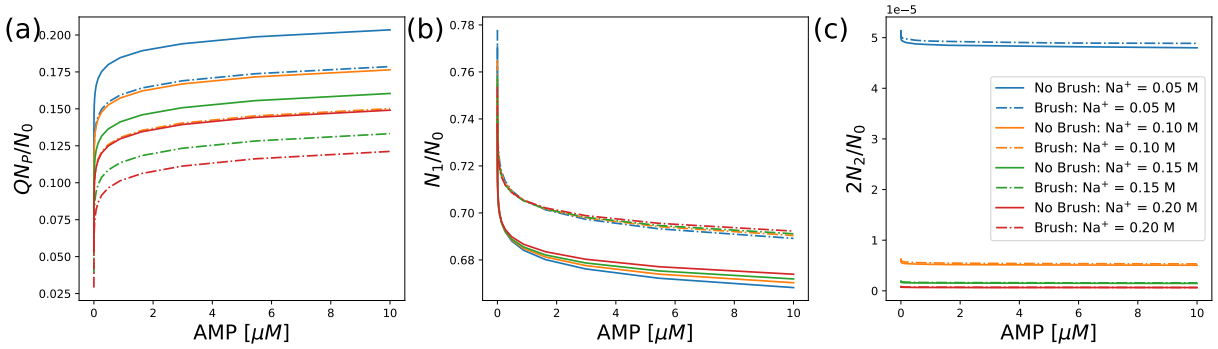

Figure 4.5: The behavioral changes in interfacial-binding peptides and ions (Mg^{2+} and Na^{+}) in response to Na^{+} concentration modulation. The solid line illustrates the LPS without the brush chain, while the dashed line represents the LPS, including the brush that allows trapping the ions and the peptides. To generate the plot, the choice of the parameters are as follows: Cell density (C_{cell}) = 1×10^5 cells/ml, peptide-brush attraction (ϵ_{att}) = -0.05 k_BT, brush length (n_r) = 15, and Mg^{2+} = 1μM. (a) The ratio of interfacially bound peptides to total binding sites with AMP being the control variate at various ranges of Mg^{2+} concentration. (b) The ratio of interfacial bound Na^{+} to total binding sites. (c) The ratio of interfacial bound Mg^{2+} to total binding sites.

questionable as to the actual ramifications since there has been no experimental research to support the following results.

Through this work, we observed how the activities of the AMPs changed as we changed Mg^{2+} and Na^{+} ions concentration. The result showed that the competing effects between the peptides and the Mg^{2+} ions are reduced when Mg^{2+} ion concentration drop close to zero, allowing the peptide to bind to the LPS easily. We further verified that the Na^{+} inhibited the binding of the peptides in the absence of Mg^{2+}, with a change in concentrations of Na^{+} as a result of the screening effects. Lastly, we observed that the binding decreased when the Na^{+} concentrations were altered, and both Na^{+} and Mg^{2+} were abundant in the environment. However, since it lacks detailed experimental evidence, it is challenging to support the results. However, the detailed examination of each subplot (b) and (c) that depicts the change in ion bindings to the peptide variations could help us clarify the binding interactions between the peptides.

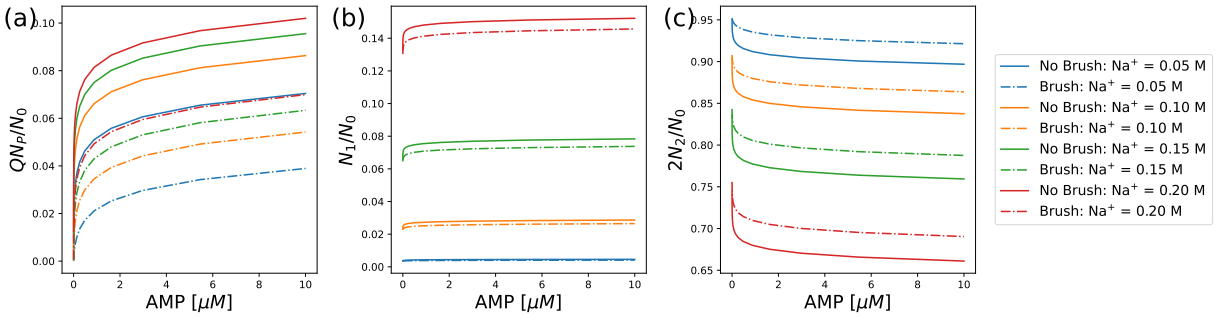

Figure 4.6: The behavioral changes in interfacial-binding peptides and ions (Mg^{2+} and Na^+) in response to Na^+ concentration modulation. The solid line depicts the LPS without the brush chain, while the dashed line represents the LPS, including the brush that allows trapping the ions and the peptides. For generating the figures, the choice of the parameters are as follows: Cell density (C_{cell}) = 1×10^5 cells/ml, peptide-brush attraction (ϵ_{att}) = -0.05 k_BT, brush length (n_r) = 15, and Mg^{2+} = 10mM. (a) The ratio of interfacially binding peptides to total binding sites with AMP being the control variate at various ranges of Mg^{2+} concentration. (b) The ratio of interfacially bound Na^+ to total binding sites. (c) The ratio of interfacial bound Mg^{2+} to total binding sites.

4.5 Conclusion

In this study, we examined the interactions between the outer bacterial membranes of the LPS layer against AMPs. Particularly, we have clarified how variations in two biologically significant factors (i.e., brush-peptide interactions, the electrostatic interactions between peptides and LPS headgroups, and brush lengths) influence the interaction of AMPs with bacterial LPS. First, we observed that LPS captured more AMPs within the brush at large attractive energy (ϵ_{att}) under high cell density and a long brush length condition. Additionally, we examined how salt concentration impacted AMP bindings to the interface of the LPS layer at different Na^+ and Mg^{2+} ions concentrations. Therefore, our model clarified the protective role of the LPS layer against cationic AMPs in a quantitative manner.

Chapter 5

Conclusion

Over the past few decades, AMPs have gained popularity as an alternative to conventional antibiotics and have been widely considered for application in various industries. Nevertheless, a thorough understanding of the interactions between AMPs and cell membranes has not been fully established and remains elusive. In this thesis, we focused on understanding the interactions between AMPs and cell membranes under various biologically relevant conditions by introducing theoretical models. In particular, we attempted to investigate the three main points, i.e., the selectivity and the activity of the AMPs in a variety of cases: bacteria-only cases, a mixture of bacteria and host cell, salinity, varying peptide-LPS interactions.

Specifically, in Chap. 2, we introduced a biophysical model of peptide activity and selectivity. Using the model, we have clarified how the presence of host cells and peptide trapping influence peptide selectivity. The result suggested a relatively insignificant dependence of the selectivity on the presence of host cells and peptide trapping. We also showed how the non-competitive selectivity acquired by combining MICs and MHCs for bacteria-only and host-cell-only solutions, respectively, differs from the competitive selectivity obtained for a mixture of both types of cells. The results demonstrated that the non-competitive selectivity can be larger than the competitive selectivity depending on how cell densities are selected.

In Chap. 3, we presented an interaction model between AMPs and bacterial membranes in electrolyte solutions containing monovalent cations Na^+. This work demonstrated how binding affinity changes with salt concentration. The binding affinity became weaker as we increased the salt concentration. As a result, the MIC was larger for higher salt concentrations.

In Chap. 4, we examined the theoretical model of the interactions between the LPS layer of the outer bacterial membrane against AMPs. To this end, we regard the LPS molecules as forming a polymer brush grafted to a charged surface and clarify the relative significance of several elements, such as brush-peptide interactions, the electrostatic interactions between peptides and LPS headgroups, and brush lengths. The result based on this model clarified the protective role of the LPS layer against cationic AMPs in a quantitative manner.

5.1 Future works

Beyond what has been accomplished in this thesis work, there remains much work to be done in the future. The remaining work from this study provides future directions. In Chap. 3, we investigated interactions between the AMPs and cell membranes with varying salt concentrations. Other studies [59, 60] have emphasized the significance of divalent ions competing with AMPs. Thus, to incorporate the divalent ions into the mean-field approach, the nonlinear Poisson-Boltzmann equation can be replaced by the linearized PB equation (i.e., the renormalized Debye Hückel approach) and further minimized with respect to the three charge densities, i.e., peptide charge density (σ_p), monovalent charge density(σ_1), divalent charge density(σ_2). With the given minimization, the total net charge density can be revised as $\sigma_{\text{net}} = Q\sigma_p + \sigma_1 - 2\sigma_2 - \sigma_0$, where the σ_0 represents the backbone charge of the peptides, which was denoted with $\sigma_0 = f_A/a_l$. With the additional terms of monovalent charge density(σ_1) and divalent charge density(σ_1), the entropy can also be revised analogous to the previous entropy formula. We hope that incorporating the divalent ions into the equation enables us to address the problem and improve both results and the method.

Furthermore, in Chap. 4, we reviewed the work of strengthening the protective layer of LPS in the presence of AMP. One caveat was that the model was assumed to have an unrealistically long brush that could not be converted into the actual model. To improve the model, we could adjust cell densities or other remaining parameters within the system to fit into the actual model.

As a final remark, in this thesis, we aim to provide a comprehensive understanding of the interaction between AMP and the cell membrane through theoretical modeling. We hope that the additional efforts related to the work carried out in this thesis become useful in the quest for ideal AMPs as therapeutic agents.

References

[1] *The Electric Double Layer*, chapter 4, pages 42–56. John Wiley & Sons, Ltd, 2003.

[2] Antimicrobial host defence peptides: functions and clinical potential. *Nature reviews. Drug discovery*, 19(5):311–332, 2020.

[3] Bruce Alberts. *Molecular biology of the cell / Bruce Alberts, Alexander Johnson, Julian Lewis, David Morgan, Martin Raff, Keith Roberts, Peter Walter ; with problems by John Wilson, Tim Hunt.* Garland Science, Taylor and Francis Group, sixth edition. edition, 2015.

[4] J M Andrews. Determination of minimum inhibitory concentrations. *Journal of antimicrobial chemotherapy*, 48 Suppl 1(suppl$_1$):5–16, 2001.

[5] James A Ayukekbong, Michel Ntemgwa, and Andrew N Atabe. The threat of antimicrobial resistance in developing countries: causes and control strategies. 6(1):47–47, 2017.

[6] Azadeh Bagheri, Sattar Taheri-Araghi, and Bae-Yeun Ha. How cell concentrations are implicated in cell selectivity of antimicrobial peptides. *Langmuir*, 31(29):8052–8062, 2015.

[7] Ali Adem Bahar and Dacheng Ren. Antimicrobial peptides. *Pharmaceuticals*, 6(12):1543–1575, 2013.

[8] Kim A Brogden. Antimicrobial peptides: pore formers or metabolic inhibitors in bacteria? *Nature reviews. Microbiology*, 3(3):238–250, 2005.

[9] Miguel A. R. B Castanho, Manuel N Melo, and Rafael Ferre. Antimicrobial peptides: linking partition, activity and high membrane-bound concentrations. *Nature reviews. Microbiology*, 7(3):245–250, 2009.

[10] Michal Ceremuga, Maksymilian Stela, Edyta Janik, Leslaw Gorniak, Ewelina Synowiec, Tomasz Sliwinski, Przemyslaw Sitarek, Joanna Saluk-Bijak, and Michal Bijak. Melittin—a natural peptide from bee venom which induces apoptosis in human leukaemia cells. *Biomolecules*, 10(2), 2020.

[11] David Leonard Chapman. Li. a contribution to the theory of electrocapillarity. *The London, Edinburgh, and Dublin Philosophical Magazine and Journal of Science*, 25(148):475–481, 1913.

[12] Ricardo A. Chaurio, Christina Janko, Luis E. Muñoz, Benjamin Frey, Martin Herrmann, and Udo S. Gaipl. Phospholipids: Key players in apoptosis and immune regulation. *Molecules*, 14(12):4892–4914, 2009.

[13] Yuxin Chen, Michael T. Guarnieri, Adriana I. Vasil, Michael L. Vasil, Colin T. Mant, and Robert S. Hodges. Role of peptide hydrophobicity in the mechanism of action of α-helical antimicrobial peptides. *Antimicrobial Agents and Chemotherapy*, 51(4):1398–1406, 2007.

[14] Hung-Lun CHU, Hui-Yuan YU, Bak-Sau YIP, Ya-Han CHIH, Chong-Wen LIANG, Hsi-Tsung CHENG, and Jya-Wei CHENG. Boosting salt resistance of short antimicrobial peptides. *Antimicrobial Agents and Chemotherapy*, 57(8):4050–4052, 2013.

[15] Pooi Yin Chung and Ramona Khanum. Antimicrobial peptides as potential anti-biofilm agents against multidrug-resistant bacteria. *Journal of Microbiology, Immunology and Infection*, 50(4):405–410, 2017.

[16] J. Michael Conlon and Milena Mechkarska. Host-defense peptides with therapeutic potential from skin secretions of frogs from the family pipidae. *Pharmaceuticals*, 7(1):58–77, 2014.

[17] Jessica Audrey Feijó Corrêa, Alberto Gonçalves Evangelista, Tiago de Melo Nazareth, and Fernando Bittencourt Luciano. Fundamentals on the molecular mechanism of action of antimicrobial peptides. *Materialia*, 8:100494, 2019.

[18] Peter Debye and Erich Hückel. Zur theorie der elektrolyte. i. gefrierpunktserniedrigung und verwandte erscheinungen. *Physikalische Zeitschrift*, 24(185):305, 1923.

[19] Anne H. Delcour. Outer membrane permeability and antibiotic resistance. *Biochimica et Biophysica Acta (BBA) - Proteins and Proteomics*, 1794(5):808–816, 2009. Mechanisms of Drug Efflux and Strategies to Combat Them.

[20] G Diamond, M Zasloff, H Eck, M Brasseur, W L Maloy, and C L Bevins. Tracheal antimicrobial peptide, a cysteine-rich peptide from mammalian tracheal mucosa: peptide isolation and cloning of a cdna. *Proceedings of the National Academy of Sciences*, 88(9):3952–3956, 1991.

[21] Ken A Dill. *Molecular driving forces : statistical thermodynamics in biology, chemistry, physics, and nanoscience / Ken A. Dill, Sarina Bromberg.* Garland Science, 2nd ed. edition, 2011.

[22] Lai Ding, Lin Yang, Thomas M Weiss, Alan J Waring, Robert I Lehrer, and Huey W Huang. Interaction of antimicrobial peptides with lipopolysaccharides. *Biochemistry (Easton)*, 42(42):12251–12259, 2003.

[23] Lai Ding, Lin Yang, Thomas M Weiss, Alan J Waring, Robert I Lehrer, and Huey W Huang. Interaction of antimicrobial peptides with lipopolysaccharides. *Biochemistry (Easton)*, 42(42):12251–12259, 2003.

[24] Julia R. Dorin, Brian J. McHugh, Sarah L. Cox, and Donald J. Davidson. Chapter 30 - mammalian antimicrobial peptides; defensins and cathelicidins. In Yi-Wei Tang, Max Sussman, Dongyou Liu, Ian Poxton, and Joseph Schwartzman, editors, *Molecular Medical Microbiology (Second Edition)*, pages 539–565. Academic Press, Boston, second edition edition, 2015.

[25] Ciara Duffy, Anabel Sorolla, Edina Wang, Emily Golden, Eleanor Woodward, Kathleen Davern, Diwei Ho, Elizabeth Johnstone, Kevin Pfleger, Andrew Redfern, K Swaminathan Iyer, Boris Baer, and Pilar Blancafort. Honeybee venom and melittin suppress growth factor receptor activation in her2-enriched and triple-negative breast cancer. *NPJ precision oncology*, 4(1):24–24, 2020.

[26] Ulrich H.N. Dürr, U.S. Sudheendra, and Ayyalusamy Ramamoorthy. Ll-37, the only human member of the cathelicidin family of antimicrobial peptides. *Biochimica et Biophysica Acta (BBA) - Biomembranes*, 1758(9):1408–1425, 2006. Membrane Biophysics of Antimicrobial Peptides.

[27] Thomas Ebenhan, Olivier Gheysens, Hendrick Gert Kruger, Jan Rijn Zeevaart, and Mike Machaba Sathekge. Antimicrobial peptides: Their role as infection-selective tracers for molecular imaging. *BioMed research international*, 2014:867381–15, 2014.

[28] R. M Epand and R. F Epand. Biophysical analysis of membrane-targeting antimicrobial peptides: membrane properties and the design of peptides specifically targeting

gram-negative bacteria. In *Antimicrobial peptides: discovery, design and novel therapeutic strategies*, pages 116–127. CABI, Wallingford, UK, 2010.

[29] Mitchell J Goldman, G.Mark Anderson, Ethan D Stolzenberg, U.Prasad Kari, Michael Zasloff, and James M Wilson. Human β-defensin-1 is a salt-sensitive antibiotic in lung that is inactivated in cystic fibrosis. *Cell*, 88(4):553–560, 1997.

[30] Gouy, G. Sur la fonction électrocapillaire. *Ann. Phys.*, 9(7):129–184, 1917.

[31] Gouy, M. Sur la constitution de la charge électrique à la surface d'un électrolyte. *J. Phys. Theor. Appl.*, 9(1):457–468, 1910.

[32] Katarzyna E Greber, Krzesimir Ciura, Mariusz Belka, Piotr Kawczak, Joanna Nowakowska, Tomasz Baczek, and Wieslaw Sawicki. Characterization of antimicrobial and hemolytic properties of short synthetic cationic lipopeptides based on qsar/qstr approach. *Amino acids*, 50(3-4):479–485, 2017.

[33] Sonia M Gregory, Allison Cavenaugh, Velvet Journigan, Antje Pokorny, and Paulo F.F Almeida. A quantitative model for the all-or-none permeabilization of phospholipid vesicles by the antimicrobial peptide cecropin a. *Biophysical journal*, 94(5):1667–1680, 2008.

[34] Chad Gu, Rob D Coalson, David Jasnow, and Anton Zilman. Free energy of nanoparticle binding to multivalent polymeric substrates. *The journal of physical chemistry. B*, 121(26):6425–6435, 2017.

[35] Robert E W Hancock, Evan F Haney, and Erin E Gill. The immunology of host defence peptides: beyond antimicrobial activity. 16(5):321–334, 2016.

[36] Robert E W Hancock and Hans-Georg Sahl. Antimicrobial and host-defense peptides as new anti-infective therapeutic strategies. *Nature biotechnology*, 24(12):1551–1557, 2006.

[37] Robert E.W Hancock and Robert Lehrer. Cationic peptides: a new source of antibiotics. *Trends in Biotechnology*, 16(2):82–88, 1998.

[38] Xue Hao, Hailong Yang, Ling Wei, Shilong Yang, Wenjuan Zhu, Dongying Ma, Haining Yu, and Ren Lai. Amphibian cathelicidin fills the evolutionary gap of cathelicidin in vertebrate. *Amino acids*, 43(2):677–685, 2011.

[39] T Heimburg and D Marsh. Protein surface-distribution and protein-protein interactions in the binding of peripheral proteins to charged lipid membranes. *Biophysical journal*, 68(2):536–546, 1995.

[40] Thomas Heimburg. *Thermal biophysics of membranes / Thomas Heimburg.* Tutorials in biophysics. Wiley-VCH Verlag, Weinheim, 2007.

[41] Thomas Heimburg, Brigitta Angerstein, and Derek Marsh. Binding of peripheral proteins to mixed lipid membranes: Effect of lipid demixing upon binding. *Biophysical journal*, 76(5):2575–2586, 1999.

[42] Yuchen Huan, Qing Kong, Haijin Mou, and Huaxi Yi. Antimicrobial peptides: Classification, design, application and research progress in multiple fields. *Frontiers in microbiology*, 11:582779–582779, 2020.

[43] Huey W Huang. Molecular mechanism of antimicrobial peptides: The origin of cooperativity. *Biochimica et biophysica acta*, 1758(9):1292–1302, 2006.

[44] Huey W Huang. Molecular mechanism of antimicrobial peptides: The origin of cooperativity. *Biochimica et biophysica acta. Biomembranes*, 1758(9):1292–1302, 2006.

[45] Norman H Lam and Bae-Yeun Ha. Surface-lattice model describes electrostatic interactions of ions and polycations with bacterial lipopolysaccharides: Ion valence and polycation's excluded area. *Langmuir*, 30(45):13631–13640, 2014.

[46] Norman H Lam, Zheng Ma, and Bae-Yeun Ha. Electrostatic modification of the lipopolysaccharide layer: competing effects of divalent cations and polycationic or polyanionic molecules. *Soft matter*, 1(38):7528–7544, 2014.

[47] Christopher N LaRock and Victor Nizet. Cationic antimicrobial peptide resistance mechanisms of streptococcal pathogens. *Biochimica et biophysica acta*, 1848(11):3047–3054, 2015.

[48] Ming-Tao Lee, Fang-Yu Chen, and Huey W Huang. Energetics of pore formation induced by membrane active peptides. *Biochemistry (Easton)*, 43(12):3590–3599, 2004.

[49] Ming-Tao Lee, Wei-Chin Hung, Fang-Yu Chen, and Huey W Huang. Many-body effect of antimicrobial peptides: On the correlation between lipid's spontaneous curvature and pore formation. *Biophysical journal*, 89(6):4006–4016, 2005.

[50] Ming-Tao Lee, Wei-Chin Hung, Fang-Yu Chen, and Huey W Huang. Mechanism and kinetics of pore formation in membranes by water-soluble amphipathic peptides. *Proceedings of the National Academy of Sciences - PNAS*, 105(13):5087–5092, 2008.

[51] Jun Lei, Lichun Sun, Siyu Huang, Chenhong Zhu, Ping Li, Jun He, Vienna Mackey, David H Coy, and Quanyong He. The antimicrobial peptides and their potential clinical applications. 11(7):3919–3931, 2019.

[52] Michelle Lin, Stephen J. Liu, and Ingrid T. Lim. Disorders of water imbalance. *Emergency Medicine Clinics of North America*, 23(3):749–770, 2005. Endocrine and Metabolic Emergencies.

[53] Ti-Yu Lin and Douglas B Weibel. Organization and function of anionic phospholipids in bacteria. *Applied microbiology and biotechnology*, 100(10):4255–4267, 2016.

[54] Karl Lohner and Florian Prossnigg. Biological activity and structural aspects of pgla interaction with membrane mimetic systems. *Biochimica et Biophysica Acta (BBA) - Biomembranes*, 1788(8):1656–1666, 2009. Amphibian Antimicrobial Peptides.

[55] Katsumi Matsuzaki. Why and how are peptide–lipid interactions utilized for self-defense? magainins and tachyplesins as archetypes. *Biochimica et Biophysica Acta (BBA) - Biomembranes*, 1462(1):1–10, 1999.

[56] Katsumi Matsuzaki. Control of cell selectivity of antimicrobial peptides. *Biochimica et Biophysica Acta (BBA) - Biomembranes*, 1788(8):1687–1692, 2009. Amphibian Antimicrobial Peptides.

[57] Katsumi Matsuzaki, Osamu Murase, Nobutaka Fujii, and Koichiro Miyajima. Translocation of a channel-forming antimicrobial peptide, magainin 2, across lipid bilayers by forming a pore. *Biochemistry (Easton)*, 34(19):6521–6526, 1995.

[58] Katsumi Matsuzaki, Osamu Murase, Nobutaka Fujii, and Koichiro Miyajima. An antimicrobial peptide, magainin 2, induced rapid flip-flop of phospholipids coupled with pore formation and peptide translocation. 35(35):11361–11368, 1996.

[59] Katsumi Matsuzaki, Ken-ichi Sugishita, Mitsunori Harada, Nobutaka Fujii, and Koichiro Miyajima. Interactions of an antimicrobial peptide, magainin 2, with outer and inner membranes of gram-negative bacteria. *Biochimica et biophysica acta*, 1327(1):119–130, 1997.

[60] Katsumi Matsuzaki, Ken-ichi Sugishita, and Koichiro Miyajima. Interactions of an antimicrobial peptide, magainin 2, with lipopolysaccharide-containing liposomes as a model for outer membranes of gram-negative bacteria. *FEBS letters*, 449(2):221–224, 1999.

[61] Neeloffer Mookherjee, Marilyn A Anderson, Henk P Haagsman, Donald J Davidson, Moleculaire afweer, and dI&I I&I-3. Antimicrobial host defence peptides: functions and clinical potential. *Nature reviews. Drug discovery*, 19(5):311–332, 2020.

[62] Robert Nawrot, Jakub Barylski, Grzegorz Nowicki, Justyna Broniarczyk, Waldemar Buchwald, and Anna Goździcka-Józefiak. Plant antimicrobial peptides. *Folia microbiologica*, 59(3):181–196, 2013.

[63] Shokoofeh Nourbakhsh, Sattar Taheri-Araghi, and Bae-Yeun Ha. Toward building a physical model for membrane selectivity of antimicrobial peptides: making a quantitative sense of the selectivity. *Soft matter*, 15(37):759–7526, 2019.

[64] Shokoofeh Nourbakhsh, Liu Yu, and Bae-Yeun Ha. Modeling the protective role of bacterial lipopolysaccharides against membrane-rupturing peptides. *The journal of physical chemistry. B*, 125(31):8839–8854, 2021.

[65] Ziv Oren and Yechiel Shai. Mode of action of linear amphipathic α-helical antimicrobial peptides. *Peptide Science*, 47(6):451–463, 1998.

[66] Niv Papo and Yechiel Shai. A molecular mechanism for lipopolysaccharide protection of gram-negative bacteria from antimicrobial peptides*. *Journal of Biological Chemistry*, 280(11):10378–10387, 2005.

[67] In Yup Park, Ju Hyun Cho, Key Sun Kim, Yun-Bae Kim, Mi Sun Kim, and Sun Chang Kim. Helix stability confers salt resistance upon helical antimicrobial peptides. *The Journal of biological chemistry*, 279(14):13896–13901, 2004.

[68] Soo-Jin Park and Min-Kang Seo. Chapter 1 - intermolecular force. In Soo-Jin Park and Min-Kang Seo, editors, *Interface Science and Composites*, volume 18 of *Interface Science and Technology*, pages 1–57. Elsevier, 2011.

[69] Gabriel G Perron, Michael Zasloff, and Graham Bell. Experimental evolution of resistance to an antimicrobial peptide. *Proceedings of the Royal Society. B, Biological sciences*, 273(1583):251–256, 2006.

[70] Andreas Peschel and Hans-Georg Sahl. The co-evolution of host cationic antimicrobial peptides and microbial resistance. *Nature reviews. Microbiology*, 4(7):529–536, 2006.

[71] Rob (Robert Brooks) Phillips. *Physical biology of the cell*. Garland Science, London ;, second edition. edition, 2013.

[72] Christian R. H Raetz and Chris Whitfield. Lipopolysaccharide endotoxins. *Annual review of biochemistry*, 71(1):635–700, 2002.

[73] Mithila Rajagopal and Suzanne Walker. Envelope structures of gram-positive bacteria. *Current topics in microbiology and immunology*, 404:1–44, 2016.

[74] Filippo Savini, Sara Bobone, Daniela Roversi, Maria Luisa Mangoni, and Lorenzo Stella. From liposomes to cells: Filling the gap between physicochemical and microbiological studies of the activity and selectivity of host-defense peptides. *Peptide science (Hoboken, N.J.)*, 110(5):e24041–n/a, 2018.

[75] Filippo Savini, Vincenzo Luca, Alessio Bocedi, Renato Massoud, Yoonkyung Park, Maria Luisa Mangoni, and Lorenzo Stella. Cell-density dependence of host-defense peptide activity and selectivity in the presence of host cells. *ACS chemical biology*, 12(1):52–56, 2017.

[76] Bethany Schefter, Shokoofeh Nourbakhsh, Sattar Taheri-Araghi, and Bae-Yeun Ha. Modeling cell selectivity of antimicrobial peptides: How is the selectivity influenced by intracellular peptide uptake and cell density. *Frontiers in Medical Technology*, 3:626481, 02 2021.

[77] Joachim Seelig. Thermodynamics of lipid–peptide interactions. *Biochimica et Biophysica Acta (BBA) - Biomembranes*, 1666(1):40–50, 2004. Lipid-Protein Interactions.

[78] Yechiel Shai. Mode of action of membrane active antimicrobial peptides. *Biopolymers*, 66(4):236–248, 2002.

[79] Zakhar O Shenkarev, Sergey V Balandin, Kirill I Trunov, Alexander S Paramonov, Stanislav V Sukhanov, Leonid I Barsukov, Alexander S Arseniev, and Tatiana V Ovchinnikova. Molecular mechanism of action of β-hairpin antimicrobial peptide arenicin: Oligomeric structure in dodecylphosphocholine micelles and pore formation in planar lipid bilayers. *Biochemistry (Easton)*, 50(28):6255–6265, 2011.

[80] Thomas J Silhavy, Daniel Kahne, and Suzanne Walker. The bacterial cell envelope. *Cold Spring Harbor perspectives in biology*, 2(5):a000414–a000414, 2010.

[81] Patrícia M Silva, Sónia Gonçalves, and Nuno C Santos. Defensins: antifungal lessons from eukaryotes. *Frontiers in microbiology*, 5:97–97, 2014.

[82] Matthew Smart, Aruna Rajagopal, Wing-Ki Liu, and Bae-Yeun Ha. Opposing effects of cationic antimicrobial peptides and divalent cations on bacterial lipopolysaccharides. *Phys. Rev. E*, 96:042405, Oct 2017.

[83] Mehdi Snoussi, John Paul Talledo, Nathan-Alexander Del Rosario, Salimeh Mohammadi, Bae-Yeun Ha, Andrej Kosmrlj, and Sattar Taheri-Araghi. Heterogeneous absorption of antimicrobial peptide ll37 in escherichia coli cells enhances population survivability. *eLife*, 7, 2018.

[84] Scott Snyder, Dennis Kim, and Thomas J McIntosh. Lipopolysaccharide bilayer structure: Effect of chemotype, core mutations, divalent cations, and temperature. *Biochemistry (Easton)*, 38(33):10758–10767, 1999.

[85] Russell K. W Spencer and Bae-Yeun Ha. How a polymer brush interacts with inclusions and alters their interaction. *Macromolecules*, 54(3):1304–1313, 2021.

[86] Charles G Starr, Jing He, and William C Wimley. Host cell interactions are a significant barrier to the clinical utility of peptide antibiotics. *ACS chemical biology*, 11(12):3391–3399, 2016.

[87] Sattar Taheri-Araghi. Private communication, 2022.

[88] Pei-Wen Tsai, Cheng-Yao Yang, Hao-Teng Chang, and Chung-Yu Lan. Human antimicrobial peptide ll-37 inhibits adhesion of candida albicans by interacting with yeast cell-wall carbohydrates. *PloS one*, 6(3):e17755–e17755, 2011.

[89] Jelske N. van der Veen, John P. Kennelly, Sereana Wan, Jean E. Vance, Dennis E. Vance, and René L. Jacobs. The critical role of phosphatidylcholine and phosphatidylethanolamine metabolism in health and disease. *Biochimica et Biophysica Acta (BBA) - Biomembranes*, 1859(9, Part B):1558–1572, 2017. Membrane Lipid Therapy: Drugs Targeting Biomembranes.

[90] G van Meer, D.R Voelker, G.W Feigenson, Membraan enzymologie, and Dep Scheikunde. Membrane lipids: where they are and how they behave. 9(2):112–124, 2008.

[91] Jean E. Vance. Phospholipid synthesis and transport in mammalian cells. *Traffic (Copenhagen, Denmark)*, 16(1):1–18, 2015.

[92] Jiajun Wang, Xiujing Dou, Jing Song, Yinfeng Lyu, Xin Zhu, Lin Xu, Weizhong Li, and Anshan Shan. Antimicrobial peptides: Promising alternatives in the post feeding antibiotic era. *Medicinal research reviews*, 39(3):831–859, 2019.

[93] Yipeng Wang, Jing Hong, Xiuhong Liu, Hailong Yang, Rui Liu, Jing Wu, Aili Wang, Donghai Lin, and Ren Lai. Snake cathelicidin from bungarus fasciatus is a potent peptide antibiotics. *PloS one*, 3(9):e3217–e3217, 2008.

[94] Zhe Wang and Guangshun Wang. Apd: the antimicrobial peptide database. *Nucleic acids research*, 32(suppl-1):D590–D592, 2004.

[95] Stephen G Wilkinson. Bacterial lipopolysaccharides—themes and variations. *Progress in lipid research*, 35(3):283–343, 1996.

[96] Michael R. Yeaman and Nannette Y. Yount. Mechanisms of antimicrobial peptide action and resistance. *Pharmacological reviews*, 55(1):27–55, 2003.

[97] Margherita Zanetti. Cathelicidins, multifunctional peptides of the innate immunity. *Journal of leukocyte biology*, 75:39–48, 02 2004.

[98] M Zasloff. Magainins, a class of antimicrobial peptides from xenopus skin: isolation, characterization of two active forms, and partial cdna sequence of a precursor. *Proceedings of the National Academy of Sciences*, 84(15):5449–5453, 1987.

[99] Michael Zasloff. Antimicrobial peptides of multicellular organisms. *Nature (London)*, 415(6870):389–395, 2002.

[100] Lijuan Zhang, Pawandeep Dhillon, Hong Yan, Susan Farmer, and Robert E. W. Hancock. Interactions of bacterial cationic peptide antibiotics with outer and cytoplasmic membranes of *Pseudomonas aeruginosa*. *Antimicrobial Agents and Chemotherapy*, 44(12):3317–3321, 2000.

[101] Ling-juan Zhang and Richard L Gallo. Antimicrobial peptides. *Current biology*, 26(1):R14–R19, 2016.

[102] Qi-Yu Zhang, Zhi-Bin Yan, Yue-Ming Meng, Xiang-Yu Hong, Gang Shao, Jun-Jie Ma, Xu-Rui Cheng, Jun Liu, Jian Kang, and Cai-Yun Fu. Antimicrobial peptides: mechanism of action, activity and clinical potential. *Military medical research*, 8(1):1–48, 2021.

[103] Huan-Xiang Zhou, Germán Rivas, and Allen P Minton. Macromolecular crowding and confinement: biochemical, biophysical, and potential physiological consequences. *Annual review of biophysics*, 37(1):375–397, 2008.

[104] S B Zimmerman and A P Minton. Macromolecular crowding: Biochemical, biophysical, and physiological consequences. *Annual review of biophysics and biomolecular structure*, 22(1):27–65, 1993.

Appendix A

Python Code Access

All code is generated using python, and the source code is accessible through GitHub for replicating the results.[1]

- Chapter 2 code is available under the repository: Membrane_Cell_Selectivity. [2]
- Chapter 3 code is available under the repository: MIC_Salt_dependent.[3]
- Chapter 4 code is available under the repository: LPS_Layer. [4]

[1] https://github.com/Suemin-Lee
[2] https://github.com/Suemin-Lee/Membrane_Cell_Selectivity
[3] https://github.com/Suemin-Lee/MIC_Salt_dependent
[4] https://github.com/Suemin-Lee/LPS_Layer